

**IDENTIFICATION OF EXOSOMES/MICROVESICLES IN THE
OVIDUCTAL LUMINAL FLUID: CHARACTERIZATION OF
MOLECULAR INTERACTIONS IN CARGO DELIVERY TO SPERM
USING NANOSCOPY, TEM, AND PMCA4 AS A MODEL**

by

Amal Ali K Aldossary

A dissertation submitted to the Faculty of the University of Delaware in partial fulfillment of the requirements for the degree of Doctor of Philosophy in Biological Sciences

Fall 2014

© 2014 Aldossary
All Rights Reserved

UMI Number: 3685093

All rights reserved

INFORMATION TO ALL USERS

The quality of this reproduction is dependent upon the quality of the copy submitted.

In the unlikely event that the author did not send a complete manuscript and there are missing pages, these will be noted. Also, if material had to be removed, a note will indicate the deletion.



UMI 3685093

Published by ProQuest LLC (2015). Copyright in the Dissertation held by the Author.

Microform Edition © ProQuest LLC.

All rights reserved. This work is protected against unauthorized copying under Title 17, United States Code



ProQuest LLC.
789 East Eisenhower Parkway
P.O. Box 1346
Ann Arbor, MI 48106 - 1346

**IDENTIFICATION OF EXOSOMES/MICROVESICLES IN THE
OVIDUCTAL LUMINAL FLUID: CHARACTERIZATION OF
MOLECULAR INTERACTIONS IN CARGO DELIVERY TO SPERM
USING NANOSCOPY, TEM, AND PMCA4 AS A MODEL**

by

Amal Ali K Aldossary

Approved: _____

Robin W. Morgan, Ph.D.
Chair of the Department of Biological Sciences

Approved: _____

George Watson, Ph.D.
Dean of the College of Arts and Sciences

Approved: _____

James G. Richards, Ph.D.
Vice Provost for Graduate and Professional Education

I certify that I have read this dissertation and that in my opinion it meets the academic and professional standard required by the University as a dissertation for the degree of Doctor of Philosophy.

Signed:

Patricia A. Martin-DeLeon, Ph.D.
Professor in charge of dissertation

I certify that I have read this dissertation and that in my opinion it meets the academic and professional standard required by the University as a dissertation for the degree of Doctor of Philosophy.

Signed:

Emanuel E. Strehler, Ph.D.
Member of dissertation committee

I certify that I have read this dissertation and that in my opinion it meets the academic and professional standard required by the University as a dissertation for the degree of Doctor of Philosophy.

Signed:

Colin Thorpe, Ph.D.
Member of dissertation committee

I certify that I have read this dissertation and that in my opinion it meets the academic and professional standard required by the University as a dissertation for the degree of Doctor of Philosophy.

Signed:

Deni S. Galileo, Ph.D.
Member of dissertation committee

I certify that I have read this dissertation and that in my opinion it meets the academic and professional standard required by the University as a dissertation for the degree of Doctor of Philosophy.

Signed:

Jia L. Song, Ph.D.
Member of dissertation committee

ACKNOWLEDGMENTS

I would like to thank God, I am thankful for the strength that keeps me standing and for the hope that keeps me believing.

I would like to express my profound gratitude and deepest appreciation to my advisor, Professor Patricia Martin-DeLeon for her excellent guidance, mentoring, and patience in correcting my writing, as well as her caring and constant encouragement throughout the few years I spent in her laboratory. Without her acceptance and guidance, this dissertation would not have been possible, and I thank her for allowing me to grow as research scientist. Under her supervision I developed a focus and became interested in Andrology. She provided me with direction, an excellent environment for doing research, technical support, and became more of a mentor and friend than a professor. The blessing, guidance, and persistent help she has given me shall carry me a long way throughout the life.

I wish to express my deep sincere gratitude to my committee member, Professor Emanuel Strehler, for his generosity of the PMCA4a antibody, guidance and useful suggestions, without which, the present work could not have been completed.

I would like to express my very great appreciation to my committee member, Professor Colin Thorpe, for his support, constructive suggestions, and allowing me to

use his lab equipment. His willingness to give his time so generously has been very much appreciated.

I would like to thank my committee member, Professor Deni Galileo, for his support, suggestions, and help with the flowcytometry.

I would like to express my deepest appreciation to my committee member, Professor Jia Song, for her encouragement, insightful comments, and help with the RT-PCR.

I would like to express my thanks to Professor Jeff Caplan, who introduced me to the 2014 Nobel prize winner technology, the super-resolved fluorescence microscopy, and whose passion for the fluorescence techniques had lasting effects on me.

I would like to express my heartfelt thanks to my beloved parents, Ali and Aisha, for their blessings, encouragements and inspiration to me throughout my entire life. Without their love and support, I would not have been at this stage of my career.

Special thanks to my siblings: Salman, Maryam, Mohammad and Khamis, and my sister in-law, Najlah. They were always supporting me and encouraging me with their best wishes.

I thank my fellow labmates in DeLeon's laboratory: Kathie, Rachel, Kris, Lauren, Deepthi, Becky, Erin, Nicolette and Ashley for their support, help and for the

fun we have had in the last few years. Assistance provided by Reetika Dutt was also greatly appreciated. I would like to thank Lauren Hurd for her assistance with calcium loading experiment.

I would like to extend my thanks to the staff of Bioimaging center at Delaware Biotechnology Institute, Deborah Powell, Shannon Modla, Jean Ross and Michael Moor for their assistance and help.

I would like to thank the University of Delaware for the opportunity to study in rich environments that help me achieve my goals. I would like to express my deepest appreciation to Dr. Mary Martin for her persistent help and encouragement. Many thanks to the former chairperson, Professor Randall Duncan, for his encouragement and support. Many thanks to chairperson, Professor Robin Morgan, faculty and staff at the Biological Sciences department for their support. A special thanks to Betty Cowgill for her assistance throughout my graduate program.

Finally, very special thanks go out to the office of laboratory Animal Medicine (OLAM) group, Mr. Frank Warren, Sandy Campbell, Minh Pham, and Francis Karani, for all of their persistent help and assistance throughout my graduate program.

In conclusion, I recognize this research would not have been possible without the financial assistance of the College of Medicine at the University of Dammam and the Saudi Arabian Cultural Mission for their financial support granted through my doctoral scholarship.

TABLE OF CONTENTS

LIST OF TABLES	xii
LIST OF FIGURES	xiii
ABSTRACT	xv

Chapter

1 INTRODUCTION	1
1.1 Spermatozoa: Their Journey during Maturation	1
1.1.1 Testicular maturation	1
1.1.2 Epididymal maturation	3
1.1.2.1 Epididymis	3
1.1.2.2 Epididymal luminal fluids- epididymosomes	4
1.1.3 Final maturation in the female reproductive tract- capacitation	6
1.2 The Plasma Membrane Calcium ATPase 4 (PMCA4)	8
1.3 Significance	12
1.4 Hypotheses and Specific Aims	14
1.4.1 Hypothesis 1: Plasma membrane Ca^{2+} -ATPase 4a (PMCA4a) is expressed and secreted in the female reproductive tract where it can be acquired on the sperm surface during sperm transit and storage (maturation) in the oviduct	14
1.4.1.1 Specific Aim 1: Determine if PMCA4a is expressed and secreted in the female luminal fluids (FLF) during the estrus cycle and if sperm can acquire PMCA4a from the fluids.	14
1.4.1.2 Specific Aim 2: Isolate and characterize membranous vesicles from female reproductive fluids and immunolocalize PMCA4a on them.	14
1.4.1.3 Specific Aim 3: Determine if oviductosomes (OVS) in the female luminal fluid are necessary and sufficient for the transfer of PMCA4a to the sperm.	14

1.4.2	Hypothesis 2: A fusogenic mechanism is involved in the delivery of PMCA4 to the sperm membrane via OVS.....	14
1.4.2.1	Specific Aim 1: Visualize the interaction between FM4-64FX pre-labeled OVS with the sperm membrane, using 3D SR-SIM.	14
1.4.2.2	Specific Aim 2: Analyze OVS-sperm interaction, using TEM and immunogold labeling of PMCA4, after co-incubation for the maximal period used in 3D SR-SIM and indirect immunofluorescence.	14
1.4.2.3	Specific Aim 3: Investigate the role of tetraspanin and/or αV integrin in OVS-sperm fusion using labeled exosomes/microvesicles and blocking of receptor-ligand interactions.	15
1.4.3	Hypothesis 3: PMCA4, carried by OVS and delivered to sperm, plays an important and crucial role in the regulation of proper Ca^{2+} handling during sperm capacitation which requires high levels of Ca^{2+}	15
1.4.3.1	Specific Aim 1: Assess litter sizes of <i>Pmca4</i> nulls, Hets and WT females mated to WT and Het males to determine the impact of PMCA4 transfer from oviductosomes to sperm <i>in vivo</i>	15
1.4.3.2	Specific Aim 2: Evaluate the impact of delivery of PMCA4 <i>in vitro</i> to <i>Pmca4</i> KO sperm by assessing Ca^{2+} -ATPase activity, Ca^{2+} handling, and progressive sperm motility following PMCA4 delivery via OVS.	15
2	MATERIALS AND METHODS	16
2.1	Mice and Reagents	16
2.2	Antibodies and Fluorescent Dyes.....	17
2.3	Analysis of Physiological Estrus Cycle.....	18
2.4	Superovulated Females.....	18
2.5	Preparation of Murine Female Reproductive Tissues	18
2.6	Collection of Luminal Fluids in Naturally Cycling Females and from Males	19
2.7	Collection of Vaginal, Uterine and Oviductal Luminal Fluids from Females after Hormonal Induction of Estrus	19
2.8	OVS Preparation.....	19
2.9	Preparation of Capacitated and Acrosome-reacted Sperm.....	20
2.10	Total RNA Isolation and Reverse Transcriptase (RT)-PCR	21

2.11	Indirect Immunofluorescence Staining and Confocal Analysis	22
2.11.1	Female reproductive tissues	22
2.11.2	Sperm suspension	22
2.12	SDS-PAGE and Western Blot Analysis	23
2.13	Analysis of <i>in vitro</i> Sperm Uptake of PMCA4a from Female Luminal Fluids (FLF)	24
2.14	Labeling of OVS with FM4-64-FX and Co-incubation of Pre-labeled OVS with Sperm	25
2.15	3D SR-SIM Analysis of OVS-sperm Interaction	26
2.15.1	Co-incubation assay.....	26
2.15.2	Co-localization of OVS with PMCA4 and α v-integrin subunit ..	26
2.15.3	3D SR-SIM imaging.....	27
2.16	TEM Analysis.....	27
2.16.1	Negative staining for TEM.....	27
2.16.2	Immunogold labeling of PMCA4a or CD9 in OVS	28
2.16.3	Pre-embedding immunogold labeling for OVS-sperm membrane interaction	29
2.17	Effect of the Tri-peptide Arg-Gly-Asp (RGD) on OVS-sperm Fusion...	30
2.18	Effect of Fibronectin (FN) or Vitronectin (VN) on OVS-sperm Fusion.	31
2.19	Breeding of <i>Pmca4</i> KO, Het and WT Females to WT or Het Males to Assess Fertility via Analysis of Litter Sizes.....	31
2.20	Ca ²⁺ -ATPase Assay	31
2.21	Evaluation of Intracellular Calcium Concentration ([Ca ²⁺] _i) in Sperm using Single Cell Imaging	33
2.22	Evaluation of Sperm Motility	34
2.23	Statistical Analysis	34
3	RESULTS.....	35
3.1	Analysis of <i>Pmca4</i> Transcripts in Murine Female Reproductive Tissues	35
3.2	Localization and Detection of PMCA4a in the Female Reproductive Tract and in its Secretion.....	37
3.3	Characterization of Membrane Vesicles from Oviductal Luminal Fluids as Exosomes and Microvesicles	42
3.4	PMCA4a is Present in the OVS of the Luminal Fluids.....	43
3.5	<i>In Vitro</i> Uptake of PMCA4a on Caudal Sperm from Unfractionated Luminal Fluids and OVS.....	44

3.6	<i>In vitro</i> OVS-sperm Interaction was Detected using FM4-64FX Dye and 3D SR-SIM.....	54
3.7	Co-localization Analysis of OVS and PMCA4a on Sperm.....	55
3.8	Analyze OVS-sperm Interaction, using TEM.....	60
3.9	CD9 and α v Subunit of $\alpha\beta$ 3 Integrin are Present on OVS and on the Membrane of Capacitated Caudal Sperm.....	63
3.10	Effect of the Adhesion Peptide Arg-Gly-Asp (RGD) for the ligand of $\alpha\beta$ 3 on OVS-sperm Fusion.....	64
3.11	Effect of Integrin Ligands, Vitronectin (VN) and Fibronectin (FN), on OVS-sperm Fusion.....	67
3.12	Fertility of <i>Pmca4</i> KO Female Mice is Unaffected.....	74
3.13	Upregulation of PMCA1 Protein in <i>Pmca4</i> ^{-/-} Oviduct.....	74
3.14	Detection of Mg ²⁺ -dependent Ca ²⁺ -ATPase Activity in Murine OVS and in <i>Pmca4</i> Null Sperm before and after Co-incubation with OVS....	74
3.15	Calcium Handling in <i>Pmca4</i> Null Sperm.....	75
3.16	Effect of Co-incubation of OVS on Progressive Motility of <i>Pmca4</i> KO Sperm.....	75
4	DISCUSSION.....	83
4.1	Expression and Secretion of PMCA4a in the Murine Female Reproductive Tract.....	83
4.2	Isolation, Identification and Characterization of Exosomes/microvesicles in the Oviductal Luminal Fluid.....	85
4.3	Transport of PMCA4a from the Female Reproductive Luminal Fluids to Sperm During Capacitation.....	86
4.4	Evidence for the Fusion of OVS and Sperm Membranes.....	87
4.5	Delivery of Transmembrane Proteins to the Sperm Surface via Membrane Fusion.....	91
4.6	The Functional Impact of Delivery Oviductosomal PMCA4 <i>in Vitro</i> to <i>Pmca4</i> null Sperm.....	92
4.7	Conclusions.....	96
4.8	Future Studies.....	97
	REFERENCES.....	98
Appendix		
A	MANUSCRIPTS.....	109
B	GLOSSARY OF ABBREVIATIONS.....	110
C	INSTITUTIONAL ANIMAL CARE AND USE COMMITTEE (IACUC) APPROVAL.....	112
D	PLOS JOURNALS STATEMENT OF AUTHORS' RIGHTS.....	116

LIST OF TABLES

Table 1.	Litter sizes born to mating pairs of different genotypes, all on FVB/N background.	76
Table 2.	Percentage of <i>Pmca4</i> KO Sperm with progressive motility after co-incubation with WT OVS for different time periods	82

LIST OF FIGURES

Figure 1.	Diagram representing the three distinct phases of sperm maturation..	2
Figure 2.	Diagrams representing the two routes of exosome formation.....	5
Figure 3.	Schematic representation of the three segments of the oviduct: the sperm reservoir, isthmus, and ampulla.....	7
Figure 4.	A schematic representation of the PMCA4 structure.....	11
Figure 5.	Semi-quantitative analysis of <i>Pmca4a, b</i> mRNA via RT-PCR in the murine female reproductive tract	36
Figure 6.	Expression of PMCA4a in mouse vaginal, uterine, and oviductal tissues following superovulation.....	39
Figure 7.	Indirect immunofluorescence of PMCA4a in the murine endometrium of the uterus during the estrus cycle.....	40
Figure 8.	Indirect immunofluorescence of PMCA4a in the murine myometrium of the uterus during the estrus cycle.....	41
Figure 9.	Detection of PMCA4a in reproductive luminal fluids and its acquisition on caudal sperm	47
Figure 10.	Characterization of membranous vesicles in OLF.....	49
Figure 11.	Electron micrographs of mouse OVS.....	50
Figure 12.	Immunodetection of PMCA4a in OVS and uterosomes	52
Figure 13.	PMCA4a uptake by caudal sperm via incubation in OVS reconstituted in PBS.....	53
Figure 14.	Co-incubation assays detect the transfer of membrane constituents from FM4-64FX-labeled OVS to the sperm membrane..	56

Figure 15.	Co-localization of FM4-64FX-labeled OVS and PMCA4a on WT and <i>Pmca4</i> KO sperm membrane following co-incubation, as detected in both wide-field fluorescence (a,c,e) and 3D SR-SIM (b,d,f)..	58
Figure 16.	FM4-64FX-labeled OVS carry and deliver different cargoes to sperm following co-incubation, using PMCA4a as an example.....	59
Figure 17.	FM4-64FX-labeled OVS and immunogold labeling in OVS fused with WT sperm membrane provide evidence for involvement of a fusogenic mechanism in the transfer of PMCA4..	62
Figure 18.	Localization of CD9 and the α_v subunit of $\alpha_v\beta_3$ integrin on sperm and OVS.....	66
Figure 19.	Effect of RGD peptide on mouse OVS-sperm in vitro fusion (via co-incubation assays), as assessed in capacitated (CAP) sperm and visualized by 3D SR-SIM.....	69
Figure 20.	Effect of fibronectin (FN) and vitronectin (VN) on mouse OVS-sperm in vitro fusion (via co-incubation assays), as assessed in sperm and visualized by 3D SR-SIM.....	71
Figure 21.	Schematic model showing molecular interactions in OVS-sperm fusion.....	73
Figure 22.	Distribution of the mean litter sizes from matings of males and females with different <i>Pmca4</i> genotypes.	76
Figure 23.	Western blot analysis of PMCA1 protein expression in oviducts (OVD) from <i>Pmca4</i> KO and WT females.....	77
Figure 24.	Determination of Mg^{2+} -dependent Ca^{2+} -ATPase activity in OVS and sperm and after their co-incubation and inhibition of mitochondrial activity with oligomycin.....	79
Figure 25.	$[Ca^{2+}]_i$ changes in Fluo-4 loaded, washed and selected sperm.	81
Figure 26.	Progressive motility rates of <i>Pmca4</i> KO sperm following co-incubation with OVS for different periods of time.	82

ABSTRACT

Plasma Membrane Calcium ATPase 4, PMCA4, is the major Ca^{2+} efflux pump in murine sperm where its deletion leads to a severe loss of hyperactivated motility and to male infertility. Here I show that *Pmca4* mRNA, 4a and 4b variants, and PMCA4a protein are highly expressed in the female reproductive luminal fluids (LF) during estrus. Transmission electron microscopy (TEM) of the pellet recovered from ultracentrifugation of the oviductal LF revealed membrane vesicles with exosomal/microvesicle orientation, size, and shape, and with the characteristic CD9 exosomal biomarker. Thus, I dubbed these exosomes/microvesicles “oviductosomes” (OVS), to which PMCA4 was immunolocalized. Co-incubation of sperm with OVS resulted in up to a ~3-fold increase of sperm PMCA4a. To determine the mechanism of delivery of PMCA4 via OVS, I defined an experimental approach for the assessment of OVS-sperm interaction at a nanoscale level, using a lipophilic dye and 3D SR-SIM. Co-incubation assays detected fusion of pre-labeled OVS with sperm, primarily over the head and midpiece. Fusion was confirmed by TEM, showing immunogold particles in OVS, and fusion stalks on sperm membrane. Both OVS and sperm carry α v-subunit of α v β 3 integrin. In capacitated and acrosome-reacted sperm, fusion was significantly inhibited by blocking integrin-ligand interactions via exogenous ligands, vitronectin and fibronectin, and their Arg-Gly-Asp recognition motif. To examine the potential impact of transfer of OVS-derived PMCA4 on sperm, Ca^{2+} -ATPase activity, Ca^{2+} loading, and motility assays were performed. Following *in*

in vitro co-incubation of *Pmca4* KO sperm with OVS from WT females, the Ca²⁺-ATPase activity was significantly increased, intracellular Ca²⁺ levels significantly decreased, and progressive motility rates significantly increased. Thus, the results are consistent with the acquisition of oviductal PMCA4 *in vivo* to meet the demand of an increased requirement for Ca²⁺ efflux in sperm during their storage, capacitation, and the acrosome-reaction, and to maintain sperm viability. Knowledge of OVS, identified for the first time, and their transfer of oviductal PMCA4 (and likely other fertility-modulating proteins) to sperm just prior to fertilization, provides new insights into molecular interactions at the fertilization site. This has important implications for increasing the fertilizing competence of sperm in the *in vitro* fertilization clinic.

Chapter 1

INTRODUCTION

1.1 Spermatozoa: Their Journey during Maturation

Testicular spermatozoa are incompetent to fertilize an oocyte. Their fertilizing ability is acquired during transit in three distinctive stages of maturation: 1) testicular maturation, 2) epididymal maturation, and 3), capacitation in the female (**Fig. 1**) (Reid et al., 2011).

1.1.1 Testicular maturation

Spermatogenesis is an intricate biological process that occurs in the testis and is responsible for the transformation of spermatogonia into spermatozoa, over an extended period of time, 40 days in mice (Hess and de Franca, 2008). During this process, spherical haploid spermatids undergo an intense morphological transformation and are converted into highly compacted spermatozoa consisting of three specialized regions: 1) a head including the acrosome which contains a matrix of enzymes, nucleus (with highly condensed chromatin in which histones are replaced with protamines for DNA compaction), cytoskeletal structure 2) midpiece, which contains approximately 100 mitochondria; and 3) a principal piece which contains a dense cytoskeleton that is used for locomotion (Gadella and Luna, 2014). The sperm contain very little cytoplasm with no organelles such as endoplasmic reticulum, ribosomes, Golgi complex, lysosomes (Jones, 1989; Cooper, 1995; Jones, 1998). Therefore, sperm are transcriptionally silent.

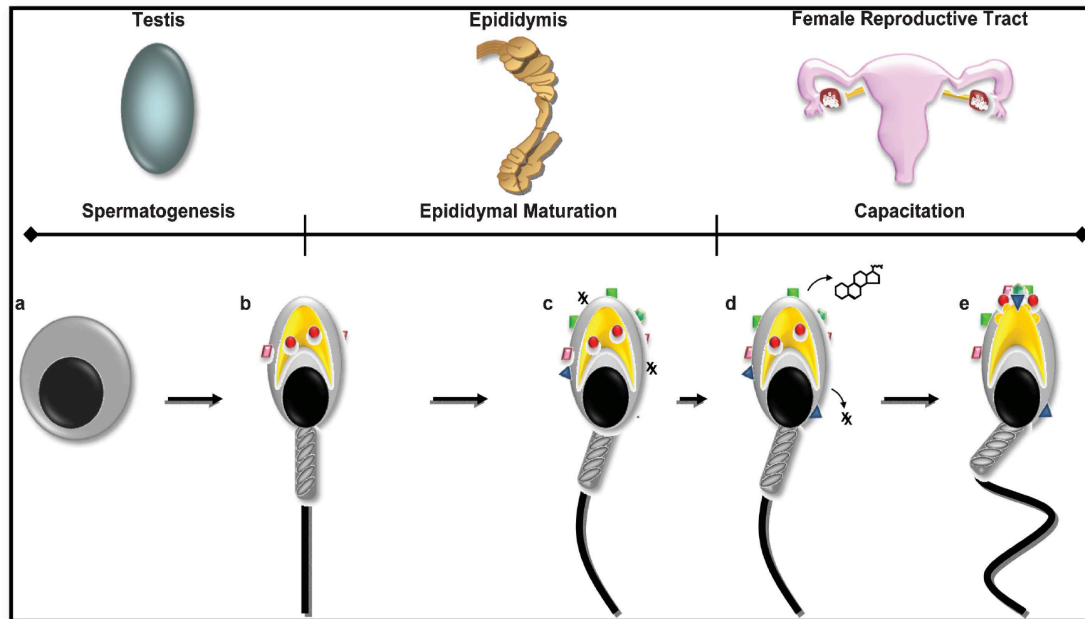


Figure 1. Diagram representing the three distinct phases of sperm maturation.

Testicular maturation (spermatogenesis), involves the sequence of cell division and morphological alterations that convert the round spermatids (**a**) into morphological mature sperm (**b**), this includes DNA condensation, removing of the cytosol organelles such as endoplasmic reticulum, Golgi complexes, ribosomes, lysosomes, the formation of the flagellum, and the concentration of mitochondria at the midpiece. Following testicular maturation, spermatozoa then undergo a second stage of maturation, epididymal maturation in which sperm are intimately associated with the luminal fluid which allows them to interact with a large number of proteins that are necessary for their maturation (**c**). They also acquire decapacitated factors that prevent sperm from undergoing premature capacitation. The final stage of sperm maturation, namely, capacitation, occurs during their transit in the female reproductive tract. At the beginning of capacitation, sperm undergo membrane surface modifications which include the loss of the inhibitory molecules: cholesterol (via efflux) and decapacitated factors (**d**). Following the initial step of capacitation, there is uptake of necessary proteins, activation of key signaling cascades, and the formation of membrane rafts which will lead to their gain of hyperactivated motility (**e**) and the competence to fertilize an oocyte. Adapted from (Reid et al., 2011).

1.1.2 Epididymal maturation

1.1.2.1 Epididymis

When sperm leave the testis they are functionally incompetent, although morphologically mature. They lack both the capacity for forward progressive motility and for binding to the zona pellucida of the oocyte (Jones, 1989; Cooper, 1995; Jones, 1998; Reid et al., 2011). Functional maturity is gained as they traverse the epididymis, a long convoluted tubule with a secretory epithelium. Sperm are bathed in complex luminal fluids that provide them with a large number of essential molecules such as proteins (Cooper, 1998; Jones, 1998). The epididymal duct is subdivided into three anatomically distinguishable regions: the caput (head), the corpus (body), and the cauda (tail) (Caballero et al., 2010). Our current understanding of the epididymis is that it is more than just a highly convoluted tube but a complex of individual cell types that contribute to the formation of a unique luminal fluid microenvironment. This microenvironment is critically important for sperm maturation: the acquisition of motility and fertilizing ability since they remain translationally silent after leaving the testis (Reid et al., 2011). Also, the acidic epididymal microenvironment is critically important to keep sperm in a quiescent state. This will conserve energy since the motor proteins (dynein ATPases), which are responsible for the flagellum movement, are pH-dependent (Christen et al., 1983; Giroux-Widemann et al., 1991).

1.1.2.2 Epididymal luminal fluids- epididymosomes

Although the precise mechanism(s) by which sperm maturation in the epididymis occurs is/are unknown, the secretion in the luminal fluid of a vast number of glycosyl phosphatidyl inositol (GPI)-linked proteins has been associated with their maturation (Kirchhoff and Hale, 1996). In addition to GPI-linked proteins from the epididymal luminal fluid (ELF), sperm also acquire molecules such as decapacitation factors to prevent them from undergoing premature capacitation. Adeoya-Osiguwa and Fraser (1996) reported that decapacitation factors prevent capacitation by stimulating the Ca^{2+} -dependent ATPase activity. Significantly, this latter event results in lowering sperm intracellular calcium concentration (Adeoya-Osiguwa and Fraser, 1996).

Most epithelial cells contain and secrete extracellular vesicles (EVs), exosomes (<100 nm in diameter) or microvesicles (100-1000 nm in diameter) (Lakkaraju and Rodriguez-Boulan, 2008; Schorey and Bhatnagar, 2008; Simpson et al., 2008; Simons and Raposo, 2009). EVs are spherical structures composed of a lipid bilayer which contains proteins and polysaccharides (Tan et al., 2013). The interior contains various bioactive molecules, including RNAs, proteins and mRNA, miRNA. Although, EVs have protein contents that are similar to those from the cells from which they are secreted (Raimondo et al., 2011), the composition of the contents may change after their release from the cell (Yoon et al., 2014). EVs have been shown to engage in diverse biological functions: in cell-cell communication, tumor promotion, immune regulation, and spreading prion proteins (Zhou et al., 2012; Ritchie et al., 2013; Yamashita et al., 2013).

The secretion of these exosomes occurs through two distinct processes: A) an apocrine pathway in which blebs dislodge from the apical membrane of the epithelium and enter the lumen, where they release the vesicles, e.g. epididymosomes (**Fig. 2A**) (Hermo and Jacks, 2002; Caballero et al., 2010) and B) by a pathway involving the multivesicular bodies (MVBs) whose outer membrane fuse with the apical membrane of epithelial cells to release their components of exosomes (**Fig. 2B**) (They et al., 2002; They et al., 2009; Turturici et al., 2014).

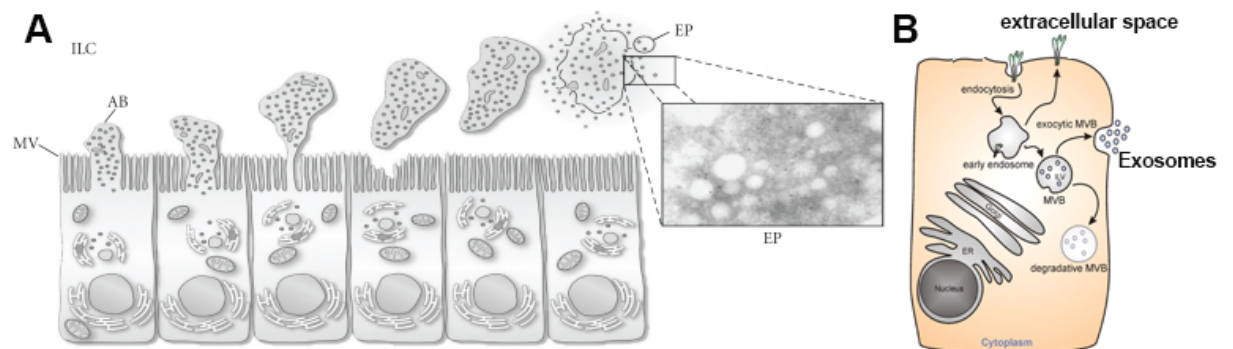


Figure 2. Diagrams representing the two routes of exosome formation. (A) Apocrine secretion, such as epididymal epithelium secretion of epididymosomes (Pisitkun et al.). ILC, intraluminal compartment; MV, microvilli; AB, apical bleb; EP, epididymosomes. Adapted from (Caballero et al., 2011). **(B)** Multivesicular bodies (MVBs). Adapted from (Turturici et al., 2014).

Exosomes can be characterized based on their a) size which is < 100 nm in diameter whereas microvesicles are larger (100 nm to 1000 nm); b) morphology which is saucer-shaped; c) the presence of an adhesion molecule biomarker, CD9, on their surface; d) their orientation (cytoplasmic-side inward). (They et al., 2002; Pisitkun et

al., 2004; They et al., 2009; Masyuk et al., 2010). Whatever their origin, they are likely to function as signaling nanovesicles and to be involved in cell-cell communication and intracellular regulation (Masyuk et al., 2010).

Exosomes such as epididymosomes have been shown to carry membrane proteins that are then transferred to the sperm plasma membrane (Frenette and Sullivan, 2001; Saez et al., 2003). Recently, we showed for the first time that murine epididymosomes carry PMCA4a, a 10-pass transmembrane protein. As expected, the soluble fraction of the ELF was devoid of the protein (Patel et al., 2013). Importantly, we found that incubation of sperm in unfractionated ELF increased sperm PMCA4a levels by ~2-fold after 30 min of co-incubation, consistent with the role of epididymosomes in PMCA4a transport (Patel et al., 2013).

1.1.3 Final maturation in the female reproductive tract- capacitation

Capacitation which occurs in the female reproductive tract is the final maturational process that mammalian sperm undergo before they are competent to effect fertilization. After their journey in the uterus they meet the oocyte at the fertilization site in the ampulla or ampullary-isthmic junction, AIJ, (Rodriguez-Martinez, 2007). Prior to ovulation, sperm are stored in the sperm reservoir, the most distal segment of the oviduct, where they adhere to the oviductal epithelial cells by lectin containing proteins that are present on the sperm membrane which bind to fucose residues present on the oviductal epithelium (Coy et al., 2012). Upon ovulation, bound sperm are released from the oviductal reservoir by the massive secretion of

fluid from the oviductal epithelial cells (**Fig. 3**) and the induction of the vigorous hyperactivated motility that is characterized by high amplitude and asymmetric flagellar beating (Coy et al., 2012).

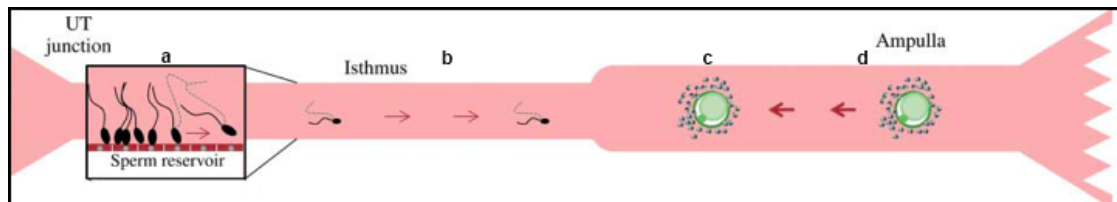


Figure 3. Schematic representation of the three segments of the oviduct: the sperm reservoir, isthmus, and ampulla. (a) At the sperm reservoir, sperm interact with oviductal epithelium and then undergo hyperactivation motility where they can free themselves from epithelial curvature, **(b)** move to the fertilization site (ampullary-isthmic junction), attach to and cross through the cumulus cells **(c)**, and **(d)** penetrate the zona pellucida. Adapted from (Coy et al., 2012).

An increase in intracellular Ca^{2+} concentration $[\text{Ca}^{2+}]_i$ levels is essential and necessary for both hyperactivated sperm motility and the induction of the acrosome reaction (de Lamirande et al., 1997). These three mechanisms (capacitation, hyperactivation, and acrosomes reaction) need to be precisely regulated to maintain sperm viability and return their cytosolic Ca^{2+} concentration to the resting level (50-100 nM) which is 4-orders of magnitude lower than the extracellular Ca^{2+} concentration (Herrick et al., 2005). There are three principal mechanisms by which murine sperm regulate their intracellular Ca^{2+} concentration: The Na^+ - Ca^{2+} exchanger (NCX) over the outer-acrosomal membrane that effluxes sequestered Ca^{2+} within intercellular stores; the mitochondrial calcium uniporter (MCU); and the plasma membrane Ca^{2+} ATPase pump (Wennemuth et al., 2003).

1.2 The Plasma Membrane Calcium ATPase 4 (PMCA4)

PMCA4, a member of the P-type family that transports ions against a concentration gradient using ATP, is an ~133 kDa cell-surface protein with 10 transmembrane domains (Strehler and Zacharias, 2001). PMCA4s are characterized by the formation of a phosphorylated (P) intermediate (which gives the family its name) during their ion transport cycle (Pedersen and Carafoli, 1987) (**Fig. 4**). The reaction cycle is characterized by two major conformational states driven by ATP hydrolysis: Enzyme 1 (E1) and enzyme 2 (E2); each stage has a different affinity for the Ca^{2+} binding site (Albers, 1967; Post et al., 1969). PMCA4s actively regulate $[\text{Ca}^{2+}]_i$ concentration and also participate in regulating intracellular pH (pH_i), since protons (H^+) are counter-transported for Ca^{2+} during the pumping mechanism (Poburko et al., 2011).

PMCA4s exist in four pumps (PMCA1-4), where PMCA4 is the major pump in murine sperm (Wennemuth et al., 2003). PMCA4 has two major splice variants 4a and 4b, and 4b is thought to play a crucial role in Ca^{2+} clearance in murine sperm (Wennemuth et al., 2003) and to be involved in signal transduction (Strehler, 2013). Of the three Ca^{2+} clearance mechanisms [NCX, MCU, and PMCA4] operative in murine sperm, PMCA4 is predominant (Wennemuth et al., 2003). It exhibits three times higher Ca^{2+} affinity and extrusion than each of the other two proteins (Wennemuth et al., 2003).

Recent studies showed that PMCA4 is synthesized in the rat (Wilhelm et al., 2008) and bovine (Brandenburger et al., 2011) epididymal epithelium. Interestingly,

bovine sperm show a progressive switch from splice variant 4b in the upper, to mainly 4a in the lower, regions of the epididymal tract (Brandenburger et al., 2011). As sperm do not engage in new mRNA transcription or protein translation, this shift has been attributed to acquisition of PMCA4a from the ELF (Brandenburger et al., 2011). The switch from 4b to 4a is physiologically relevant because sperm face a steeper Ca^{2+} efflux requirement for hyperactivated motility in the female tract and PMCA4a has a higher basal activity and is more efficient than 4b in returning Ca^{2+} to resting levels (Caride et al., 2007; Brandenburger et al., 2011). Thus it would readily meet the demands of maintaining homeostasis in conditions of high $[\text{Ca}^{2+}]_i$ during capacitation.

Deletion of *Pmca4* disrupts Ca^{2+} homeostasis and leads to loss of both progressive and hyperactivated sperm motility and ultimately to infertility (Okunade et al., 2004; Schuh et al., 2004). To our knowledge, it has not yet been reported how PMCA4 deletion results in loss of motility. However, there are at least two possible mechanisms, either of which or both may be involved. The absence of PMCA4, the major efflux pump in murine sperm, is known to cause elevated $[\text{Ca}^{2+}]_i$, resulting in Ca^{2+} overload in mitochondria (Okunade et al., 2004). This increased mitochondrial Ca^{2+} could result in collapse of the mitochondrial membrane potential and cause depletion in ATP production and sperm pH_i which would lead to decreased activity of the highly pH -dependent dynein ATPases, proteins that generate the flagellar beat (Christen et al., 1983; Giroux-Widemann et al., 1991). Decreased flagellar beat would ultimately result in loss of motility. However, this mechanism is highly unlikely as the DeLeon Lab has unpublished data showing that the mitochondrial membrane potential in *Pmca4* null sperm is undisturbed. Further, a similar finding for *Jam-A* null sperm

which demonstrate the Ca^{2+} overload in the mitochondria due to decreased PMCA4 activity has been reported (Aravindan et al., 2012). Secondly, the activation of nitric oxide synthases and oxidative stress might underlie the loss of motility. Both of the constitutive nitric oxide synthases, neuronal nitric oxide synthase (nNOS) and endothelial NOS (eNOS) are present in sperm and are rapidly activated by Ca^{2+} (Knowles and Moncada, 1994). Because PMCA4 negatively regulates the NOSs (Schuh et al., 2001; Holton et al., 2010), in its absence in *Pmca4* null sperm there would be elevated levels of nitric oxide (NO) which readily reacts with superoxide ($\text{O}_2^{\bullet-}$) to form a powerful oxidant [peroxynitrite (ONOO^-)]. Elevated levels of NO and ONOO^- in the absence of NOS regulation by PMCA4, would result in the oxidization of polyunsaturated fatty acids (PUFA) which are enriched in sperm plasma membrane, causing lipid peroxidation (Aitken, 1995; Zalata et al., 1998) which is a key mechanism in the loss of sperm motility (Hellstrom et al., 1994; Weinberg et al., 1995). DeLeon and co-workers have provided evidence supporting this second mechanism as they have documented the presence of elevated levels of NO and ONOO^- , as well as germ cell apoptosis which results from oxidative stress in *Pmca4* null sperm (Martin-DeLeon et al., *in preparation*).

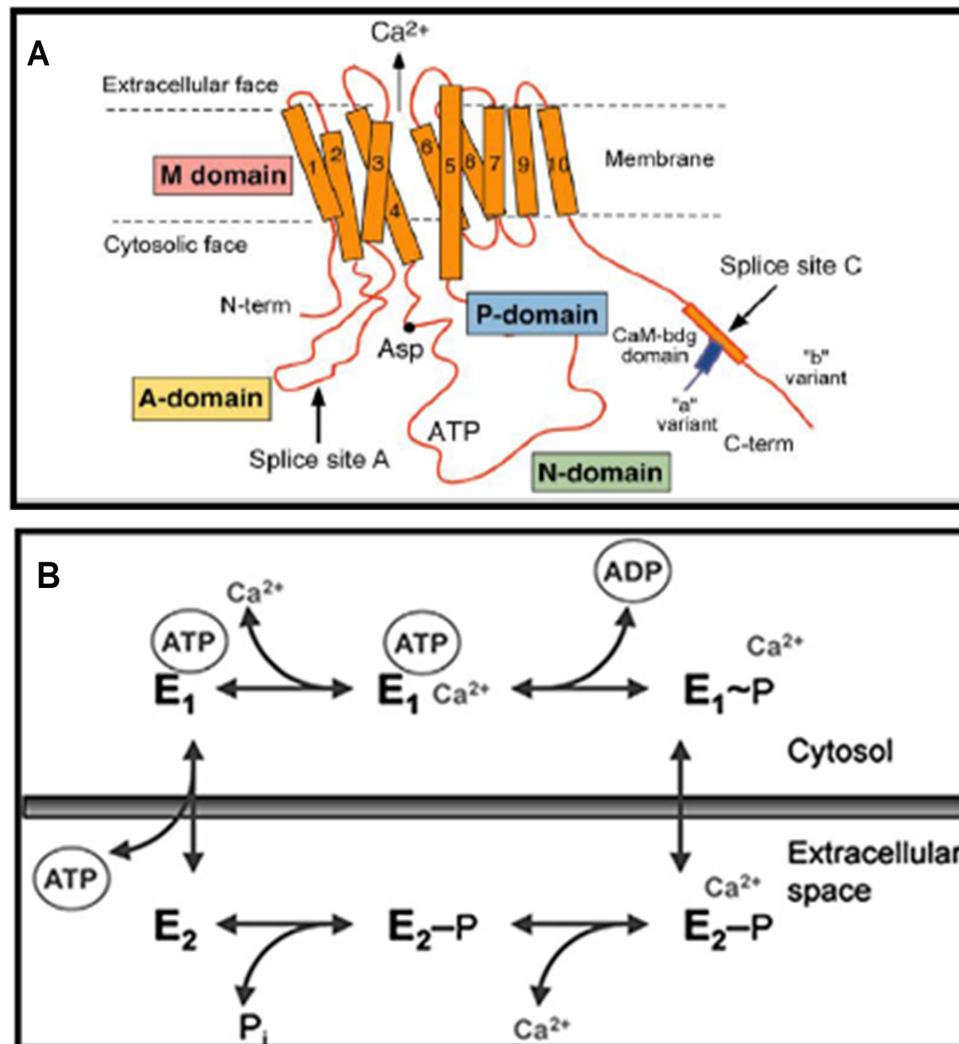


Figure 4. **A schematic representation of the PMCA4 structure (A).** PMCA has 10 membrane-spanning regions and two major cytoplasmic loops, the larger of which contains the catalytic core. Splicing at the site C results in major splice variants “a” and “b”, which differ in their C-termini due to a reading frame shift. Adapted from (Strehler, 2013). **(B)** A diagram of the Ca²⁺ transport cycle. The PMCA reaction cycle contains two main conformational states E1 and E2. Hydrolysis of one ATP molecule is responsible for transport of one Ca²⁺ ion against the Ca²⁺ concentration gradient through the plasma membrane. Adapted from (Di Leva et al., 2008).

1.3 Significance

Reduced sperm motility occurs in mice due to the absence of PMCA4 (Okunade et al., 2004; Schuh et al., 2004). Recently, we showed that *Pmca4* is also expressed in the epididymis where both PMCA4 splice variants, 4a and 4b, are secreted in the mouse epididymal luminal fluid (Patel et al., 2013). Variant 4a was shown to be transferred *in vitro* to the membrane of caudal sperm via epididymosomes (membranous vesicles), suggesting its involvement in epididymal maturation. Notably, caudal sperm from the distal epididymal region have a 5-fold increase of PMCA4a over that in caput sperm from the proximal region (Patel et al., 2013).

Since caput sperm have 2-6 times higher cytosolic calcium concentration ($[Ca^{2+}]_c$) than caudal sperm and are incapable of progressive motility (Yeung, 2002), the uptake of PMCA4a during epididymal transit may play a direct and vital role in sperm acquisition of sperm motility. It is intriguing to conceive that PMCA4a can be acquired by sperm during their transit in the female reproductive tract. In the female tract sperm may need to acquire additional PMCA4a to: a) preserve their fertility in the storage reservoir of the oviduct by avoiding premature capacitation and b) maintain viability after the demand for the high $[Ca^{2+}]_i$, required for hyperactivated motility in the ampullary isthmus junction (AIJ) (Coy et al., 2012) and for the acrosome reaction (de Lamirande et al., 1997).

During transit in both the male and female tracts and during ejaculation, the sperm plasma membrane undergoes extensive modifications in which it acquires a variety of proteins (Kirchhoff et al., 1997). To date, it is unknown how transmembrane proteins are delivered to the sperm membrane. However, the DeLeon Lab has shown that glycosyl phosphatidylinositol- (GPI)-linked proteins are acquired on the sperm membrane from both vesicular and membrane-free soluble fractions of the epididymal luminal fluid (ELF) via hydrophobic interactions with the outer leaflet of the lipid bilayer on sperm (Griffiths et al., 2008a; Griffiths et al., 2009). Since transmembrane proteins, such as PMCA4, are unlikely to be acquired via hydrophobic interactions, it is highly likely that they are acquired by a mechanism involving the fusion of OVS with the sperm membrane. **Thus the following central hypotheses were advanced:**

1.4 Hypotheses and Specific Aims

1.4.1 Hypothesis 1: Plasma membrane Ca^{2+} -ATPase 4a (PMCA4a) is expressed and secreted in the female reproductive tract where it can be acquired on the sperm surface during sperm transit and storage (maturation) in the oviduct.

1.4.1.1 Specific Aim 1: Determine if PMCA4a is expressed and secreted in the female luminal fluids (FLF) during the estrus cycle and if sperm can acquire PMCA4a from the fluids.

1.4.1.2 Specific Aim 2: Isolate and characterize membranous vesicles from female reproductive fluids and immunolocalize PMCA4a on them.

1.4.1.3 Specific Aim 3: Determine if oviductosomes (OVS) in the female luminal fluid are necessary and sufficient for the transfer of PMCA4a to the sperm.

1.4.2 Hypothesis 2: A fusogenic mechanism is involved in the delivery of PMCA4 to the sperm membrane via OVS.

1.4.2.1 Specific Aim 1: Visualize the interaction between FM4-64FX pre-labeled OVS with the sperm membrane, using 3D SR-SIM.

1.4.2.2 Specific Aim 2: Analyze OVS-sperm interaction, using TEM and immunogold labeling of PMCA4, after co-incubation for the maximal period used in 3D SR-SIM and indirect immunofluorescence.

- 1.4.2.3 Specific Aim 3:** Investigate the role of tetraspanin and/or αV integrin in OVS-sperm fusion using labeled exosomes/microvesicles and blocking of receptor-ligand interactions.
- 1.4.3 Hypothesis 3:** PMCA4, carried by OVS and delivered to sperm, plays an important and crucial role in the regulation of proper Ca^{2+} handling during sperm capacitation which requires high levels of Ca^{2+} .
- 1.4.3.1 Specific Aim 1:** Assess litter sizes of *Pmca4* nulls, Hets and WT females mated to WT and Het males to determine the impact of PMCA4 transfer from oviductosomes to sperm *in vivo*.
- 1.4.3.2 Specific Aim 2:** Evaluate the impact of delivery of PMCA4 *in vitro* to *Pmca4* KO sperm by assessing Ca^{2+} -ATPase activity, Ca^{2+} handling, and progressive sperm motility following PMCA4 delivery via OVS.

Chapter 2

MATERIALS AND METHODS

2.1 Mice and Reagents

Sexually mature 4-12 week old female and 10-12 week old male mice (FVB/N strain; Harlan, Indianapolis, IN) were used throughout the investigation. In addition to these wild-type (WT) mice, *Pmca4* null mice were used to provide caudal sperm for the immunofluorescence analysis of the uptake of PMCA4-carrying OVS on sperm and their impact sperm function. These mutant mice were a generous gift from Dr. Gary Shull in whose laboratory they were generated. Breeding and genotyping of these mice were described previously (Okunade et al., 2004). Studies were approved by the Institutional Animal Care and Use Committee at the University of Delaware and were in agreement with the Guide for the Care and Use of Laboratory Animals published by the National Research Council of the National Academies, 8th ed., Washington, D.C. (publication 85-23, revised 2011). All enzymes and chemicals were purchased from Fisher Scientific Co. (Malvern, PA), Sigma (St. Louis, MO) or Invitrogen (Carlsbad, CA), unless otherwise specified.

2.2 Antibodies and Fluorescent Dyes

Rabbit polyclonal antibodies against peptides specific for bovine PMCA4a have been generated and previously validated (Filoteo et al., 1997; Brandenburger et al., 2011). Sequence analysis suggested a high probability of cross-reactivity with mouse PMCA4a, and studies in mice revealed the specificity of the antibodies for this species (Patel et al., 2013). Thus these antibodies were used in Western blots, immunofluorescence, immunoelectron microscopy, and flow cytometric studies, all of which further demonstrated their competence to specifically detect mouse PMCA4a. Goat polyclonal anti-PMCA4 antibody, which detects isoforms 4a and 4b, (SC-22080) (Patel et al., 2013), rat monoclonal anti-CD9 antibody (SC-18869) and mouse monoclonal anti-HSC70 antibody (sc-7298) were purchased from Santa Cruz Biotechnology, Dallas, TX (Al-Dossary et al., 2013). Rabbit polyclonal anti- α v integrin (AB1930) was from Millipore, Temecula, CA. Rabbit monoclonal anti- β -actin antibody (4970) was obtained from Cell Signaling (Boston, MA). Rabbit monoclonal anti-PMCA1 antibody (ab190355) was obtained from Abcam (Cambridge, MA). Alexa Fluor 405 donkey anti-rabbit (AB175651) was from Abcam, Cambridge, MA. FM4-64FX (F34653) was purchased from Life Technologies, Grand Island, NY. DRAQ5TM (DR05500) was purchased from Biostatus Limited, Leicestershire, United Kingdom. Fluoro-Gel (17985-10) and Fluoro-Gel II with DAPI (17985-50) were purchased from Electron microscope sciences, Hatfield, PA. Fluo-4/AM (Cat. # F-14201) purchased from Molecular Probes, Eugene, OR.

2.3 Analysis of Physiological Estrus Cycle

Eight to 12 week- old virgin female mice were used in this investigation. Females were categorized by the stages of estrus cycle based on the proportion of different cell types observed in the vaginal secretion (Goldman et al., 2007). Uterine tissues were collected from females at diestrus, proestrus, estrus, and metestrus. Tissues were then processed for indirect immunofluorescence and Western blot analysis as described below.

2.4 Superovulated Females

Four to 6-week-old C57BL/6 female mice were induced into estrus by sequential administration of pregnant mare serum gonadotropin (7.5 i.u.) and human chorionic gonadotropin (7.5 i.u.) spaced 48 h apart. Reproductive tissues (uterus, vagina, oviduct) were removed, after sacrificing females 13.5-14 h following the last hormonal injection.

2.5 Preparation of Murine Female Reproductive Tissues

Vaginas, uteri and oviducts were removed immediately after sacrifice and frozen at -80°C for subsequent expression analysis, or they were flushed with PBS to remove the LF and immediately frozen at -80°C.

2.6 Collection of Luminal Fluids in Naturally Cycling Females and from Males

Reproductive luminal fluids were collected from 4 females in proestrus and estrus (combined), and from 4 in metestrus and diestrus (combined), as previously described (Griffiths et al., 2008a; Griffiths et al., 2009). Briefly, vaginas, uterine horns and oviducts were flushed with PBS plus protease inhibitors by inserting a 26-gauge needle attached to a 1 ml syringe into the lumen and fluids were collected. Centrifugation at 3,500 x g for 10 min was used to exclude tissue fragment and cells and to clarify the fluids. Caudal luminal fluids, used as controls, were collected from the epididymal caudae pooled from 2-3 WT ICR mice, using a method that was previously described (Griffiths et al., 2009; Patel et al., 2013).

2.7 Collection of Vaginal, Uterine and Oviductal Luminal Fluids from Females after Hormonal Induction of Estrus

Vaginal luminal fluid (VLF), uterine luminal fluid (ULF) and oviductal luminal fluid (OLF) were obtained from 6-8 superovulated female mice per experiment. The methodology of collecting the fluid is similar to described above (Griffiths et al., 2009).

2.8 OVS Preparation

Clarified OLF, was collected from 10 superovulated females as described above. To fractionate the OLF we used a methodology similar to previously described

(Al-Dossary et al., 2013). Briefly, the clarified FLFs (OLF, ULF, and VLF combined) were subjected to ultracentrifugation at 120,000 x g for 2 h, at 4°C using a Beckman Optima 2-70 k ultracentrifuge and a Ti60 rotor. The resulting pellets (OVS), which contain both exosomes and microvesicles, were re-suspended in homogenization buffer and protease inhibitor, for Western blot analysis, or in PBS to a final concentration of 1.3 mg/ml proteins to be used for co-incubation with sperm or transmission electron microscopy (TEM).

2.9 Preparation of Capacitated and Acrosome-reacted Sperm

Mouse spermatozoa were harvested from the caudal epididymides of 2 sexually mature males per experiment, by mincing the caudae in warm Human Tubal Fluid (HTF, Cat. # 2002, *InVitroCare*, Frederick, MD) as described earlier (Chen et al., 2006) and kept at 37°C for 10 min to allow sperm to swim out of the tissue. After gravity settling of the tissues the supernatant was collected. Next, 3.4×10^7 sperm were aliquoted into 1.5-ml tubes (final concentration, 8.5×10^5 sperm) and 100 μ l of capacitation medium (HTF) for 90 min at 37°C. Calcium ionophore A23187 was then added at a final concentration of 20 μ M for 60 min of incubation at 37°C to induce the acrosome reaction (AR) as previously described (Deng et al., 1999).

2.10 Total RNA Isolation and Reverse Transcriptase (RT)-PCR

Female reproductive tissues (vagina, uterus, oviduct) were collected from two virgin females after superovulation, and total RNAs were extracted using RNeasy Mini Kit (Qiagen, Valencia, CA) according to the manufacturer's directions and RNA samples were further treated with DNAase (Turbo DNA-Free, Ambion Inc., Austin, TX). Total RNA (1µg) was used to synthesize cDNA using the iScript™ cDNA synthesis kit (BioRad, Hercules, CA). Samples without the addition of reverse transcriptase served as controls. To amplify cDNA samples, PCR reactions (25 µl final volume) were performed with 2 µl cDNA for 30 cycles (ABI Veriti Thermocycler), using *Pmca4a* and *4b* primers as follows: forward primer sequence was 5'- GGA CGA GAT TGA CCT TGC CG -3' and the reverse 5'- CAC CAT CCA ACA GGA GCA CAC T-3'. PCR amplification was performed for 35 cycles at denaturation for 30 sec at 96°C, annealing for 30 sec at 59°C, extension for 1 min at 72°C, and a final extension of 5 min at 72°C. *Gapdh* was used as an internal control, Using commercial mouse *Gapdh* primers (Qiagen, Valencia, CA), PCR amplification was performed for 34 cycles at denaturation for 10 sec at 95°C, annealing for 30 sec at 55°C, extension for 90 sec at 72°C, and a final extension of 10 min at 72°C. The total RNA extracted from testis was used as positive control. RT-PCR products (10 µl) were run on 2% Nusieve agarose gel in TAE (40 mM Tris-acetate, 2 mM EDTA, pH 8.5) containing ethidium bromide (10 µg/ml), along with a 100 bp ladder (Invitrogen).

2.11 Indirect Immunofluorescence Staining and Confocal Analysis

2.11.1 Female reproductive tissues

Vaginal, uterine, and oviductal tissues were collected from superovulated females and immediately embedded in optimum cutting temperature media (OCT) (Tissue Tek, Torrance, California) and frozen at -80°C, or were frozen immediately after flushing to remove the luminal fluids. Cryostat sections (20 µm) were made and kept in -80°C until processing. Slides were fixed in 1:1 acetone:methanol pre-chilled for 20 min at -20°C and then allowed to air-dry for 10 min before being placed in protein blocker [1% bovine serum albumin (BSA) in PBS] for 1-2 h at RT. They were then incubated overnight at 4°C with the anti-PMCA4a primary antibody diluted at 1:50 in blocking solution, or with PBS or rabbit IgG for the negative controls, followed by washing with PBS (2X, 20 min). Sections were then incubated for 1h at RT with Alexa Fluor 568-conjugated goat anti-rabbit IgG (Molecular Probes, Eugene Oregon, 1:200) containing 1:2000 Draq-5 as a nuclear stain (Biostatus Limited, Leicestershire, United Kingdom), followed by (2X, 20 min) washing with PBS. Finally, the samples were mounted with mounting media and cover-slipped. Slides were visualized using a Zeiss LSM780 confocal microscope (Carl Zeiss, Inc, Gottingen, Germany) using a plan-Apochromatic 20x objective.

2.11.2 Sperm suspension

Immunofluorescence staining was performed as previously described (Reese et al., 2010; Modelski et al., 2014). Briefly, capacitated sperm were fixed with 4%

paraformaldehyde diluted in PBS (Cat. #15710, Electron Microscopy Sciences, Hatfield, PA) for 30 min. After (3x, 5 min) washes in PBS, they were permeabilized with 0.1% Triton X-100 in PBS. Then they were washed (3x, 5 min) in PBS, blocked for 30 min in 2% BSA in PBS and then incubated with the primary antibodies (rat anti-CD9 or rabbit anti- α v integrin, 1:200, 1 h, overnight). Subsequently, they were treated with the appropriate secondary antibodies (1:500 dilution, Alexa Fluor 488 anti-rat or Alexa Fluor 568 anti-rabbit, respectively) for 1 h at RT, and washed (4x, 5 min) in PBS and suspensions placed on slides. Following mounting with fluoro-Gel II with DAPI, cells were imaged, using a Zeiss LSM 780 confocal microscope. Controls were prepared by replacing primary antibody with the appropriate IgG isotype.

2.12 SDS-PAGE and Western Blot Analysis

Preparation of protein extracts from vagina, uterus, and oviduct was performed as described previously (Zhang and Martin-DeLeon, 2003), using caudal sperm as a positive control. Total protein concentration in the lysates was determined using the bicinchoninic acid protein assay Kit (Pierce), according to the manufacturer's protocol. Samples for electrophoresis were diluted in 2x Laemmli sample buffer with DTT (final concentration 100 mM) and urea (125 mg/ml) and incubated for 10 min at 37°C. Twenty and 40 μ g of proteins from tissues and fluids, respectively, were loaded per lane on 10% polyacrylamide gels and transferred onto a nitrocellulose membrane (Amersham Biosciences). Western blotting was performed with the WesternBreeze Chemiluminescent Immunodetection Kit (Invitrogen) according to the manufacturer's instructions. Blots were blocked for 1h at RT and incubated in rabbit polyclonal anti-

PMCA4a primary antibody (1: 500), rat monoclonal anti-CD9 primary antibody (1:1000), rabbit polyclonal anti- α v integrin primary antibody (1: 500), or rabbit monoclonal PMCA1 primary antibody (1: 2000) overnight at 4°C. Non-specific binding of antibody was removed using 5x washes of TBST (20 mM Tris, pH 8.0, containing 150 mM NaCl and 0.5% Tween 20) before incubation in the alkaline phosphatase (AP)- conjugated anti-rabbit IgG (Invitrogen, diluted 1:2000) or AP-conjugated anti-rat IgG (Sigma-Aldrich, diluted 1:32,000) for 1 h at 4°C. The membrane was again washed (6x, 15 min) using TBST before chemiluminescence was detected by using the ECL kit (Bio-Rad, Hercules, CA). The membrane was re-probed with HSC70 or β -actin antibody which was used as internal loading control and for normalization.

2.13 Analysis of *in vitro* Sperm Uptake of PMCA4a from Female Luminal Fluids (FLF)

In Vitro sperm uptake assay of PMCA4a was similar to that previously described from our lab (Chen et al., 2006; Griffiths et al., 2008a; Griffiths et al., 2009; Patel et al., 2013). Briefly, caudal sperm were incubated in exosomes or unfractionated FLF (combined VFL, OFL and ULF), recovered as described above in PBS supplemented with 200 μ M zinc acetate and protease inhibitor, pH 7.0. This PBS-zinc acetate solution was used for incubating equal aliquots of control sperm samples. After co-incubation of sperm and FLF for periods of 2-3 h at 37°C, control and test samples were washed (3X, collected with centrifugation at 500 x g for 15 min) using PBS with 200 μ M zinc acetate. They were then fixed with 1.5%

paraformaldehyde for 1 hr at RT, washed (3X, 15 min) with PBS and then permeabilized with 0.1% Triton X-100 for 10 min at RT. After washing cells with blocking buffer (2% BSA in PBS) they were incubated in blocking buffer for 30 min at RT. Permeabilized cells were then incubated in anti-PMCA4a primary antibody (1:200 dilution in blocking solution, applied to the cells at 4°C, for 1h), followed by washing (3X, 15 min) with PBS. Alexa Fluor 488-conjugated donkey anti-rabbit IgG (Molecular Probes, Eugene Oregon) diluted 1:200 in blocking solution was used as a secondary antibody in which cells were incubated at RT for 30 min in the dark, followed by washing (3X, 20 min) with PBS. Stained sperm were analyzed by flow cytometry on a FACSCalibur or a FACS AriaTM II (BD Sciences, San Jose, CA), equipped with an argon laser at 488 nm excitation. Analysis was performed using standard protocols and quantification criteria to assess PMCA4a uptake by sperm.

2.14 Labeling of OVS with FM4-64-FX and Co-incubation of Pre-labeled OVS with Sperm

OVS were collected as described above and re-suspended in PBS. The incorporation of FM4-64FX, a lipophilic fluorescent dye into OVS was performed as previously described (Griffiths et al., 2008a). FM4-64FX (5 mM) was used at 1:100 dilution in the OVS suspension. The mixture was kept at 37°C overnight. Subsequently, OVS were recovered by ultracentrifugation 120,000 x g, 1h and washed in PBS. The resulting pellet was re-suspended in PBS. Fifty µg of FM4-64-FX labeled OVS was co-incubated with fresh caudal sperm (8.5×10^5 sperm/ tube) for 3 h at 37°C in HTF medium or PBS. Post-coincubation, sperm were washed (4x, 5 min) in PBS at

500 x g. The resulting pellet with sperm was used for further analysis (3D SR-SIM, TEM) as described below. Control sperm were incubated in the supernatant penultimate wash for 3 h at 37°C or directly in FM4-64FX.

2.15 3D SR-SIM Analysis of OVS-sperm Interaction

2.15.1 Co-incubation assay

Following co-incubation of FM4-64FX-labeled OVS with sperm as described above, samples were post-fixed with 4% paraformaldehyde for 30 min at RT, washed with PBS (4x, 5 min) and mounted with Fluoro-Gel II with DAPI.

2.15.2 Co-localization of OVS with PMCA4 and α v-integrin subunit

After the co-incubation of sperm with FM4-64FX pre-labeled OVS for 3 h the cells were permeabilized with 0.1% Triton X-100 for 10 min at RT. After washing the cells with blocking buffer (2% BSA in PBS) they were incubated in blocking buffer for 30 min at RT. Permeabilized cells were then incubated in rabbit anti-PMCA4a antibody or rabbit anti- α v integrin antibody (1:200 dilution in blocking solution, applied to cells at 4°C, for 1 h), followed by washing with PBS (3x for 5 min). Next, cells were incubated with the secondary antibody, Alexa Fluor 405-conjugated donkey anti-rabbit (1:200 dilution) and DRAQ5TM (1:2000 dilution) at RT for 1 h. They were then washed in PBS (4x, 5 min) and cell suspensions placed on slides which were mounted with Fluoro-Gel.

2.15.3 3D SR-SIM imaging

Images were captured with a 63x plan-Apochromat Oil immersion objective (numerical aperture of 1.4), using SR-SIM (Zeiss Elyra PSI SIM, Carl Zeiss, Inc, Germany). The FM4-64FX channel was obtained with 488 nm laser excitation and LP 655 nm emission filter. The Alexa Fluor 405 channel was obtained with 405 nm laser excitation and a BP 420-480 nm emission filter; The DAPI channel with 405 nm laser excitation of an Argon laser and band pass (BP) 420-480 nm emission filter; and the DRAQ5 channel with 642 nm laser excitation and a LP 655 nm emission filter. The 3D SR-SIM and wide-field images were reconstructed with ZEN 2011 (Carl Zeiss, Inc, Germany). Images were generated from z-stacks containing 5 phase shifts and 5 rotations per z-slice (0.091 μm interval) and then processed in the Zen 2011 software. For channel alignment, a multicolored bead slide was imaged using the same image acquisition settings and used for an affine alignment of channels.

2.16 TEM Analysis

2.16.1 Negative staining for TEM

The methodology of negative staining is similar to that previously described (Al-Dossary et al., 2013). Nickel TEM grids (Electron Microscopy Sciences), 400 mesh with a formvar/carbon film, were floated on a drop of the fractions of purified OLF pellet suspension. The grids were then washed with several drops of water and then stained with 1% uranyl acetate, a phospholipid stain, before being subjected to

microscopic analysis. Membrane vesicles were imaged using the TEM (Zeiss LIBRA 120).

2.16.2 Immunogold labeling of PMCA4a or CD9 in OVS

The methodology of immunogold labeling is similar to previously described (Pisitkun et al., 2004). Briefly, following ultracentrifugation, vesicle suspensions were mixed 1:1 with 4% paraformaldehyde in 0.15 M Sorensen's phosphate buffer pH 7.4 then were applied to 400-mesh nickel grids. The grids were then washed on 3 drops of PBS then incubated with 0.05 M glycine in PBS for 15 min. After blocking with goat block (Aurion, Wageningen, Netherlands) for 30 min and washing, the grids were incubated with primary anti-PMCA4a antibody diluted 1:10 in 0.1 % BSA-cTM containing 0.02 % Triton X-100 (to permeabilize the vesicle membranes) for 2 h or CD9 antibody diluted 1:10 in 0.1 % BSA-cTM. Grids were then washed 6X, 5 min each, with 0.1 % BSA-cTM (Aurion) and then were exposed to goat anti-rabbit or goat anti-rat secondary antibodies conjugated to 6 nm gold particles (Aurion) diluted 1:20 in 0.1 % BSA-cTM (Aurion) for 2 h. The grids were then washed 6X, 5 min each, with 0.1% BSA-c and then with PBS 3x, 5 min each. Grids were post-fixed with 2% glutaraldehyde in PBS for 5 min and then washed with PBS for 5 min, followed with filtered double de-ionized water 5X, 2 min each. The membrane vesicles on the grids underwent negative staining with 1% uranyl acetate. After drying, the grids were examined with a Zeiss LIBRA 120 electron microscope operated at 120 kV. Control samples were processed identically, except that rabbit IgG or rat IgG were substituted for the primary antibody.

2.16.3 Pre-embedding immunogold labeling for OVS-sperm membrane interaction

The methodology of immunogold labeling is similar to previously described (Pisitkun et al., 2004; Al-Dossary et al., 2013). Briefly, after co-incubation for 3 h at 37°C, the mixture was centrifuge at 500 x g for 10 min and re-suspended in PBS and a droplet was applied to a 22 mm round thermanox coverslip coated with poly-l-lysine. Sperm were allowed to adsorb to the surface of the coverslip for 15 min. Samples were then fixed with 4% paraformaldehyde in 0.1M Sorensens' phosphate buffer pH 7.2 for 30 min and washed 3x for 15 min each with 0.1M Sorensens' phosphate buffer pH 7.2. To inactivate residual aldehyde groups present after aldehyde fixation a solution of 0.1% sodium borohydride (NaBH₄) in 0.1 M Sorensens' phosphate buffer (freshly prepared) is used for 10 min. After, washing 4x for 5 min in 0.1 M Sorensens' phosphate buffer pH 7.2, sperm cells were permeabilized with 0.05% Triton-X-100 in PBS for 10 min followed with PBS washes, 3x for 10 min. After blocking with AURION Donkey Solution for 30 min, the coverslips containing the sperm sample were incubated with goat anti-PMCA4 diluted 1:50 in BSA-c, overnight at 4°C. Controls consisted of replacing the primary antibody with normal goat IgG (1:2900 dilution) and replacing the primary antibody with BSA-c. Next day, samples were washed with BSA-c and incubated with donkey anti-goat IgG ultra-small gold-conjugated secondary antibody (800.311, Aurion Immuno Gold Reagents & Accessories, Wageningen, The Netherlands) diluted 1:100 overnight at 4°C. After being washed with BSA-c and PBS, samples were fixed with 2% glutaraldehyde in 0.1 M Sorensens' phosphate buffer pH 7.2 for 30 min, washed, and post-fixed with 1% osmium tetroxide (aq) for 15 min. Following extensive water washes, samples were

silver-enhanced for 20 min using the Aurion R-Gent SE-EM silver enhancement kit (500.033, Aurion Immuno Gold Reagents & Accessories, Wageningen, The Netherlands). Samples were then washed, dehydrated in an ascending acetone series, infiltrated with EMBED-812 epoxy resin, and polymerized at 60°C overnight. Samples were sectioned on a Reichert Jung UltracutE ultramicrotome, and ultrathin sections were collected onto 200 mesh formvar/carbon coated nickel grids. Sections were post-stained with uranyl acetate dissolved in methanol and Reynolds' lead citrate and imaged on a Zeiss Libra 120 TEM operated at 120kV. Images were acquired with a Gatan Ultrascan 1000 CCD.

2.17 Effect of the Tri-peptide Arg-Gly-Asp (RGD) on OVS-sperm Fusion

To test the effect of RGD peptide on OVS-sperm membrane fusion before *in vitro* fusion, either pre-labeled OVS or WT sperm or both were separately pre-incubated for 40 min at 37°C in HTF medium supplemented with RGD at 1 mM or 1 mg/ml. Then, they were co-incubated in HTF medium at 37°C for 3 h with final concentration of 8.5×10^5 sperm/ tube. After co-incubation sperm were washed (3x, collected with centrifugation at 500 x g for 15 min), using PBS. Then they were fixed with 4% paraformaldehyde for 30 min at RT, washed (5x, 5 min) with PBS and placed on slides. Slides were mounted with fluoro-Gel II with DAPI. Images were captured as described above (see 3D SR-SIM analysis section). A minimum of 33 sperm were analyzed for the number of microvesicles present.

2.18 Effect of Fibronectin (FN) or Vitronectin (VN) on OVS-sperm Fusion

Capacitated sperm (final concentration 8.5×10^5 sperm/ tube) were treated with 10 $\mu\text{g/ml}$ FN similarly to that used by Geho and others for platelet adhesion (Geho et al., 2003) or 0 $\mu\text{g/ml}$ FN (control) for 40 min prior to co-incubation with pre-labeled OVS for 3 h at 37°C. Acrosome-reacted sperm (final concentration 8.5×10^5 sperm/ tube) were treated with 600 nM (Thys et al., 2012) VN or 0 nM VN (control) for 40 min prior co-incubation with pre-labeled OVS for 3 h at 37°C. After co-incubation, sperm were placed on slides and subjected to 3D SR-SIM analysis as described above.

2.19 Breeding of *Pmca4* KO, Het and WT Females to WT or Het Males to Assess Fertility via Analysis of Litter Sizes

Eight *Pmca4* (-/-) KO and *Pmca4* (+/-) heterozygous (Het) female mice were mated to WT or Het males. Their progeny were carefully observed and the numbers recorded. The mating of WT females with WT males served as control. The mean litter sizes (including the number of perinatal deaths) from these matings were recorded and subjected to statistical analysis.

2.20 Ca^{2+} -ATPase Assay

Following 3 h incubation of OVS with caudal WT or *Pmca4* KO sperm, sperm were recovered by centrifugation. They were then homogenized in a homogenization

buffer [25 mM maleate pH 7.4, 1 mM EDTA, 1 mM DTT, 250 mM sucrose and protease inhibitor completeTM (1 tablet / 50 ml, Roche Diagnostics, Mannheim, Germany), pH 7.4]. The homogenate was centrifuged for 10 min at 14,000 x g at 4°C, and the supernatant subjected to ultracentrifugation at 100,000 x g for 60 min at 4°C to yield microsomal membrane. The microsomal membrane pellet was re-suspended in 100 µl of homogenization buffer (pH 7.4) containing 1.5% *n-octyl-β-D-glucopyranoside* (detergent) for 15 min at 4°C as previously described (Sikdar et al., 1991). Protein concentration was determined using the bicinchoninic acid protein assay Kit (Pierce), according to the manufacturer's protocol. Mg²⁺-dependent Ca²⁺-ATPase activity was measured in homogenate mixture according to the method previously described by Sikdar et al. (1991). To assay the activity of Mg²⁺-dependent Ca²⁺-ATPase, 2 µg proteins and 60 mM ATP were added to reaction buffer containing 250 mM Tris / maleate, 2 M KCl, 100 mM EGTA, 100 mM MgCl₂ and 100 mM CaCl₂ in a total volume of 100 µl (Kosk-Kosicka, 1999). Two µg/mL oligomycin, a specific blocker of mitochondrial ATPases, was added to the reaction buffer. The reaction was stopped by adding 28 µl ice-cold trichloroacetic acid after 30 min. Thereafter, the samples were diluted with 220 µl distilled water. An aliquot of 40 µl 1.75% ammonium molybdate and of 40 µl 2% ascorbic acid was added to the samples to determine the amount of released inorganic phosphate. After a 10-min incubation, the complexed Pi was measured colorimetrically at 820 nm. Enzyme activity was calculated in micromoles Pi per milligram protein per hour (µM Pi/mg protein per h). The Ca²⁺-ATPase activity was determined as the differences between the rate of ATP hydrolysis in WT OVS and *Pmca4* KO OVS, in WT sperm or *Pmca4* KO sperm before and after co-incubation with OVS.

2.21 Evaluation of Intracellular Calcium Concentration ($[Ca^{2+}]_i$) in Sperm using Single Cell Imaging

$[Ca^{2+}]_i$ was evaluated as previously described (Hirst et al., 1999; Aravindan et al., 2012). Briefly, uncapacitated WT and *Pmca4* KO sperm (8.5×10^5 sperm/group) were co-incubated with OVS ($50 \mu\text{g}/\text{group}$) for 3 h at 37°C , using WT or *Pmca4* KO sperm without OVS co-incubation, respectively, as positive and negative control. After washing, sperm re-suspended in PBS (final concentration 8.5×10^5 sperm/ dish) and loaded into a small-volume imaging dish (35 mm diameter, MatTek Crop., Cat. # P35G-0-14-C, Ashland, USA) coated with poly-D-lysine. Sperm were loaded with Fluo-4/AM (fluorescent Ca^{2+} indicator, lipophilic membrane permeant acetoxymethyl (AM) esters, $10 \mu\text{M}$ final concentration, in DMSO supplemented with 0.5% pluronic F-127), for 15 min at 37°C in the dark, followed by two washes with Hank's Balanced Salt Solution (HBSS, Fisher Scientific). $[Ca^{2+}]_i$ was visualized with a 40x C-Apochromat Water immersion objective, using a high speed confocal microscope (Zeiss 5 LIVE DUO, Carl Zeiss, Inc, Germany). The Fluo-4 channel was obtained with 488 nm laser excitation and LP 505 nm emission filter and change in fluorescence intensity was measured over time. Images were gathered over 2-5 min to establish baseline calcium values. Images were analyzed using Zeiss Zen Physiology software module (2012). The experiment was repeated 2 times with 3 dishes per round of experimentation, using the same protocol and configuration setting. Statistical analyses were performed using one-way ANOVA followed with Tukey-Kramer post hoc.

2.22 Evaluation of Sperm Motility

Sperm motility was objectively assessed by visual estimation (Roca et al., 2000; Shao et al., 2008). Briefly, after co-incubation of *Pmca4* KO sperm (8.5×10^5 sperm) with OVS (50 μg) resuspended in PBS at 37°C for various periods of time (0 h- 3 h, a drop of 2 μl of sperm was loaded into 100 μm deep disposable chambers (Cytonix, Microtool-20-4), which are coated with a crystal clear coating that prevents sperm adhesion to the glass surface (Armant and Ellis, 1995), pre-warmed at 37°C. The preparation was then examined using a Video camera (5.0MP) [model # A3550U, Microscopenet], attached to a phase-contrast microscope. At least 200 spermatozoa and five fields were recorded from each group. The mean numbers of progressively motile sperm were recorded from the videos and expressed as a percentage of the total number of sperm.

2.23 Statistical Analysis

Two-way ANOVA and Student's *t*-tests or one-way analysis of variance (ANOVA) followed by Tukey-Kramer post hoc test was performed on the means \pm SEM for 3 replicates. *P*-values were calculated and $*P < 0.05$ was considered significant.

Chapter 3

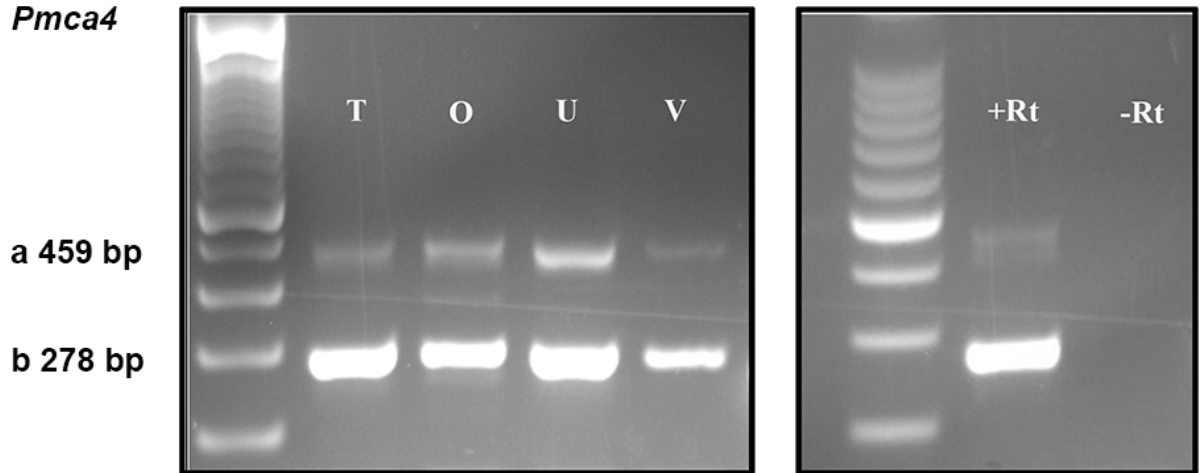
RESULTS

3.1 Analysis of *Pmca4* Transcripts in Murine Female Reproductive Tissues

To obtain information on the expression of transcripts from the C-terminal splice variants of *Pmca4* in the murine female reproductive tract, I performed RT-PCR using specific primers. Testis tissues were used as a positive control. As shown in **Fig. 5A**, mRNA for *Pmca4a* and *4b* variants was present throughout the female tract in tissues recovered following superovulation. The expected PCR products of 469 and 278 bp were observed in all three regions: the oviduct, uterus, and vagina. The mRNA distribution varied in the tissues. Of the two variants *Pmca4b* mRNA is more abundant in all three regions (**Fig. 5B**). Sequence analysis of the 469 and 278 bp PCR products matched the cDNA sequence of PMCA4a and the alternatively spliced PMCA4b, respectively. A negative control for the PCR showed no product for the reaction in the absence of reverse transcriptase.

A

Variant a & b (Ex 19 - Ex 21)



B

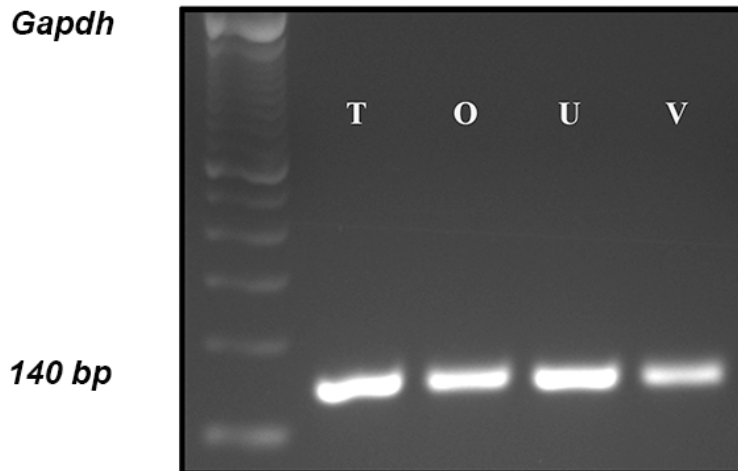


Figure 5. Semi-quantitative analysis of *Pmca4a, b* mRNA via RT-PCR in the murine female reproductive tract (A) The 469 bp PCR product represents *Pmca4a*, and that of 278 bp corresponds to *Pmca4b*. Murine testis (T) cDNA served as positive control. Negative control was performed in the absence of reverse transcriptase (-RT). *Gapdh* mRNA was used as an internal control (B). Pronounced expression of *Pmca4b* was detected in the uterus, whereas *PMCA4a* showed more prominent expression in the oviduct than in the testis. A 100 bp ladder was run in the left lane of each panel. O, oviduct; U, uterus, and V, vagina.

3.2 Localization and Detection of PMCA4a in the Female Reproductive Tract and in its Secretion

To determine the expression and localization pattern of the PMCA4a protein in the female reproductive tract, sections of vaginal, uterine, and oviductal tissues from superovulated virgins were subjected to indirect IF analysis using the polyclonal PMCA4a antibody. The results in **Fig. 6A** show that PMCA4a is mostly present in the luminal and glandular epithelial cells of the endometrium of the uterus. In the vagina a strong signal of PMCA4a was detected in the mucosa and within the epithelial layers at the apical membrane near the lumen (yellow arrowhead) and a weaker staining at the basement membrane (white arrowhead). In the oviduct the signal for PMCA4a is strongest in the luminal epithelia of the convoluted epithelial lining on the apical membrane. The presence of PMCA4a on the apical membrane of the luminal epithelial cells suggests that PMCA4a is secreted in the lumen.

The uterine expression pattern of PMCA4a in naturally cycling females was determined after vaginal smears were examined to identify the stages of the estrus cycle. Uterine tissues collected from virgins at the four stages of the estrus cycle were analyzed. Interestingly, only in the pro-estrus and estrus phases was expression of PMCA4a detectable in both the luminal and glandular epithelium, while it was absent or marginally present in the metestrus and diestrus phases in these regions (**Fig. 7, insets**). In contrast, the myometrium showed strong expression of PMCA4a in all four phases of the estrus cycle (**Fig. 8**).

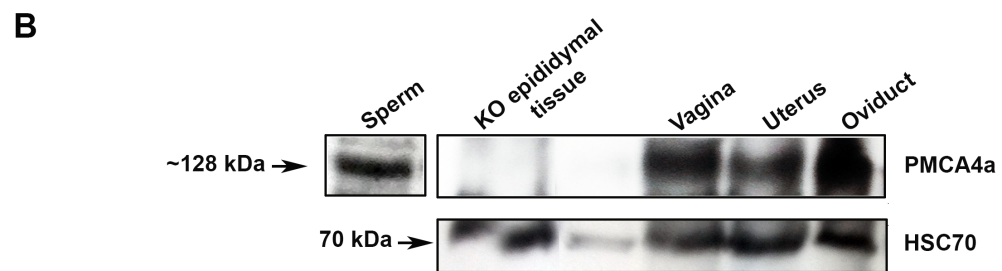
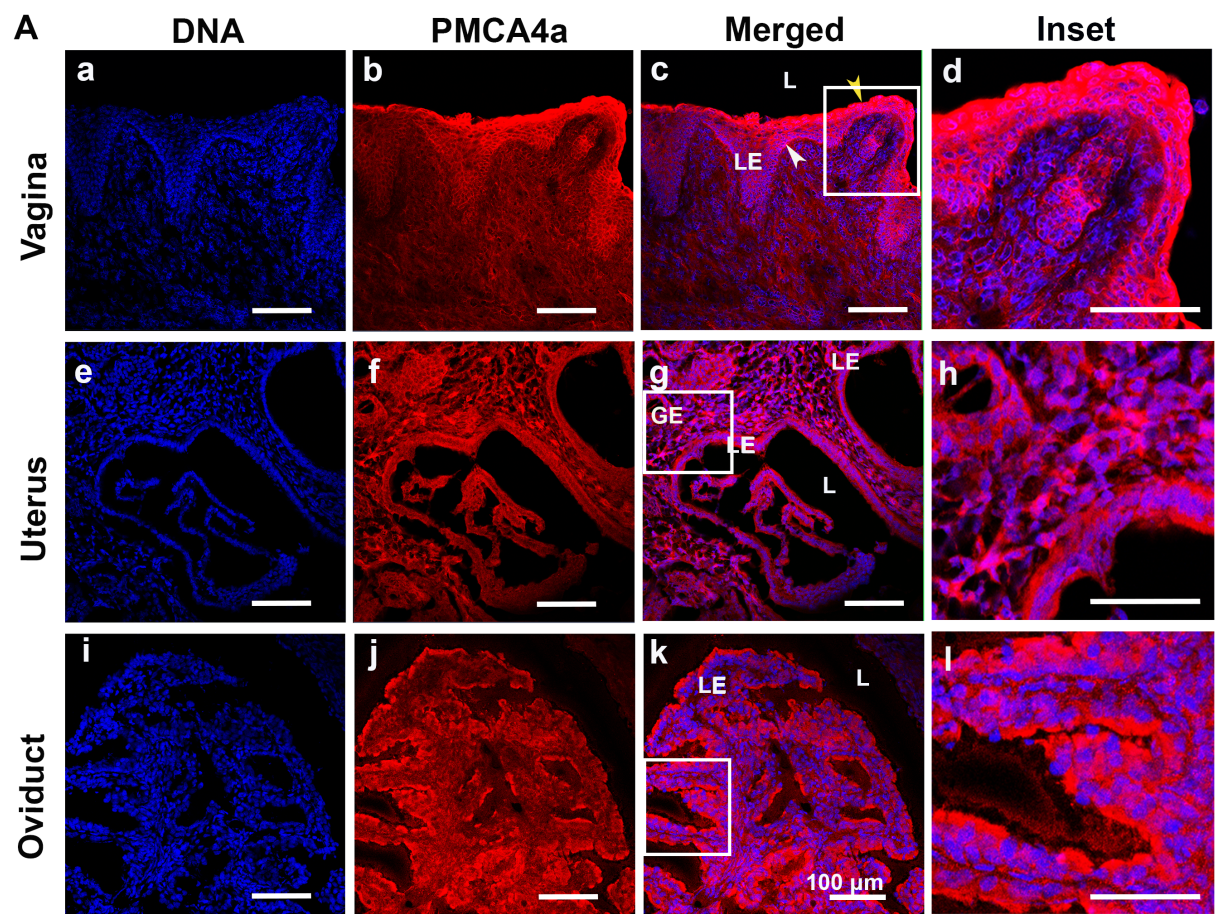


Figure 6. Expression of PMCA4a in mouse vaginal, uterine, and oviductal tissues following superovulation (A) Indirect immunofluorescence was performed on frozen sections (a-d) of vaginal tissues using anti-PMCA4a antibody and an Alexa Fluor-conjugated secondary antibody (red), and the nuclei were visualized by staining with Draq-5 (blue). Strong PMCA4a staining was detected at the epithelial layers at the luminal edge (yellow arrowhead) and was decreased at the basement membrane (white arrowhead). (e-h) In uterine tissue PMCA4a was abundantly expressed in both the luminal and glandular epithelia and also in the stroma. (i-l) In oviductal tissue strong PMCA4a staining is detected at the apical boundaries of the epithelial cells that line the oviductal lumen. (d, h, and l) Insets are seen from vagina, uterus and oviduct. Negative controls in PBS or IgG of the tissues showed no staining, similar to that in Fig. 3, 4. The images were captured using confocal microscopy with a 20x objective lens (a plan-Apochromatic). L= lumen; LE = luminal epithelium; GE = glandular epithelium. Bar = 100 μ m (same scale for all micrographs, and 200 μ m insets). (B) Western blot analysis performed with anti-PMCA4a antibody on tissues recovered after superovulation, using sperm as a positive control, revealed the ~128 kDa PMCA4a in all tissues and its absence in epididymal tissues of *Pmca4* null mice, used as a negative control (Top panel). In the lower panel, equal loading of protein is demonstrated by detection of HSC 70 in the tissue lysates. The amount of proteins loaded was 20 μ g per lane.

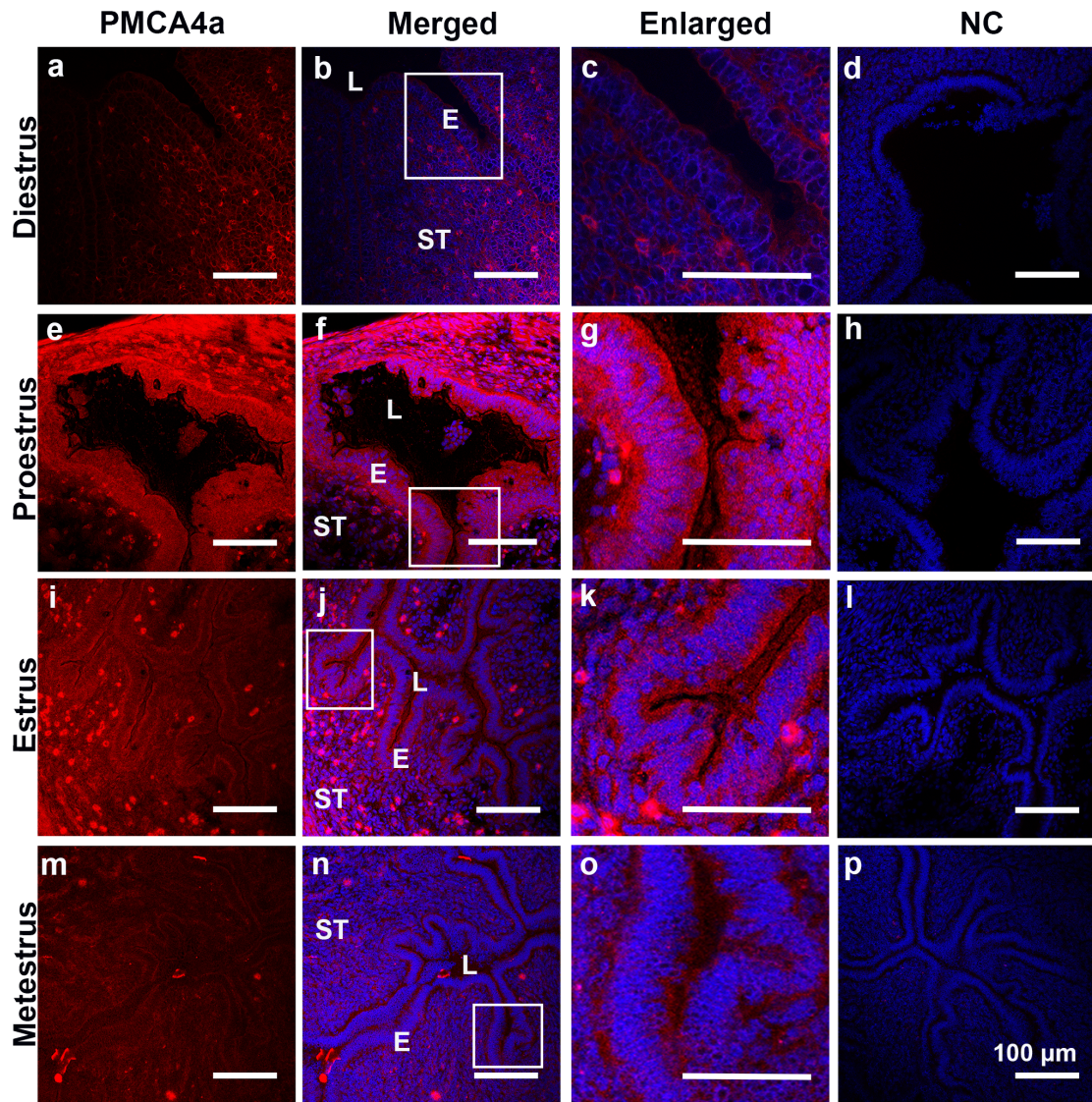


Figure 7. Indirect immunofluorescence of PMCA4a in the murine endometrium of the uterus during the estrus cycle Using frozen sections PMCA4a immunoreactivity (red) was detected in the uterine luminal epithelium in pro-estrus (e - g) and estrus phases (i - k) but not during metestrus (m - o) and diestrus (a - c). The nuclei were visualized by staining with Draq-5 (blue). Negative controls (NC) in PBS or IgG are shown in d, h, l, and p. The images were captured using confocal microscopy and a 20x (a plan-Apochromatic) objective lens. LE = luminal epithelium; L= lumen; ST= stroma. Bar = 100 μ m (same scale for all micrographs, and 200 μ m for insets).

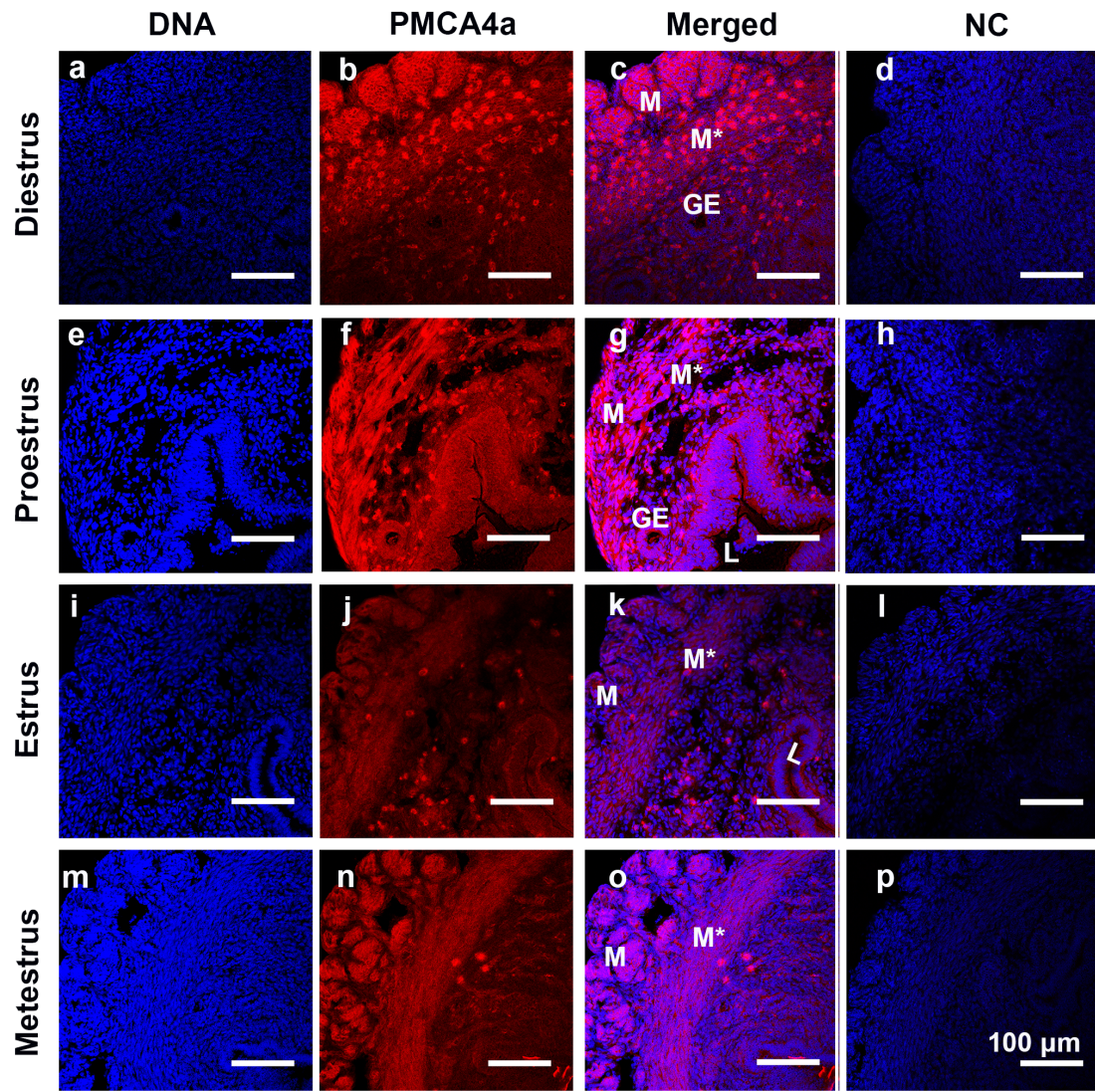


Figure 8. Indirect immunofluorescence of PMCA4a in the murine myometrium of the uterus during the estrus cycle In addition to the endometrium, the muscles and mesothelium of the myometrium (M*, M, respectively) were positively stained for PMCA4a. Elevated levels of PMCA4a immunoreactivity were detected at the boundaries of the epithelial cells lining the pro-estrus uterine glands (g). The nuclei were visualized by staining with Draq-5 (blue). Negative controls (NC) of diestrus, pro-estrus, estrus, and metestrus phases are respectively shown (**d, h, l, and p**). The images were captured using confocal microscopy and a 20x (a plan-Apochromatic) objective lens. GE = glandular epithelium; L = lumen; ST= stroma. Bar = 100 μ m (same scale for all micrographs).

To confirm the IF data, I performed Western blotting analysis on tissues recovered after superovulation. In all three regions of the female reproductive tract the ~128 kDa PMCA4a band was detected (**Fig. 6B**), corroborating the IF findings. Western analysis also revealed that while females in proestrus/estrus secreted PMCA4a in the luminal fluids combined (FLF) those in metestrus/diestrus had only marginal levels of the protein (**Fig. 9A**). As expected females brought into estrus by superovulation also displayed PMCA4a in the luminal fluids from the vagina (VLF), uterus (ULF), and the oviduct (OLF), as shown in **Fig. 9B**. Densitometric analysis showed that the level of expression of PMCA4a in the LFs varied, being lowest in the VLF and highest in the OLF which is secreted at the site of fertilization. The 9-fold higher level of PMCA4a in OLF over VLF (**Fig. 9C**) represents a significant increase ($P = 0.03$).

3.3 Characterization of Membrane Vesicles from Oviductal Luminal Fluids as Exosomes and Microvesicles

Oviductal fluid was collected from females hormonally-induced into estrus. Using TEM, the pellet isolated from the oviductal fluid by differential ultracentrifugation was shown to be rich in EVs, consisting of both exosomes and microvesicles (**Fig. 10A, Fig. 11**).

Using antibodies which recognize the extracellular domains of CD9 tetraspanin, one of the most abundant proteins found on the exosomal membrane (They et al., 2002; Caballero et al., 2013), I detected the presence of the 24 kDa CD9 by Western analysis of the OLF pellets as well as of the uterosomes (**Fig. 10C**). The

band was however absent in the supernatant. The presence of CD9 in the OLF membrane vesicles was confirmed by TEM analysis and immunogold labeling on the membrane where the gold particles were seen on the exterior (**Fig. 10D**), an orientation that typifies exosomes (Pisitkun et al., 2004). Therefore, consistent with the requirements for defining membrane vesicles as exosomes/microvesicles, I show that vesicles in the OLF: 1) are within a size range of 25-1000 nm in diameter, as detected by negative staining and TEM (**Fig. 10B, Fig 11**), 2) have exosomal/microvesicle shape, 3) are enriched with CD9 tetraspanin, a biomarker of exosomes (They et al., 2002; Caballero et al., 2013) (**Fig. 10C**), and 4) have membrane proteins in the exosomal/microvesicle orientation. Thus, I defined these vesicles, purified from oviductal fluid, as exosomes/microvesicles and termed them "oviductosomes" or OVS.

3.4 PMCA4a is Present in the OVS of the Luminal Fluids

When the nitrocellulose membranes used for the detection of CD9 in the exosomes from ULF and OLF (**Fig. 10C**) were re-probed with anti-PMCA4a antibodies in Western blotting analysis, the ~128 kDa PMCA4a band was detected, but was absent from the supernatant (**Fig. 12A**). For the uterosomes, there was a cross-reactive ~100 kDa band that was not seen in the OLF and whose origin is unknown. Our findings indicate that 100% of PMCA4a in the luminal fluids resides in the particulate fraction, or the OVS. More importantly, our results indicate that PMCA4a is carried on CD9-positive OVS.

I confirmed the presence of PMCA4a on CD9-positive OVS by TEM and immunogold labeling. Control samples incubated in the presence of rabbit IgG showed randomly dispersed 6 nm immunogold particles on the grids, but none localized to vesicles (**Fig. 12B, 1-4**). In test samples treated with the primary antibody, immunogold, particles detecting PMCA4a were observed on both the OVS (**Fig. 12B, 5-8, Fig. 11**) and the uterosomes (**Fig. 12B, 9-12**). It should be noted that gold particles were not randomly distributed and were rarely localized outside of the vesicles on the grids. Importantly, on the vesicles, the particles detecting the localization of PMCA4a (**Fig. 12B**) required gentle permeabilization of the vesicles in order for the PMCA4a antibodies to gain access to, and recognize an epitope on, the cytoplasmic-side of the molecule. This further confirms that the OVS are exosomes/microvesicles, and not endosomes which have the cytoplasmic side of the molecule in the exterior orientation (Pisitkun et al., 2004).

3.5 *In Vitro* Uptake of PMCA4a on Caudal Sperm from Unfractionated Luminal Fluids and OVS

The presence of PMCA4a in the luminal fluid during estrus, the only phase when sperm traverse the female tract, suggested that the pump may be transferred to the sperm surface during their transit and storage in the oviduct. Fresh caudal epididymal sperm were incubated for 2-3 h in PBS supplemented with Zn^{2+} (carrier control), which are known to prevent the acrosome reaction (Andrews et al., 1994), or in FLF suspended in PBS containing Zn^{2+} (added in the form of zinc acetate). Sperm were then fixed and stained with anti-PMCA4a primary and Alexa Fluor-488 conjugated secondary antibodies as described in the Materials and Methods. Flow

cytometry, used to quantify fluorescence intensity as a measure of PMCA4a uptake in 50,000 sperm/group, revealed that after 2 h incubation in FLF there was a right peak shift in fluorescence intensity, compared to the PBS control (**Fig. 9D**). After 3 h co-incubation of sperm and reconstituted OVS, there was a remarkable ~3-fold increase in uptake compared to the PBS control (**Fig. 13**). In general, the flow cytometric data reveal *in vitro* acquisition of PMCA4a on caudal sperm and suggest that the plasma membrane in these cells is not all fully saturated with this transmembrane protein when sperm leave the male.

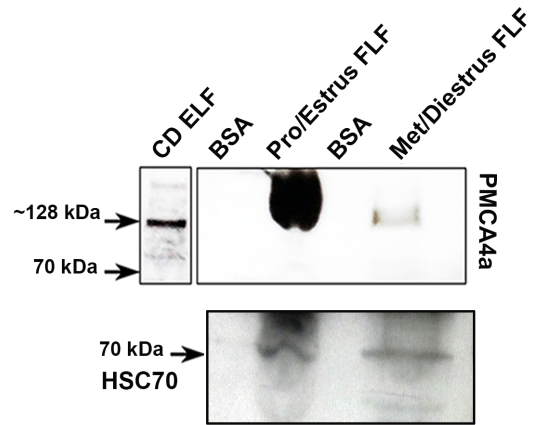
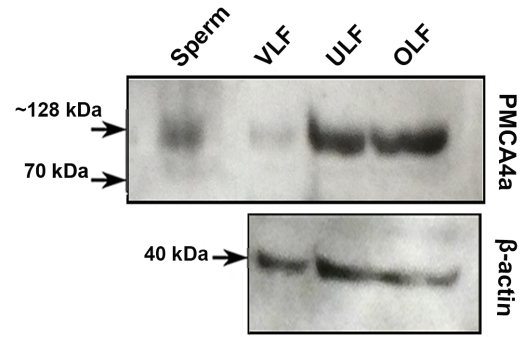
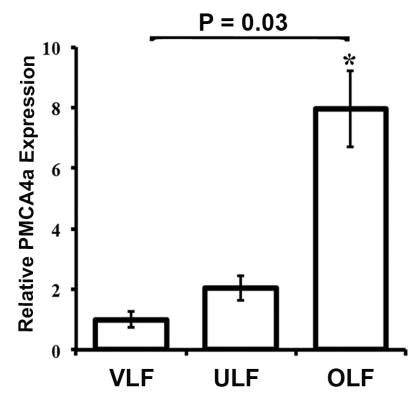
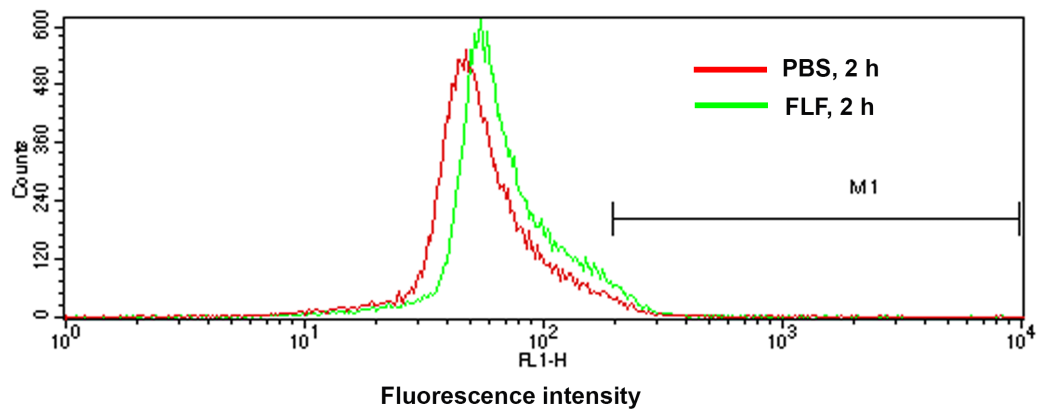
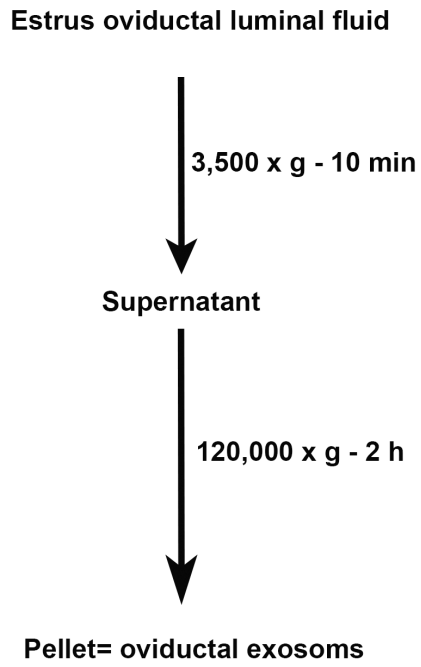
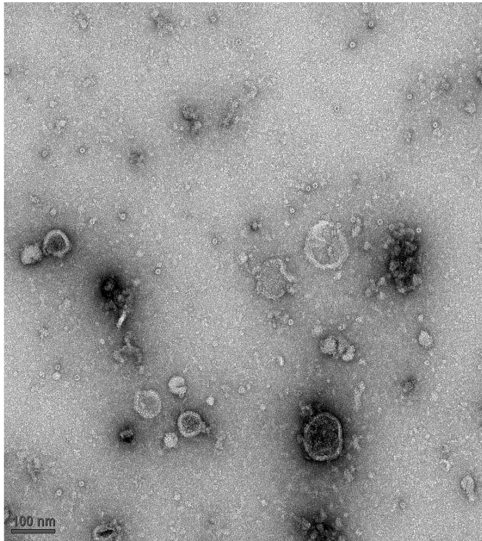
A**B****C****D**

Figure 9. Detection of PMCA4a in reproductive luminal fluids and its acquisition on caudal sperm (A) Representative Western blot of FLFs collected during pro-estrus and estrus and metestrus and diestrus (40 μ g proteins loaded). The ~128 kDa PMCA4a is seen in pro-estrus and estrus and is marginally present at metestrus and diestrus. Caudal epididymal luminal fluid was used as a positive control. The membrane was stripped and re-probed for HSC70 as a loading control. (B) Western blots of VLF, ULF, and OLF recovered after superovulation demonstrate the presence of the ~128 kDa PMCA4a. Sperm protein was used as a positive control. The membrane was stripped and re-probed for β -actin as a loading control. (C) Quantitation of Western blot data shown in B; the relative expression was determined using VLF as 1. The data represent the mean (\pm SEM) of a minimum of three independent experiments, and the intensity was quantified by Image J software. ANOVA and *t*-tests were performed on the mean and *P* values were calculated. **P* = 0.03 indicates a significantly increase amount of PMCA4a in OLF compared to that in VLF. (D) A peak shift of fluorescence intensity to the right, indicates increase amounts of PMCA4a in sperm incubated in FLF compared to PBS for 2 h and treated as described in Materials and Methods.

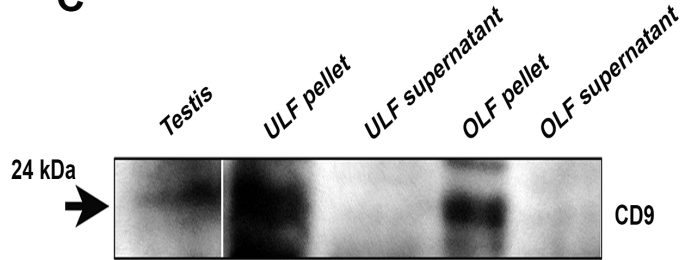
A Purification of oviductal exosomes



B



C



D

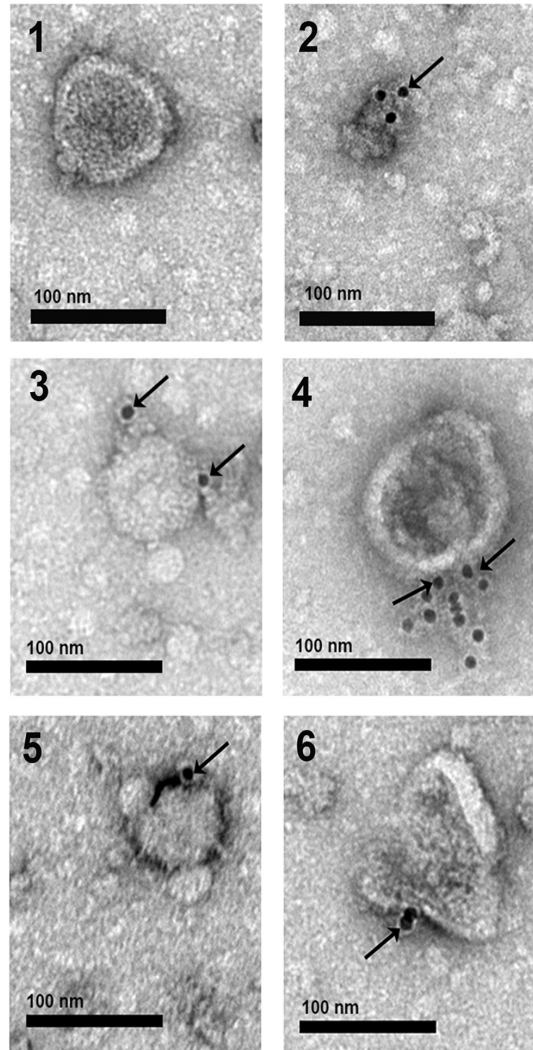


Figure 10. Characterization of membranous vesicles in OLF (A) Protocol used to isolate oviductal exosomes by ultracentrifugation of oviductal fluids. **(B)** TEM of negative staining for the particulate fraction from OLF reveals the presence of membranous vesicles ranging in size from 25-100 nm in diameter. **(C)** Western blots detected CD9 (24 kDa) in protein extracts from membranous vesicles removed from OLF and uterosomes, but not in the supernatants. Testis protein was used as a positive control. Each lane contains 40 μ g of protein. Results are representative of three experiments. **(D)** Immunogold labeling (6 nm gold particles) of CD9 is shown in oviductal membranous vesicles termed “oviductosomes”. Gold particles on individual OVS are seen arrowed in 2-6 on the exterior of the membrane. In the absence of primary antibodies and the presence of rat IgG, gold particles were absent (1), indicating the specificity of the antibody. Scale bar =100 nm in panel B, D.

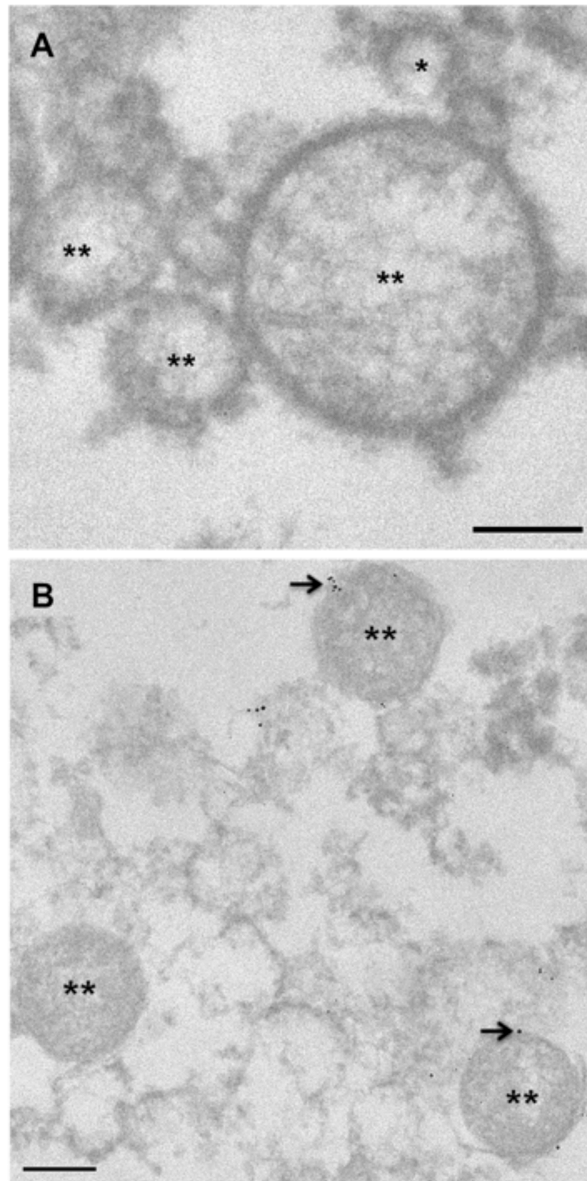
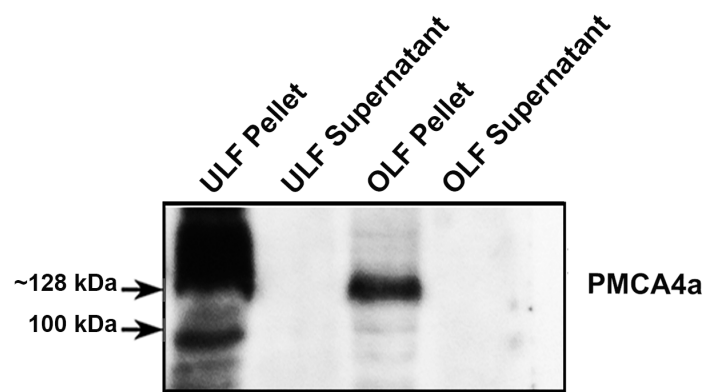


Figure 11. Electron micrographs of mouse OVS. (A-B) OVS, exosomes* and microvesicles**, were isolated using differential ultracentrifugation. Prior to imaging with transmission electron microscopy grids were stained with uranyl acetate, a heavy metal stain that binds to lipids and proteins. **(A)** Microvesicles from IgG control ranged in sizes from 0.1 μm to 1 μm in diameter and exosomes are < 100 nm, and showed no immunogold particles. **(B)** Immunogold labeling of PMCA4 (arrows) showed ultra small gold particles on microvesicles. Bar = 200 nm.

A



B

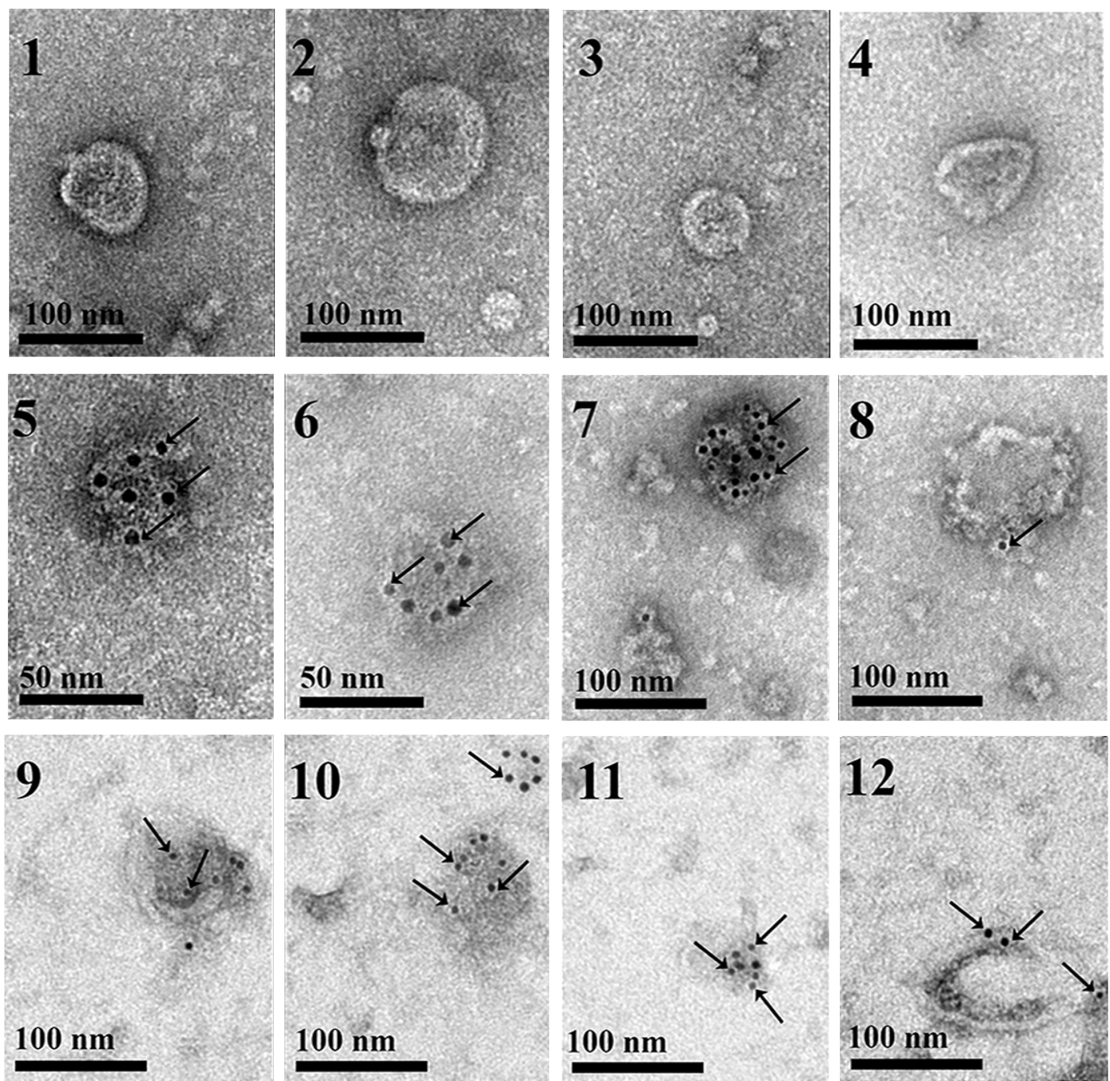


Figure 12. Immunodetection of PMCA4a in OVS and uterosomes (A)

Nitrocellulose membrane with CD-positive pellets and supernatants (Fig. 6C), when stripped and re-probed with PMCA4a antibodies in a Western blot, revealed the presence of the ~128 kDa PMCA4a band in the pellets only. A band of unknown origin at ~100 kDa is also seen in the uterosomes. Each lane contains 40 µg of proteins. Results are representative of three experiments. **(B)** Immunogold labeling (6 nm gold particles) of PMCA4a is shown in OVS in 5-8 and in uterosomes in 9-12. Gold particles localized on the cytoplasmic-side of the membrane are seen arrowed. They were rarely seen elsewhere on the grids. In the absence of primary antibodies and the presence of rabbit IgG, gold particles were absent (1-4) indicating the specificity of the antibody. Scale bar = 50-100 nm.

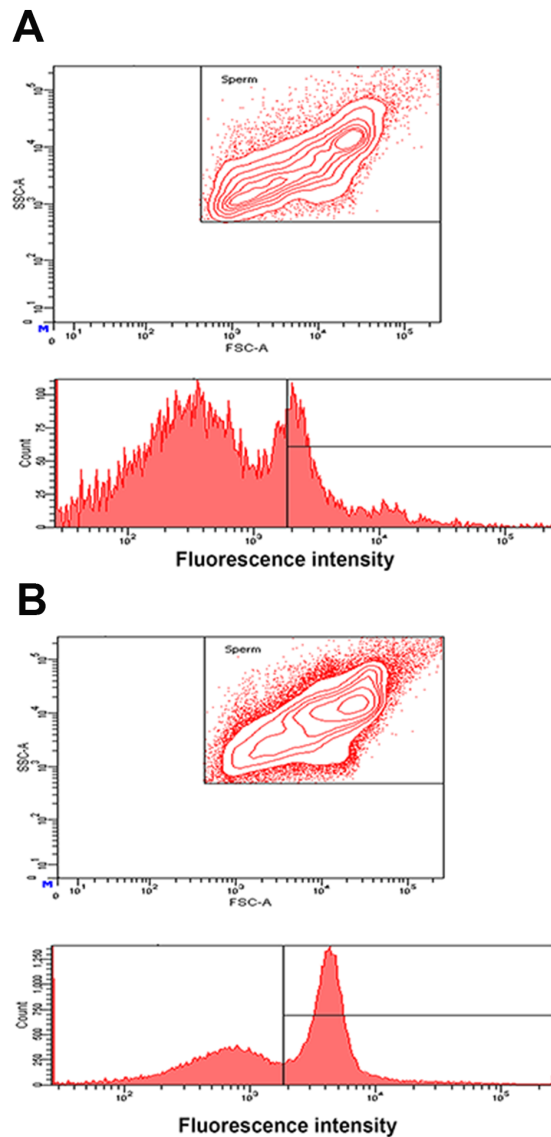


Figure 13. PMCA4a uptake by caudal sperm via incubation in OVS reconstituted in PBS OVS were isolated from FLFs after superovulation. **(A)** Flow cytometric analysis of sperm co-incubated in PBS (negative control). The contour plot above reveals two subpopulations of sperm, as represented by the small inner circles at top right and bottom left. The graph shows that the majority of the fluorescence falls below the gated region. **(B)** Sperm incubated in FLF OVS (2 mg/ml protein) show a unimodal distribution (a single inner circle) and a ~3 fold increase of fluorescence intensity (peak shift to the right) compared to A in the gated region. The co-incubation period was 3 h for both A and B.

3.6 *In vitro* OVS-sperm Interaction was Detected using FM4-64FX Dye and 3D SR-SIM

To gain insights into the mechanism of delivery transmembrane proteins to the sperm membrane, a novel experimental approach for the assessment of OVS-sperm interaction was executed, using 3D SR-SIM. OVS pre-labeled with a fluorescent membrane dye, FM4-64FX, and co-incubated with caudal sperm in a co-incubation assay were shown to accumulate on the sperm membrane after 2-3 h (**Fig. 14A-B**). Labeled OVS were first detected over the acrosome, followed by other areas on the head, the midpiece (**Fig. 14A-B**), and the proximal principal piece where they were occasionally seen (data not shown). In addition to the detection of the punctate red signal detecting microvesicles there was continuous red decoration of the midpiece with the FM4-64FX red signal, likely due to the coalescence of exosomes attached or fused with the sperm membrane over the midpiece (**Fig. 14A**). In contrast with the negative control sperm samples that were incubated in the supernatant dye solution collected after removing the labeled OVS (**Fig. 14C**). Not only do these control sperm lack the punctate signal on the head, but they also lack the continuous staining on the midpiece, while sperm incubated directly in the dye showed broad labeling over the entire membrane (internal positive control, data not shown).

3.7 Co-localization Analysis of OVS and PMCA4a on Sperm

Immunofluorescence analysis of WT and *Pmca4* KO sperm after co-incubation with pre-labeled OVS revealed co-localization of the OVS with PMCA4a (**Fig. 15**). Interestingly, 3D SR-SIM allowed us to visualize PMCA4a molecules located on the inner acrosomal membrane (IAM) (**Fig. 15A, c-d**), identified for the first time. PMCA4a was also detected on the midpiece (**Fig. 15; Fig. 16**) where it was delivered by both microvesicles and exosomes, as detected by the merging of the green and red signal to give a yellow coloration. I consistently detected an accumulation of signal for endogenous PMCA4a in the posterior head near the neck (**Fig. 15A, c-d; Fig. 16A-B**), and its delivery to *Pmca4* null sperm via OVS in this region (**Fig. 15B, c-d**). Prominent PMCA4a signal was detected on the midpiece where it does not reside in mature caudal sperm, suggesting that over time it relocates to the proximal principal piece where lipid rafts exist (Travis et al., 2001). Importantly, there is evidence to suggest that all OVS do not carry/deliver the identical cargo as some with and without PMCA4a were detected on the plasma membrane over the same sperm head (**Fig. 16**).

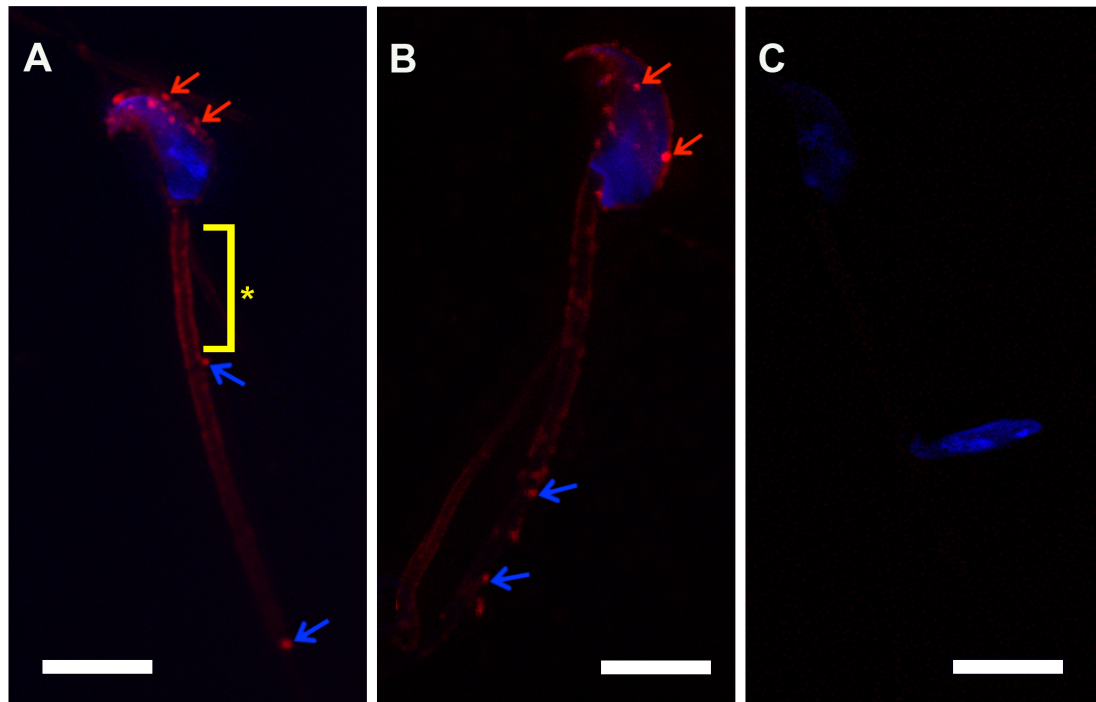


Figure 14. Co-incubation assays detect the transfer of membrane constituents from FM4-64FX-labeled OVS to the sperm membrane. (A-B) Labeled OVS [(microvesicles), (red, 0.1 -1 μm in diameter)] were detected over the acrosome (red arrows) and the midpiece (blue arrows) after 3 h co-incubation with sperm in PBS. Continuous red staining on the midpiece indicates the OVS (exosomes) fused with the sperm membrane (*). **(C)** Negative control shows the absence of labeling in caudal sperm incubated in supernatant FM4-64FX-dye solution. Sperm nuclei were stained blue with DAPI. Images were acquired with a 63x Plan-Apochromat oil immersion objective (numerical aperture of 1.4), using 3D SR-SIM.

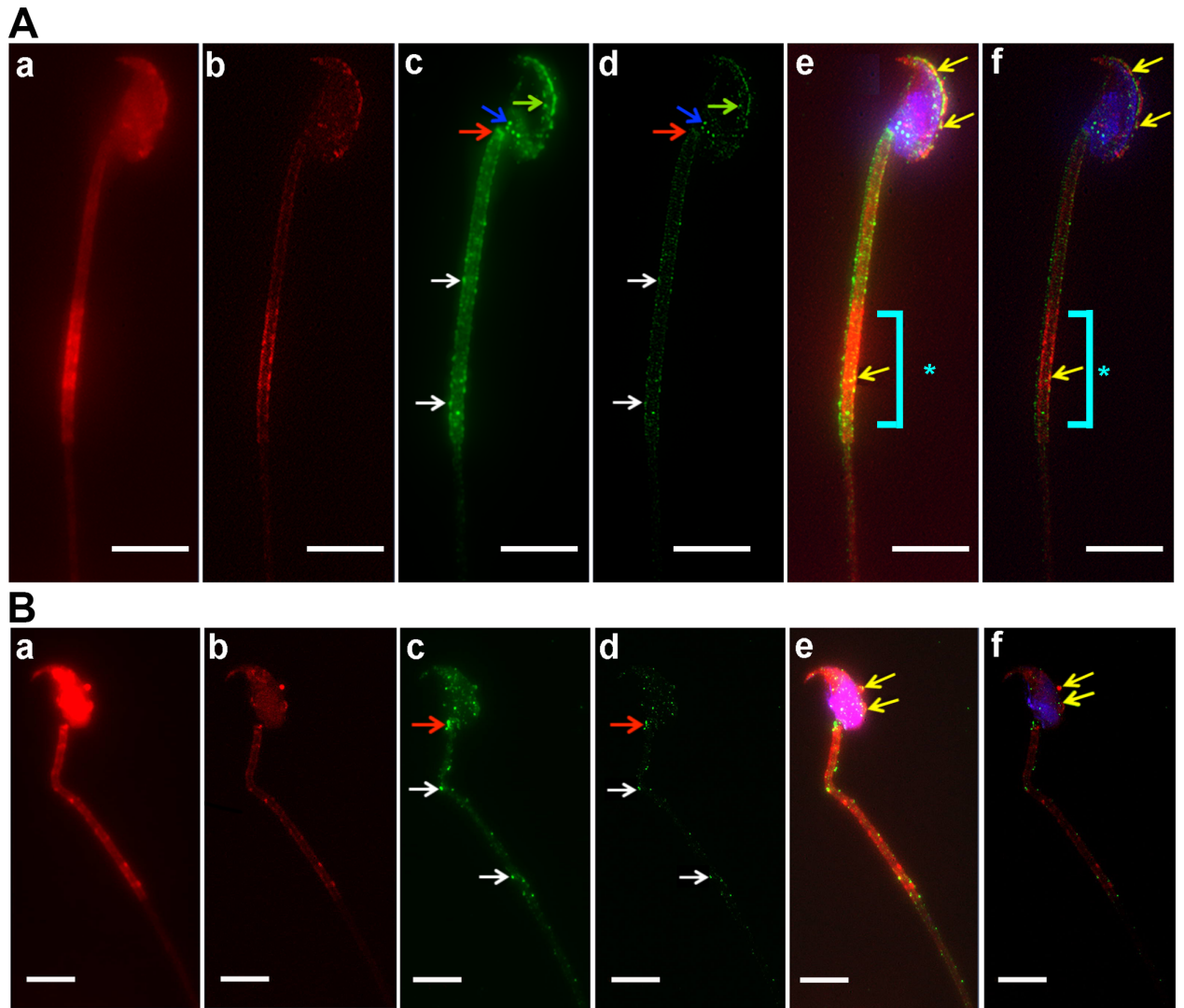


Figure 15. Co-localization of FM4-64FX-labeled OVS and PMCA4a on WT and *Pmca4* KO sperm membrane following co-incubation, as detected in both wide-field fluorescence (a,c,e) and 3D SR-SIM (b,d,f). WT (A) and (B) *Pmca4* KO sperm were incubated with FM4-64FX-labeled OVS microvesicles. Transferred PMCA4a protein (green, c and d) from FM4-64FX-labeled OVS (red, a and b) was identified as a co-localized signal (yellow) over the acrosome (green arrows), on the midpiece (white arrows) after the images were merged (yellow arrows, e and f). Endogenous PMCA4a protein was identified for the first time on the inner acrosomal membrane (A-c and d, green arrows), on the posterior head (blue arrows), on the neck (red arrows), and on the midpiece (white arrows). * The distal midpiece shows intense staining of FM4-64FX-labeled OVS. Sperm nuclei were stained with DRAQ5 (blue). Images were acquired with a 63x Plan-Apochromat oil immersion objective (numerical aperture of 1.4). Scale Bars = 5 μ m.

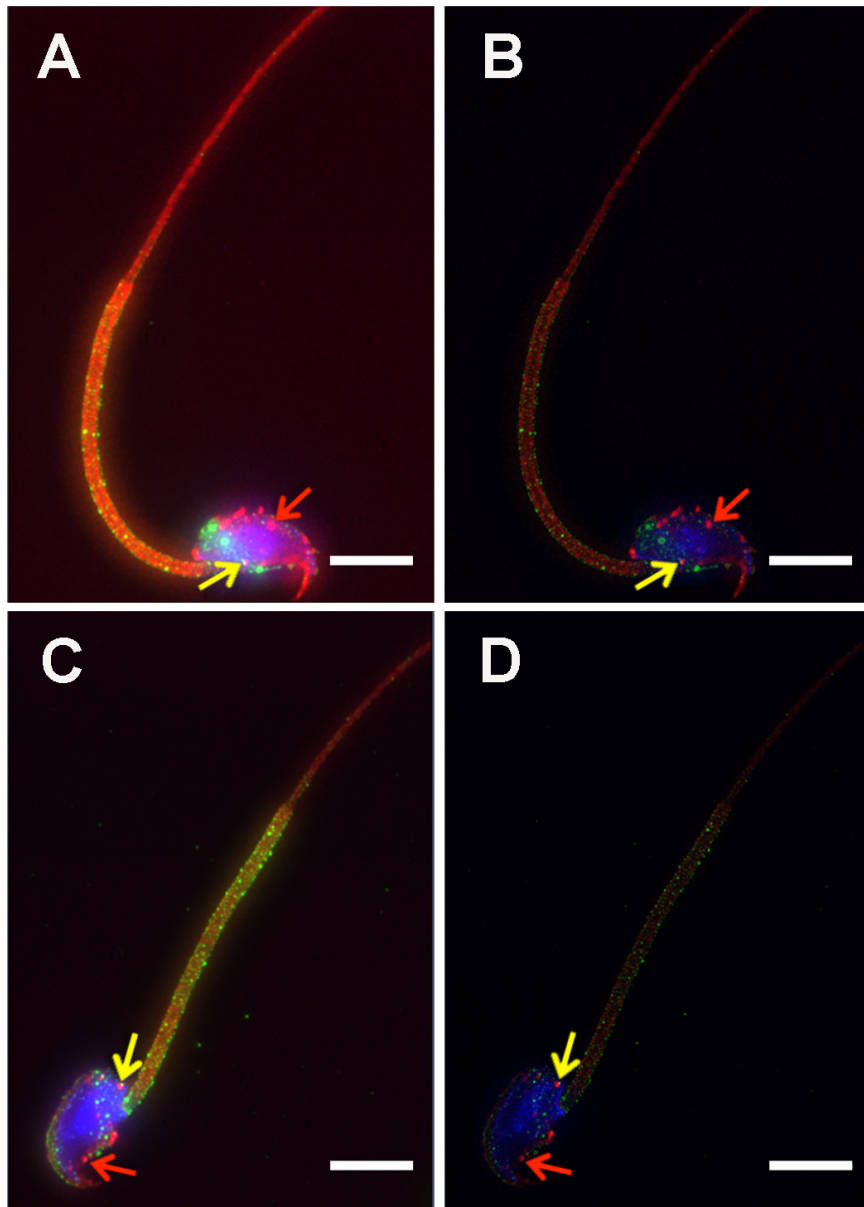


Figure 16. FM4-64FX-labeled OVS carry and deliver different cargoes to sperm following co-incubation, using PMCA4a as an example. Some FM4-64FX-labeled OVS (red) co-localized with PMCA4a (green) signal (yellow arrow) and some did not (red arrow), indicating the absence of PMCA4a and suggesting that OVS carry different cargoes. Sperm nuclei were stained with DRAQ5 (blue). Images shown as simulated wide-field (A, C) and SR-SIM (B, D) reconstructions. Scale bars = 5 μm .

3.8 Analyze OVS-sperm Interaction, using TEM

High magnification TEM analysis was performed to confirm the observations detected by 3D SR-SIM (**Fig. 17A**). Following co-incubation of caudal sperm with unlabeled OVS for 3h (a period in which large numbers of microvesicles on the sperm membrane and bright continuous staining over the midpiece were detectable, via SR-SIM), sperm were sectioned and immunostained for PMCA4a. Detection of immunogold particles in TEM analysis revealed that microvesicles fuse with the sperm plasma membrane in delivering PMCA4a (**Fig. 17B**). Fusion in delivery is seen in 3D SR-SIM where integrated red OVS, on both the membrane over the head (**Fig. 17A**) and the midpiece, merge with the green PMCA4a signal to give a yellow coloration (**Fig. 17C**). **Fig. 17D** demonstrates that not only microvesicles (100-1000 nm), but also exosomes (<100 nm) fuse with sperm membrane, and their alignment along the membrane in TEM images is consistent with the continuous red signal seen with SR-SIM. These results (**Fig. 17A-D**) clearly indicate that OVS fuse with the sperm membrane in the transfer of their constituents, as exemplified by PMCA4 (**Fig. 17B, C**).

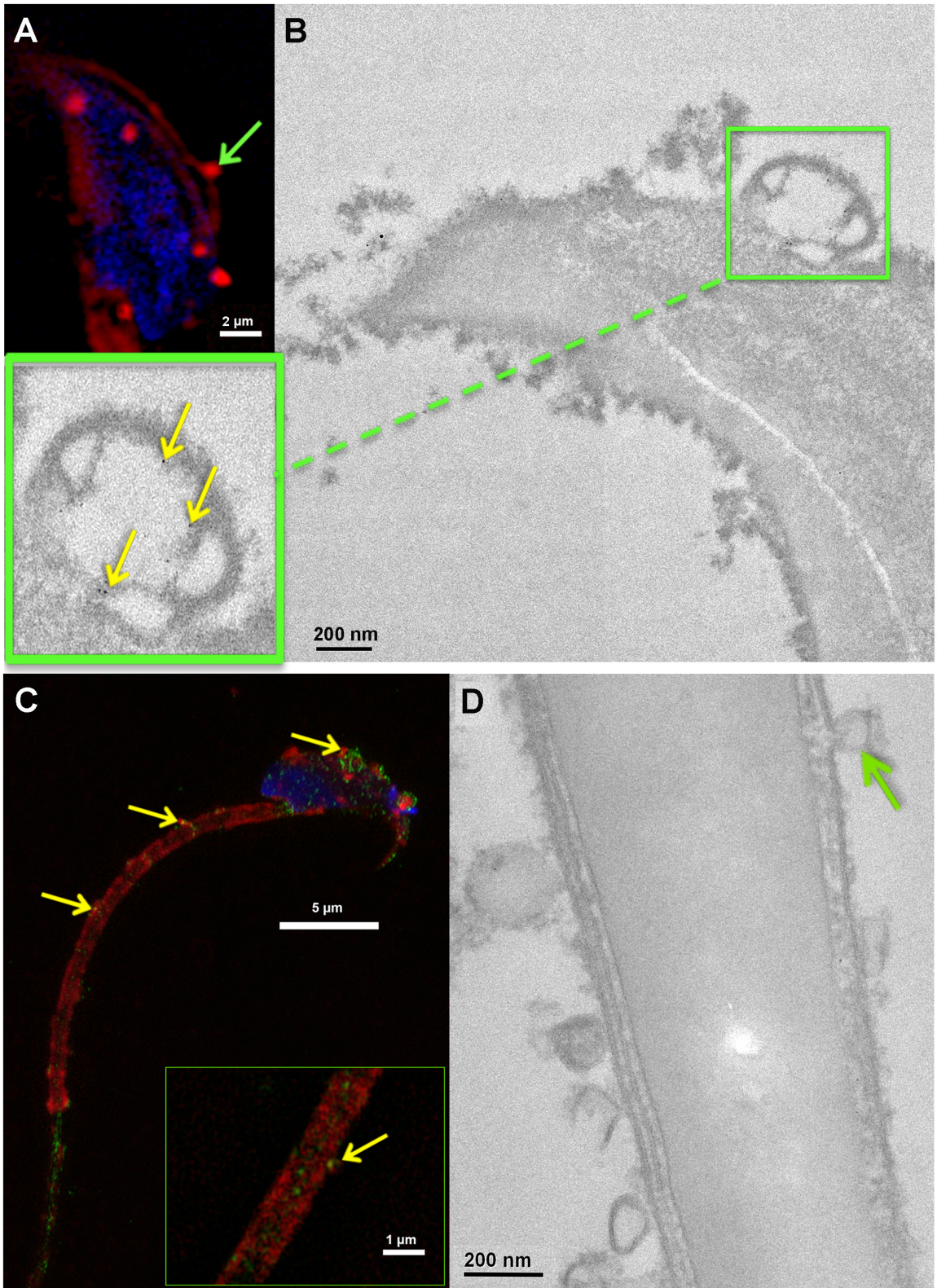


Figure 17. FM4-64FX-labeled OVS and immunogold labeling in OVS fused with WT sperm membrane provide evidence for involvement of a fusogenic mechanism in the transfer of PMCA4. (A) Fusion of a FM4-64FX-labeled microvesicle (green arrow) with the sperm membrane over the acrosome was seen in SR-SIM images. Sperm nuclei were stained with DAPI (blue). (A, C) SR-SIM demonstrated that sperm incubated in labeled OVS acquire the label (green arrows) in a pattern similar to the localization of PMCA4 (yellow arrows), on the plasma membrane overlying the acrosomal cap. The green staining on the proximal principal piece is endogenous PMCA4. Transferred PMCA4 from OVS was detected on the midpiece (yellow arrows). Sperm nuclei were stained with DRAQ5 (blue). (B, D) TEM analysis demonstrates and confirms fusion (green arrow) and transfer of gold particles (PMCA4, yellow arrow) from labeled OVS to the sperm membrane over the acrosome. Control IgG shows the alignment of OVS along the sperm membrane with the absence of immunogold labeling (D).

3.9 CD9 and α v Subunit of α v β 3 Integrin are Present on OVS and on the Membrane of Capacitated Caudal Sperm

How do the lipid bilayers of the OVS and the sperm membrane come close to each other to facilitate fusion? In an attempt to investigate the molecular interactions underlying the fusion of OVS with sperm membrane, I investigated the presence and localization of CD9 and the α v subunit of α v β 3 integrin which are known to facilitate membrane fusion (Escrevente et al., 2011), on OVS and sperm. Western blotting and indirect immunofluorescence analysis were carried out with anti-CD9 and anti- α v integrin antibodies. Immunofluorescence data showed the presence and distribution patterns of CD9 and α v integrin subunit on sperm membrane over the head, the midpiece, and on the principal piece. CD9 was less abundant on the head than on the flagellum where it was confined to the proximal principal piece (**Fig. 18A, a-b**). However, the α v integrin extended distally beyond the proximal region of the principal piece (**Fig. 18A, c-d**). Control sperm samples treated with the IgG isotype gave no signal (**Fig. 18A, e-f**), confirming the specificity of the antibodies. Western blotting analysis revealed the presence of CD9 (24 kDa) and α v integrin subunit (130 kDa) on OVS from both induced estrus oviductal fluid as well as from spontaneous proestrus/estrus and diestrus/metestrus (**Fig. 18B**). 3D SR-SIM analysis revealed that α v integrin subunit co-localized with OVS after *in vitro* fusion with sperm (**Fig. 18C, a-b**). Interestingly, endogenous α v integrin subunit was seen on both the head and the flagellum (midpiece and principal piece) with an accumulation of the signal at the neck (**Fig. 18C, b**), similar to PMCA4a (**Fig. 15, 16**). Exogenous α v integrin transferred by OVS was also seen in these regions. This spatial relationship of α v integrin and PMCA4a suggests that α v β 3 integrin might be involved in the delivery of PMCA4 to the sperm surface.

3.10 Effect of the Adhesion Peptide Arg-Gly-Asp (RGD) for the ligand of $\alpha v\beta 3$ on OVS-sperm Fusion

Having demonstrated the presence of αv integrin subunit on mouse sperm and OVS, I next investigated its involvement in their fusion. I elected to study microvesicles on the sperm membrane instead of exosomes, as the latter are not individually detectable with SR-SIM due to the coalescence of the dye from adjacent vesicles. The average number of microvesicles that fused with sperm in the presence or absence of the RGD peptide, the recognition sequence for αv integrin ligand, was determined in four groups. **Fig. 19A** shows that in Group1, the control group, the average # of microvesicles binding to sperm was 18.6. This is significantly different from the 4.7 and 2.8 in Groups 2 and 3, respectively where OVS or sperm were pre-incubated with 1mM RGD (**Fig. 19B,C**). In Group 4 where both OVS and sperm were separately pre-incubated with 1 mM RGD, the greatest reduction in OVS binding/fusion was seen with a mean of 2 (\pm SEM) (**Fig. 19D**). ANOVA revealed that Groups (2-4) showed significantly reduced OVS-sperm fusion ($P < 0.001$) compared to the control (group 1) (**Fig. 19E**).

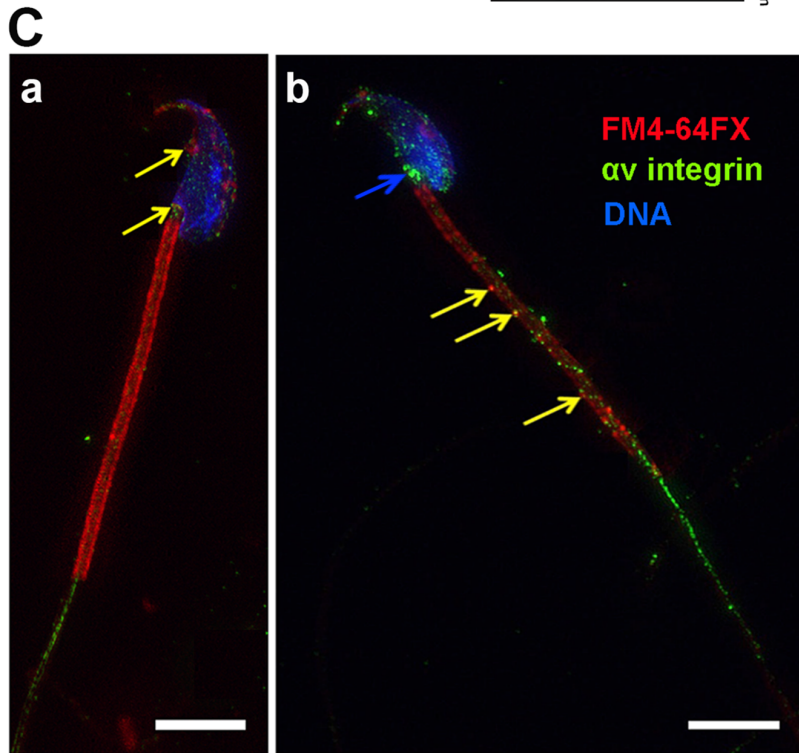
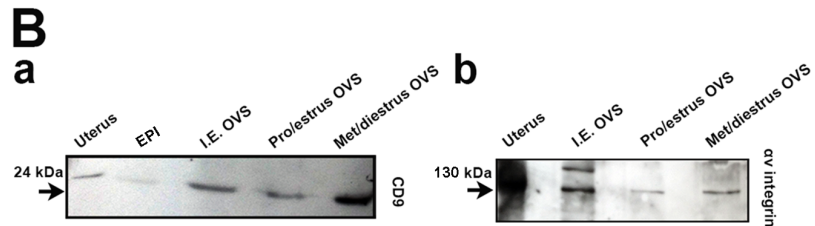
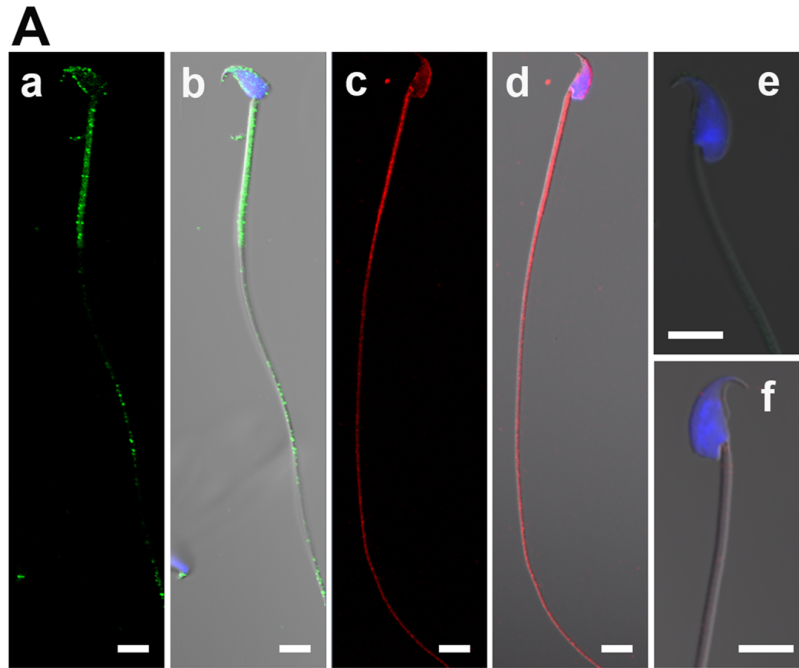


Figure 18. Localization of CD9 and the αv subunit of $\alpha v \beta 3$ integrin on sperm and OVS. (A) Distribution of CD9 and αv integrin on sperm studied by immunofluorescence and confocal microscopy. CD9 (green, a-b) and αv integrin (red, c-d) localized on the midpiece, the proximal principal piece, and the over the acrosome. Sperm nuclei were stained with DAPI (blue). IgG control did not give any signal (e-f). (B) Western blotting analysis performed with anti-CD9 (a) and anti- αv integrin (b) antibodies on OVS recovered from oviductal fluid, proestrus and estrus combined and metestrus and diestrus combined, as well as hormonally-induced estrus (I.E OVS), using epididymosomes (EPI) and uterus as positive controls, respectively. The 24 kDa CD9 and the 130 kDa αv integrin are present in all the OVS. (C) Co-localization of FM4-64FX-labeled OVS and αv integrin on caudal sperm following co-incubation and in vitro fusion, using 3D SR-SIM. Immunofluorescence reveals that αv integrin co-localizes with OVS on the sperm membrane. The localization pattern is similar to PMCA4a, over the acrosome, neck (blue arrow), mid-piece and the proximal principal piece of sperm flagellum. The yellow arrow shows the overlap between the red FM4-64FX and the green αv integrin signal. Sperm nuclei were stained blue with DRAQ5. Images were captured with a 63x Plan-Apochromat oil immersion objective (numerical aperture of 1.4). Scale bars = 5 μm .

3.11 Effect of Integrin Ligands, Vitronectin (VN) and Fibronectin (FN), on OVS-sperm Fusion

To confirm the inhibitory effect of the RGD peptide on OVS-sperm fusion, exogenous ligands (with the RGD interaction motif) for two integrin receptors, $\alpha v\beta 3$ known to be abundantly expressed on the head in acrosome-reacted mouse and human sperm (Fusi et al., 1996; Boissonnas et al., 2010) and $\alpha 5\beta 1$ in capacitated human sperm (Bronson and Fusi, 1996; Fusi et al., 1996), were used to block receptor-ligand interaction in co-incubation assays. Using acrosome-reacted and capacitated sperm in the assay with the appropriate ligand, VN and FN, respectively; our study revealed a marked reduction in the number of microvesicles present on the sperm membrane. There was a mean # of 27.7 (\pm SEM) on control sperm which differed significantly ($P < 0.001$) from the 17 seen in the presence of 10 μ g/ml FN in the incubation mixture (**Fig. 20A**). For acrosome-reacted sperm in the presence of 600 nM VN, respectively, the inhibitory effect was greater with the mean numbers of microvesicles being 32.3 *versus* 1.03 ($P < 0.001$) (**Fig. 20B**). It should be noted that microvesicles were detected on both the flagellum and the inner acrosomal membrane, indicating that cargo delivery occurs on the sperm head after the AR.

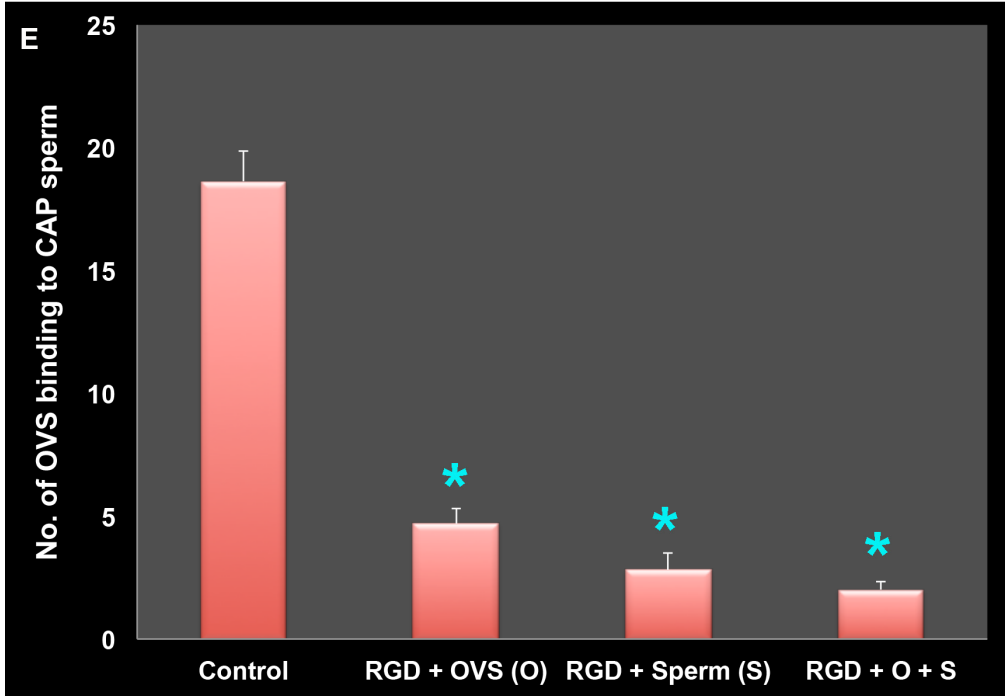
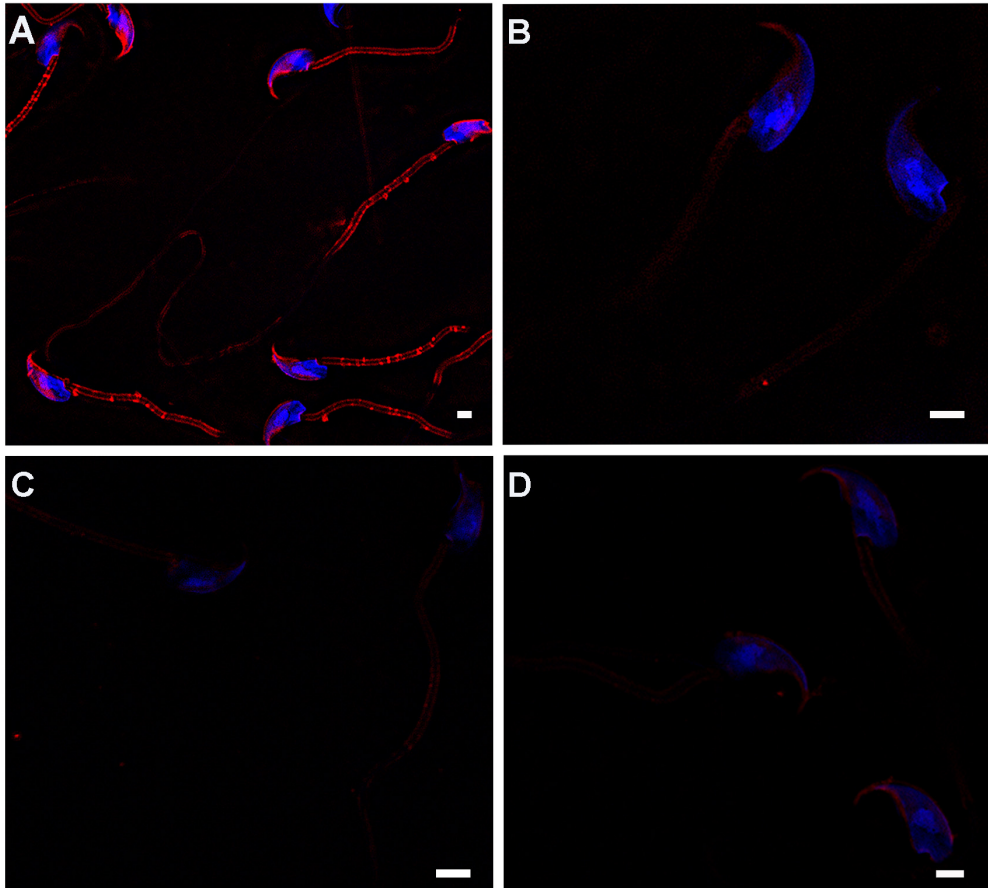


Figure 19. Effect of RGD peptide on mouse OVS-sperm in vitro fusion (via co-incubation assays), as assessed in capacitated (CAP) sperm and visualized by 3D SR-SIM. (A) Control sperm (group 1) acquire pre-FM4-64FX-labeled OVS following co-incubation in the presence of 0 mM RGD. **(B-D)** The effect of 1 mM RGD peptide on OVS-sperm fusion following pre-incubation of OVS (group 2), sperm (group 3), or both (Group 4), respectively; for 40 min at 37°C is demonstrated. Sperm nuclei were stained blue with DAPI. Scale bars = 1 μ m. **(E)** OVS-sperm fusion was significantly ($*P < 0.001$) inhibited in the presence of RGD in each of the 3 groups (2-4) compare to control (group 1), with the effects appearing to be additive in group 4. Data are presented as the average # of OVS (microvesicles) per sperm in each group. Data represent (mean \pm SEM).

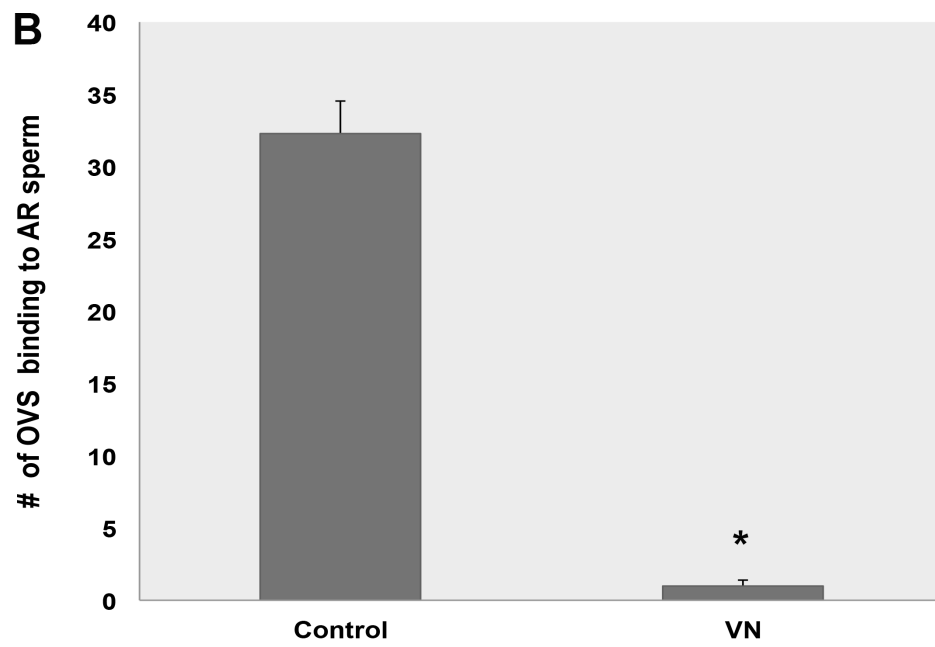
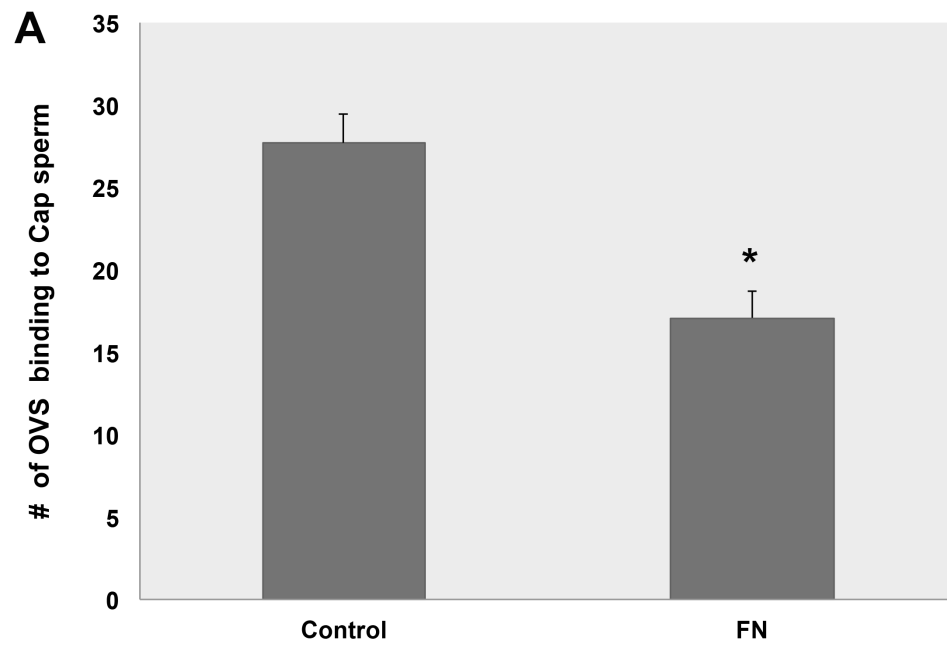


Figure 20. Effect of fibronectin (FN) and vitronectin (VN) on mouse OVS-sperm in vitro fusion (via co-incubation assays), as assessed in sperm and visualized by 3D SR-SIM. Fusion rate or mean (\pm SEM) number of OVS (microvesicles) fused with capacitated (**CAP, A**) or acrosome-reacted (**AR, B**) sperm was calculated following co-incubation of pre-FM4-64FX-labeled OVS and sperm in HTF medium supplemented with 10 μ g/ml FN or 600 nM VN, respectively; for 3 h at 37°C in dark. Data presented as the average # of OVS per sperm in each group. Data represent (mean \pm SEM). *Values are significantly different from control with 0 μ g/ml FN ($P < 0.001$) or 0 nM VN ($P < 0.001$).

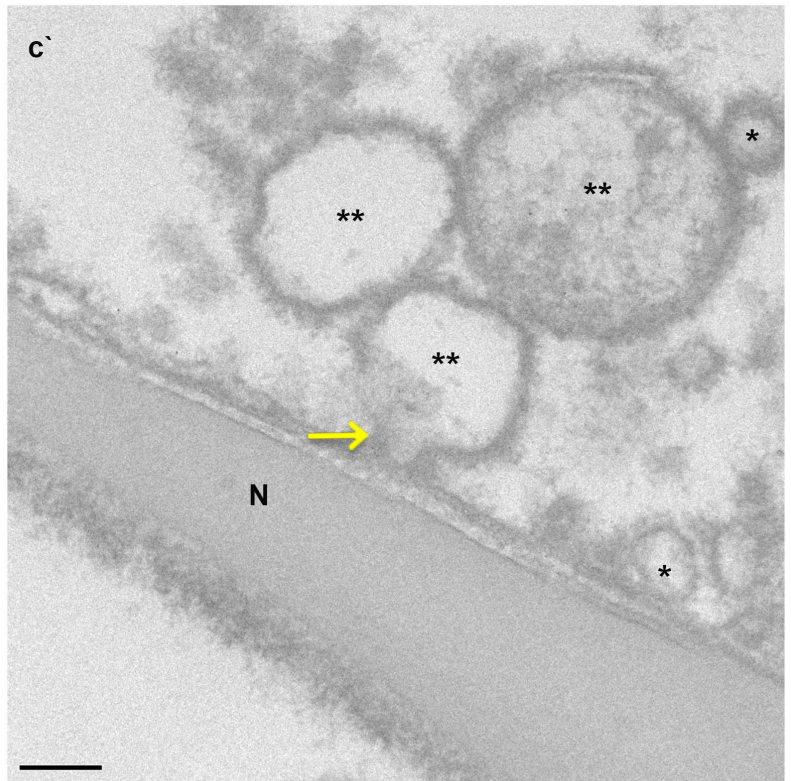
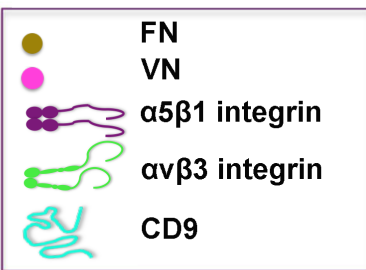
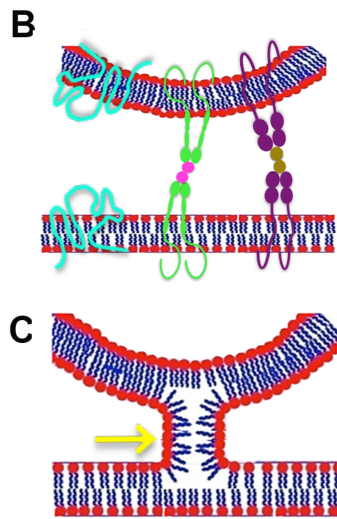
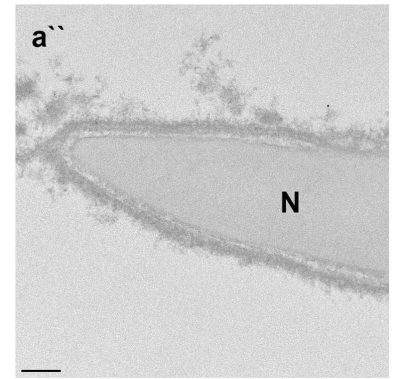
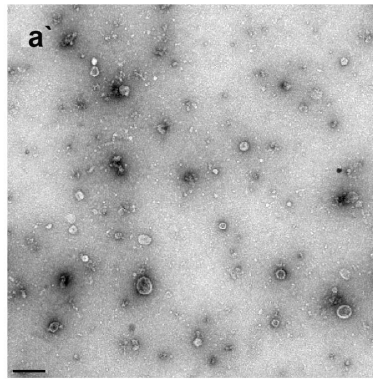
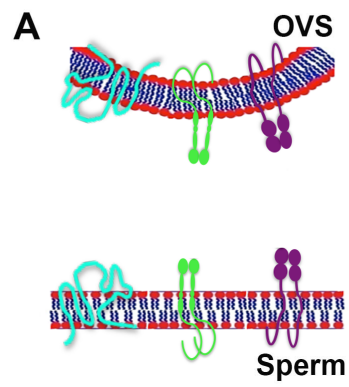


Figure 21. Schematic model showing molecular interactions in OVS-sperm fusion. (A) CD9 generates fusion-competent sites on the membranes of both the OVS and the sperm. OVS (a`) and sperm membrane (a`) carry adhesion proteins such as $\alpha 5\beta 1$ and $\alpha v\beta 3$ integrins. (B) The respective ligands for these integrins, fibronectin (FN) and vitronectin (VN) bind to their activated receptor upon capacitation and acrosome reaction, respectively. These integrins facilitate the adhesion of the two membranes by bringing them close together. (C) Close proximity of the membranes leads to electrostatic repulsion between the apposed polar heads of the lipids and the opening of the outer leaflets of the membranes resulting in a fusion stalk formation (c`, yellow arrow). Transmission electron micrographs (a`, a`, c`) support the proposed model of membrane fusion. N = nucleus; * = exosomes (size < 100 nm); ** = microvesicles (size ranging from 100 nm to 1 μ m). Bar represents 200 nm.

3.12 Fertility of *Pmca4* KO Female Mice is Unaffected

To determine the impact of the acquisition of oviductal PMCA4 on sperm via OVS, it was important to assess the fertility of *Pmca4* null females. To investigate the fertility level of *Pmca4* null females, matings of *Pmca4*^{+/+} (WT) males and females, *Pmca4*^{+/+} males and *Pmca4*^{+/-} females, *Pmca4*^{+/-} males with *Pmca4*^{+/-} females, and *Pmca4*^{+/-} males with *Pmca4*^{-/-} females were set up. There were no significant differences in the mean litter sizes in the four mating groups. **Table 1** and **Fig. 22** shows that *Pmca4*^{-/-} females are fully fertile with a mean litter sizes 8.7 ± 0.6 pups [$n = 32$, where n is the number of litters]) versus control WT female mated to WT male (8.4 ± 0.4 pups [$n = 53$]) or *Pmca4*^{+/-} female mated with WT or *Pmca4*^{+/-} male (9.2 ± 0.8 pups [$n = 14$] or 8.6 ± 0.5 pups [$n = 60$]), respectively.

3.13 Upregulation of PMCA1 Protein in *Pmca4*^{-/-} Oviduct

Western blot analysis revealed an increase in of PMCA1 protein expression in *Pmca4* null oviduct (KO, 5.03 ± 0.176 versus WT, 1.4 ± 0.34 normalized using brain; $P < 0.001$; $n = 3$ for each group (**Fig. 23**).

3.14 Detection of Mg²⁺-dependent Ca²⁺-ATPase Activity in Murine OVS and in *Pmca4* Null Sperm before and after Co-incubation with OVS

Ca²⁺-ATPase activity was observed in WT and *Pmca4* KO OVS (**Fig. 24A**). Following co-incubation of sperm and OVS, there were significant increases in Ca²⁺-

ATPase activity in WT sperm with WT OVS ($P < 0.01$) and *Pmca4* KO sperm with WT OVS ($P < 0.003$) (**Fig. 24B**).

3.15 Calcium Handling in *Pmca4* Null Sperm

$[Ca^{2+}]_i$ level in WT and *Pmca4* KO sperm before and after co-incubation with OVS was studied. $[Ca^{2+}]_i$ level in *Pmca4* KO sperm was significantly ($*P = 0.022$) increased compared to WT (**Fig. 25 A**), as expected. Interestingly, $[Ca^{2+}]_i$ level in *Pmca4* KO sperm was returned to near normal (control value of WT, **Fig. 24 B**) after co-incubation with OVS for 3 h (**Fig. 25 C**), suggesting the successful delivery of oviductosomal PMCA4 to *Pmca4* KO sperm, $*P = 0.015$. Also, for WT sperm co-incubation with OVS for 3 h $[Ca^{2+}]_i$ decreased to levels that approached significance ($P = 0.05$) (**Fig. 25 B**).

3.16 Effect of Co-incubation of OVS on Progressive Motility of *Pmca4* KO Sperm

I observed a significant increase in the percentages of progressive motility in *Pmca4* KO sperm after *in vitro* co-incubation for 0.5 h-2 h with OVS ($*P = 0.001$, $*P = 0.0004$ and $*P = 0.007$, respectively), compared to *Pmca4* KO in PBS (0.5 h - 2 h) (**Table 2; Fig. 26**).

Table 1. Litter sizes born to mating pairs of different genotypes, all on FVB/N background.

Genotypes of Mating Pairs Female x male	# Pairs	# Litters	Total # of pups	Mean # pups/ Litter.	± SEM	<i>P</i>
<i>Pmca4</i> ^{+/+} x <i>Pmca4</i> ^{+/+}	1	53	443	8.4	± 0.386	N/A
<i>Pmca4</i> ^{+/-} x <i>Pmca4</i> ^{+/+}	1	14	101	9.2	± 0.835	N/A
<i>Pmca4</i> ^{+/-} x <i>Pmca4</i> ^{+/-}	1	60	517	8.6	± 0.455	N/A
<i>Pmca4</i> ^{-/-} x <i>Pmca4</i> ^{+/-}	1	32	278	8.7	± 0.613	N/A

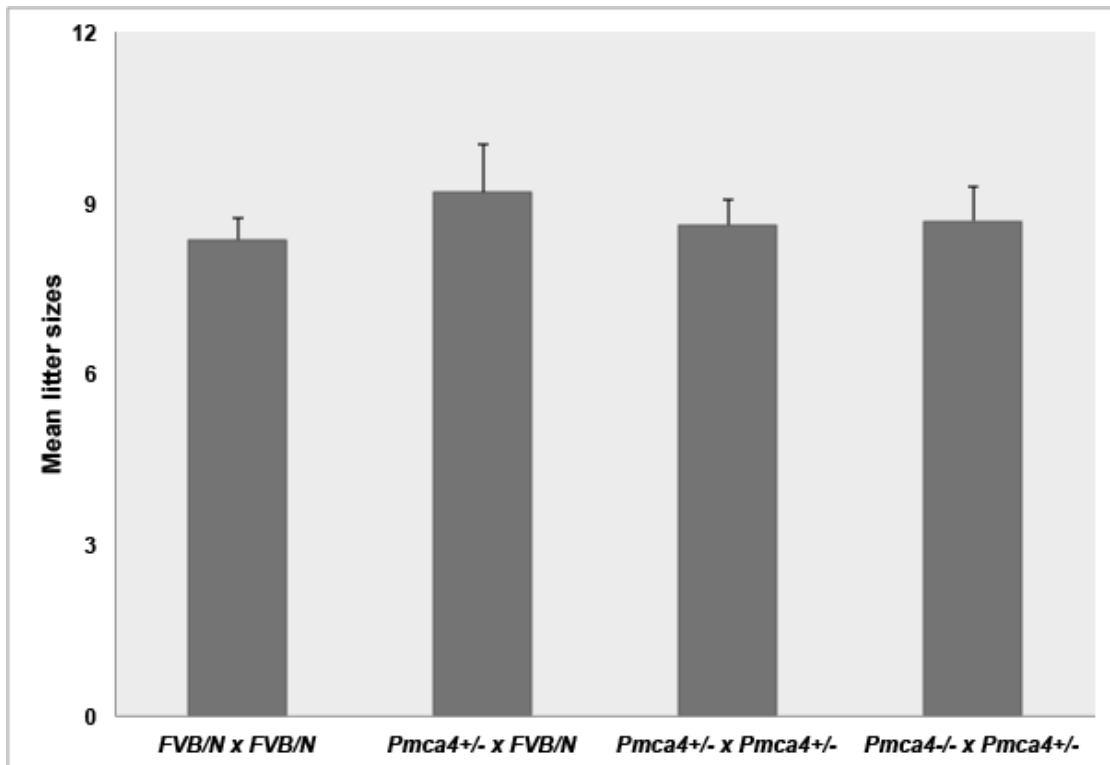


Figure 22. Distribution of the mean litter sizes from matings of males and females with different *Pmca4* genotypes. No significant difference in mean litter sizes was detected for *Pmca4*^{-/-} female mating compared to WT and heterozygous female matings.

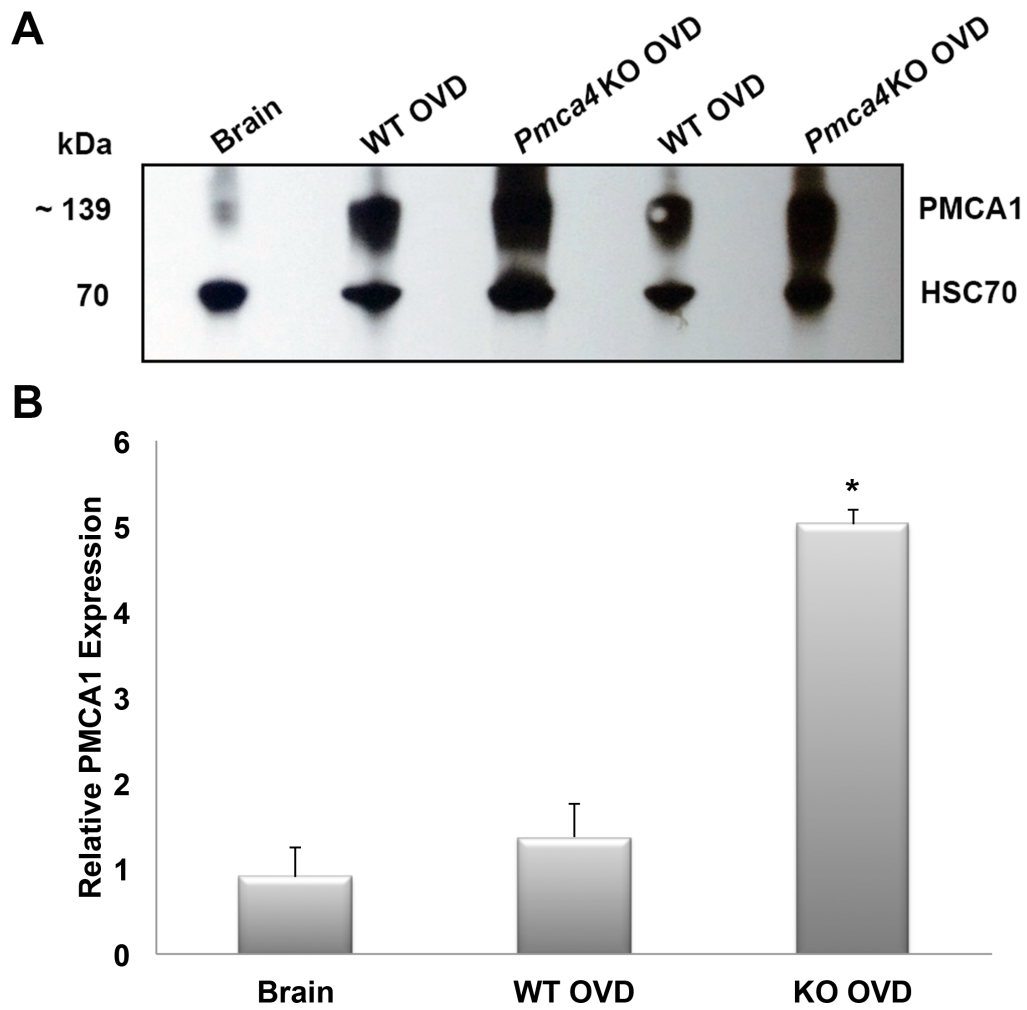
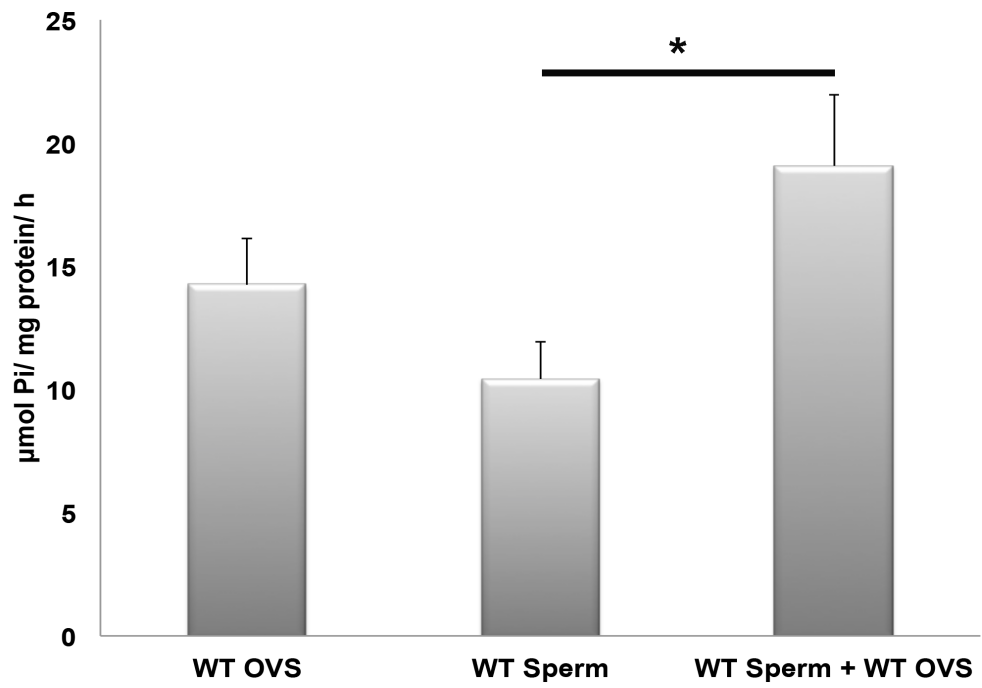


Figure 23. Western blot analysis of PMCA1 protein expression in oviducts (OVD) from *Pmca4* KO and WT females. A representative membrane (A) is shown above the bar graphs (B). Data in the graph represent mean intensities \pm SEM of three independent experiments ($*P < 0.001$). Brain tissue extract was used as a positive and HSC70 as a reference protein (loading control).

Ca²⁺-ATPase activity in WT caudal sperm



Ca²⁺-ATPase activity in KO caudal sperm

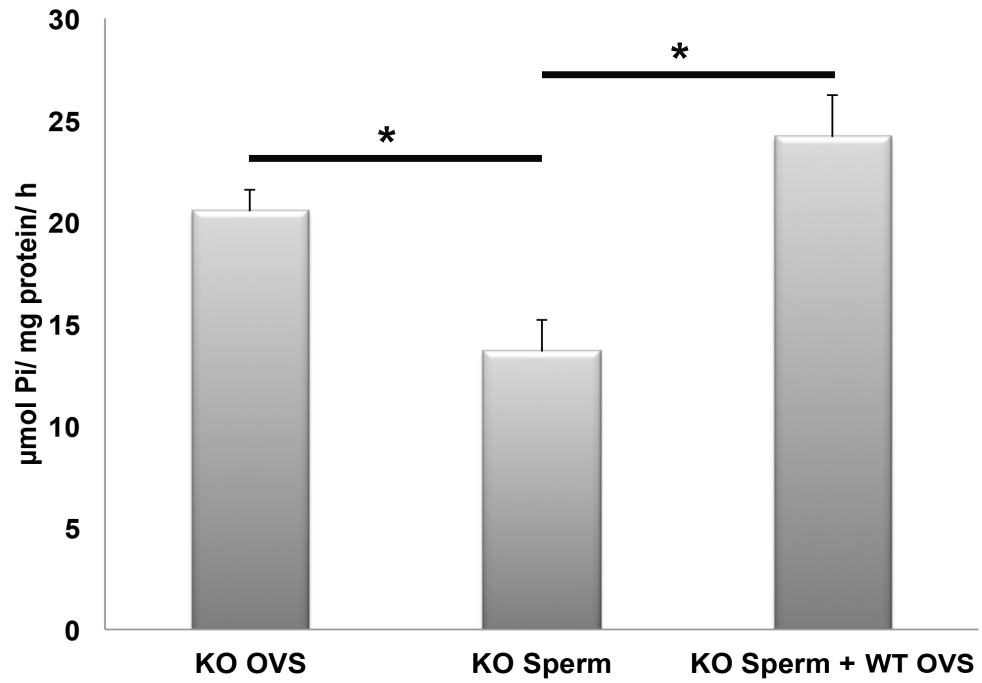


Figure 24. Determination of Mg²⁺-dependent Ca²⁺-ATPase activity in OVS and sperm and after their co-incubation and inhibition of mitochondrial activity with oligomycin. (A) OVS from WT and oviductal fluids showed higher levels Ca²⁺-ATPase activity than WT sperm and there is a significant ($P < 0.01$) higher Ca²⁺-ATPase activity after co-incubation with OVS. **(B)** Ca²⁺-ATPase activity was detected in OVS from *Pmca4* KO oviductal fluids which is significantly ($P < 0.004$) higher than *Pmca4* KO sperm. Co-incubation of *Pmca4* KO sperm with WT OVS showed a significant higher Ca²⁺-ATPase activity ($P < 0.003$), compared to *Pmca4* KO sperm without co-incubation. Data are expressed as means \pm SEM from three independent experiments. Vertical bars indicate SEM. *Statistically significant differences.

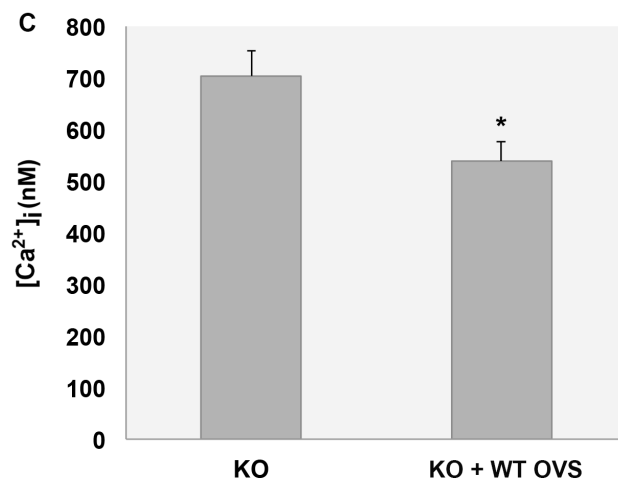
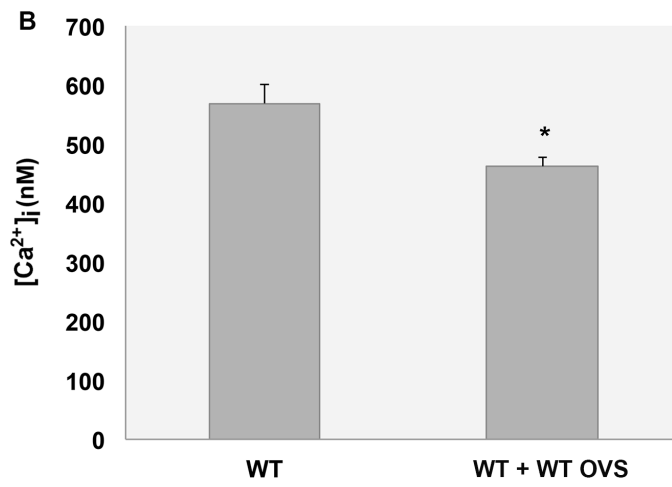
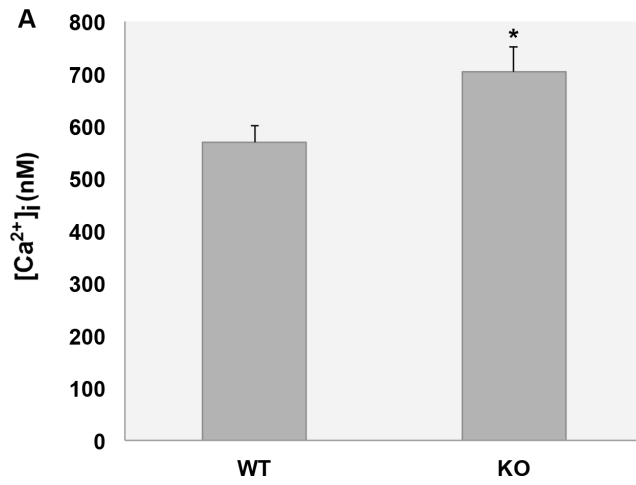


Figure 25. $[Ca^{2+}]_i$ changes in Fluo-4 loaded, washed and selected sperm. (A-C) Histograms of the mean (\pm SEM) basal $[Ca^{2+}]_i$ levels in selected uncapacitated sperm in the absence of Ca^{2+} during Fluo-4 loading. **(A)** Significant ($*P = 0.022$) increase in $[Ca^{2+}]_i$ level in *Pmca4* KO sperm, compared to WT (n = 21 for each group). **(B)** Near significant ($P = 0.05$) decrease in $[Ca^{2+}]_i$ level in WT sperm after co-incubation with OVS, compared to WT (n = 8 and 21, respectively). **(C)** Significant ($*P = 0.015$) decrease in $[Ca^{2+}]_i$ level in *Pmca4* KO sperm after co-incubation with OVS, compared to *Pmca4* KO sperm (n = 14 and 21, respectively).

Table 2. Percentage of *Pmca4* KO Sperm with progressive motility after co-incubation with WT OVS for different time periods (0.5 h - 2 h). *

Time points (h)	0.5 h		1 h		2 h	
Group	C	T	C	T	C	T
# Motile	12	43	8	41	2	19
# Immotile	281	275	260	302	243	284
Total	293	318	268	343	235	303
Motility (%) \pm SEM	4.42 \pm 0.4	16.02 \pm 0.1	3.24 \pm 0.09	12.56 \pm 1.6	0.88 \pm 0.08	7.56 \pm 1.9
<i>P</i> value	* <i>P</i> = 0.0001		* <i>P</i> = 0.0004		* <i>P</i> = 0.007	

*n = 3 for test and control (C)

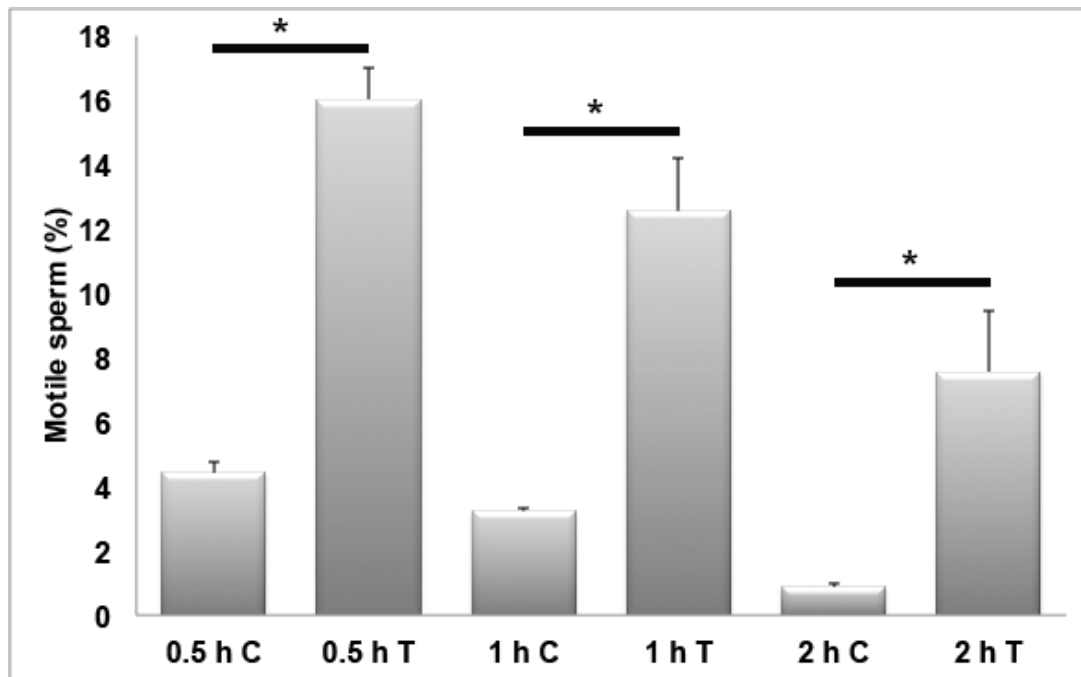


Figure 26. Progressive motility rates of *Pmca4* KO sperm following co-incubation with OVS for different periods of time. Significant increase in progressive motility rates were observed after 0.5h -2h (**P* = 0.01, *P* = 0.0004 and **P* = 0.007, respectively), compared to control co-incubated in PBS.

Chapter 4

DISCUSSION

4.1 Expression and Secretion of PMCA4a in the Murine Female Reproductive Tract

Of the two major splice variants of PMCA4, 4a and 4b, 4a is faster in extruding Ca^{2+} and returning cytosolic Ca^{2+} concentration to resting levels (Caride et al., 2007). Since sperm in the oviduct, particularly the AIJ, have high levels of intracellular Ca^{2+} (Suarez and Pacey, 2006), they need effective efflux mechanisms to prevent Ca^{2+} overload in order to maintain their viability and fertilizing ability. The mRNA data (**Fig. 5A**) revealed that both *Pmca4a* and *4b* isoforms are expressed in reproductive tissues collected from all three regions of the tract of females undergoing estrus. Since estrus, is the only time when females are receptive to the male and when sperm are likely to be present in the tract, the presence of *Pmca4a* and *4b* mRNAs may be related to sperm capacitation. Therefore their presence in the oviduct, where sperm undergo hyperactivation, with the activation of Ca^{2+} influx by CatSper (Qi et al., 2007), may be physiologically relevant. The RT-PCR results were corroborated by the high level of PMCA4a in the oviductal apical epithelium and in the OLF. This elevated expression of the more efficient PMCA4a appears to be necessary to maintain Ca^{2+} homeostasis when the demand for efflux is great.

When PMCA4a protein was examined by IF in naturally cycling females, it was found to be expressed in the uterine myometrium in all four stages of the estrus cycle (**Fig. 8**). This suggests that the pump plays a key role in the maintenance of uterine function by helping to regulate membrane potential and intracellular Ca^{2+} .

However, during the estrus and pro-estrus phases, unlike metestrus and diestrus, in addition to its presence in the myometrium, there was up-regulation of PMCA4a in the uterine endometrium, as seen in the luminal and glandular epithelia. This suggests that the transcription of the *Pmca4* gene and/or the alternative splicing of its primary RNA transcripts are/is under the control of female hormones. Indeed, a bioinformatics analysis of the promoter region of the *Pmca4* gene for the presence of estrogen response elements (EREs) revealed at -313-335 a potential ERE sequence, 5'-GGGCTgacTGACC-3'. Although this sequence contains two mismatches compared to the consensus ERE (Driscoll et al., 1998), it fulfills the requirement for ER-ERE binding for estrogen responsive genes (Driscoll et al., 1998). Further studies will be needed to determine the mechanism of estrogen-mediated up-regulation of PMCA4a expression in the female reproductive tract.

To study PMCA4a during estrus, virgins were superovulated and sections of all three regions of the female tract analyzed. IF revealed that in addition to the uterus, the vagina and the oviduct showed high expression of PMCA4a. The low mRNA levels seen in the vagina might be due to inter-individual variation in mice in estrus since different animals were used for protein and mRNA assays. Importantly, all three ductal regions had the strongest PMCA4a staining on the luminal side of the apical membrane of the epithelium. This finding parallels that seen in the epididymis (Patel et al., 2013) and is consistent with the secretion of PMCA4a in these tissues into the lumen as seen in other tissues for other PMCA4s (Belan et al., 1996; Lee et al., 1997; Reinhardt et al., 2000; Post et al., 2002).

Western analysis corroborated the IF results and revealed the presence of the ~128 kDa PMCA4a band in all female reproductive tissues as well as in the luminal fluids. Interestingly, in naturally cycling females while fluids collected during metestrus/diestrus had only marginal levels of PMCA4a, those collected during proestrus/estrus had elevated levels of the protein, as seen after induction of superovulation (**Fig. 9A**). Here, PMCA4a was most abundant in OLF. These findings are similar to that for SPAM1, a GPI-linked sperm protein which was found to be present on uterosomes, vesicular particles in the uterine fluid (Griffiths et al., 2008b) during estrus. However, unlike GPI-linked proteins that are found in both the particulate and the soluble fraction of the LF (Zhang and Martin-DeLeon, 2003; Griffiths et al., 2008a), I found PMCA4a exclusively in the particulate fraction of the oviductal LF and the uterosomes. This localization is consistent with the PMCA4a's transmembrane structure which has its catalytic domain on the cytosolic side of the membrane (Strehler et al., 2007).

4.2 Isolation, Identification and Characterization of Exosomes/microvesicles in the Oviductal Luminal Fluid

OVS (exosomes/microvesicles) were identified for the first time, and characterized as exosomes and microvesicles based on negative staining, shape, size, membrane orientation (cytoplasmic-side inward), and the CD9 exosomes biomarker. These OVS are likely to originate as internal vesicles of multivesicular bodies (MVBs) with a unique orientation (cytoplasmic-side inward) (Pisitkun et al., 2004; They et al., 2009). It is also possible that they could result from an apocrine pathway resulting from blebbing of the apical membrane of the epithelial lining, as reported for

epididymosomes in the male reproductive tract (Hermo and Jacks, 2002). Whatever their origin, they are likely to play a role in cell-cell communication.

4.3 Transport of PMCA4a from the Female Reproductive Luminal Fluids to Sperm During Capacitation

EVs are thought to be the vehicle of transport of proteins from luminal fluids to the sperm surface (Frenette and Sullivan, 2001; Saez et al., 2003). Accordingly, I detected the transfer of PMCA4a from unfractionated FLF and from OVS to caudal sperm *in vitro* with increases of up to ~3-fold. Our finding strongly suggests that PMCA4a is acquired by sperm *in vivo* during their transit in the female tract. **Fig. 13** provides some initial insight into the mechanism of uptake, as I detected that OVS are not only necessary but are sufficient for the transfer of PMCA4a to the sperm. The presence of PMCA4a's uptake from reconstituted OVS, in the absence of soluble proteins in the FLF, is supportive of this conclusion.

To date, it is unknown how exosomes/microvesicles deliver transmembrane proteins to the sperm membrane. Our lab showed epididymosomes and uterosomes docking on the sperm membrane during the delivery of SPAM1, a GPI-linked protein (Griffiths et al., 2009). Schwarz and others proposed a fusogenic mechanism (Schwarz et al., 2013). CD9 is present in OVS and is known to facilitate fusion (Caballero et al., 2013). Based on these reports, I proposed that OVS fuse with the sperm membrane.

4.4 Evidence for the Fusion of OVS and Sperm Membranes

The use of nanoscopy or 3D SR-SIM provided some understanding of the mechanism by which sperm interact with EVs. Sperm analyzed by nanoscopy after incubation with fluorescently-labeled OVS revealed the label predominantly on the head, the midpiece and the proximal principal piece. This distribution of the label is similar to that previously reported on mouse sperm for epididymosomes and uterosomes, with confocal microscopy (Griffiths et al., 2008a). With 3D SR-SIM I was able to detect distinct punctate, as well as continuous, labeling on the sperm membrane, reflecting the contributions from microvesicles and exosomes, respectively. High magnification TEM analysis of sperm co-incubated with unlabeled OVS confirmed the contribution of both types of EVs to the sperm plasma membrane, as both could be seen in various stages of attachment to the sperm membrane (**Fig. 17B, D**). These stages include the stalk formation (**Fig. 21a, a'', c**), which is a major step in membrane fusion (Kozlov et al., 1989).

Prior to fusion, the membrane lipid bilayers must establish close proximity (a distance of < 0.5 nm) within a small area ~ 10 nm (Leikin et al., 1987; Kozlov et al., 1989; Chernomordik and Kozlov, 2003). This will increase the electrostatic repulsion between apposed polar heads of the lipid molecules of the bilayers leading to an opening of the monolayers at the interacting area (**Fig. 21**). This tension leads to the rupture of the separated monolayers, followed by formation of a stalk formation and hydrophilic pore (**Fig. 21**). The aqueous environment in the hydrophilic pore will ultimately lead to spreading of the membrane to complete fusion of the membrane (Leikin et al., 1987; Kozlov et al., 1989; Chernomordik and Kozlov, 2003). It is

known that vesicular curvature enhances fusion (Pencer et al., 2008). Thus it is likely that exosomes with their smaller size and therefore greater curvature would have a greater fusion rate than the larger microvesicles. Our observation of the continuous bright fluorescent label on the midpiece (**Fig. 15, 16**) and the close alignment of exosomes on the sperm plasma membrane detected by TEM in this region, as well as on the head (**Fig. 17D**), would be consistent with a greater fusion rate for exosomes on the sperm surface. In general our findings are in support of a fusogenic mechanism proposed by Schwartz et al. for the transfer of PMCA4 to bovine sperm via epididymosomes (Schwarz et al., 2013).

The use of nanoscopy uncovered the localization of PMCA4 in different subcellular compartments of murine sperm. To date, PMCA4 has been localized on the membrane over the acrosome and on the proximal principal piece of the flagellum of murine sperm (Wennemuth et al., 2003; Okunade et al., 2004; Schuh et al., 2004; Aravindan et al., 2012). In addition to being present over the acrosome, with nanoscopy PMCA4 was detected on the inner acrosomal membrane (IAM), the posterior head, and the neck where the staining often appeared to be intense. Its presence on the IAM and neck may be of physiological relevance. Additional PMCA4 on the IAM would be advantageous to return Ca^{2+} to resting levels after the markedly high influx associated with the AR (O'Toole et al., 2000; Ho et al., 2002; Ho and Suarez, 2003; Suarez and Ho, 2003), particularly after the loss of PMCA4 molecules on the plasma membrane over the acrosome following this reaction. While the significance of PMCA4 at the neck is not readily apparent, it is known that in human sperm there is a Ca^{2+} store at the neck (Costello et al., 2009), where PMCA4

immunostaining has been shown to be intense in human sperm (Andrews and Martin-DeLeon, *in preparation*). If such a Ca^{2+} store exists in the neck of the murine sperm, its close proximity to PMCA4 would be parallel to the situation in humans and would highlight the spatially regulated nature of Ca^{2+} signaling.

In addressing the molecular forces that underpin the fusion of OVS and sperm membrane, I focused my attention on CD9 tetraspanin, which is known to build scaffolds and fusion competent sites (They et al., 2002; They et al., 2009), and αv integrin which is a subunit of $\alpha v\beta 3$. The latter is an adhesion molecule (Seftor et al., 1992; Danen et al., 1994) known to be present on the sperm head and to play a role in sperm-egg fusion (Boissonnas et al., 2010). I report for the first time the presence of both CD9 and αv integrin subunit on the murine sperm flagellum, with the latter extending distally in the principal piece and thereby being more broadly distributed than CD9 which is predominantly on the midpiece (**Fig. 18**). Interestingly, both of these proteins were earlier shown to be present on the IAM and to increase in abundance after the acrosome reaction (Boissonnas et al., 2010; Ito et al., 2010). Because I detected that OVS are able to bind to the IAM after the acrosome reaction, as well as the plasma membrane (**Fig. 20, 14**), CD9 and αv integrin subunit could be temporally and spatially related to OVS on the sperm head. However, their presence on the midpiece and the proximal principal piece to which OVS preferentially bind is relevant to sperm-OVS fusion. Thus, I investigated their existence in OVS and show their presence by Western blot analysis (**Fig. 18B**). Having previously shown the presence of CD9 in OVS by immunoelectron microscopy (Al-Dossary et al., 2013), I confirmed the presence of αv integrin in OVS, using 3D SR-SIM to detect their co-

localization on sperm (**Fig 18**). Thus there is clear evidence that both molecules are present on OVS and sperm at the primary regions where fusion of OVS has been detected.

To detect a functional involvement of αv integrin subunit in OVS-sperm interaction and to support my finding of a fusogenic mechanism by which OVS interact with sperm membrane, I used integrin antagonist peptides [a receptor-ligand blocking assay]. Both the RGD ligand recognition sequence and vitronectin, the ligand for $\alpha v\beta 3$, were able to significantly block sperm-OVS fusion (**Fig. 19, 20**). A similar effect was seen when fibronectin, the ligand for $\alpha 5\beta 1$ integrin which is known to be increased on both human and mouse sperm (Fusi et al., 1992; Fusi et al., 1996), was added to the co-incubation assay (**Fig. 20**). These findings indicate that integrins play an important role in OVS-sperm interaction and fusion. Since it has been shown that mammalian sperm express fibronectin and vitronectin as well as their receptors, $\alpha 5\beta 1$ integrin and $\alpha v\beta 3$ integrin at their surface after capacitation and acrosome reaction, respectively (Fusi and Bronson, 1992; Fusi et al., 1996; Thys et al., 2012), our data provide support for a receptor-ligand interaction in sperm-OVS interaction and fusion. Based on the finding that the effect of the RGD blocking on both the sperm and the OVS appeared to be additive, compared to blocking each separately (**Fig. 19**) as well as an analogous receptor-ligand interaction reported for sperm-oocyte interaction (Boissonnas et al., 2010), I propose a schematic model in **Fig. 21**. In this model I show the involvement of CD9 which acts as a scaffold protein (Peddibhotla et al., 2013) to tether adhesion molecules such as $\alpha v\beta 3$ integrin (Peddibhotla et al., 2013) with which it co-localizes on sperm. During capacitation and acrosome reaction when OVS are

released and the ligands are increased on sperm (Bronson and Fusi, 1996; Fusi et al., 1996) the ligands will form a connecting bridge between the membranes of sperm and OVS, bringing them in close proximity. It is likely that exogenous ligand could prevent the membranes from coming in close proximity and thereby decrease the ability of the membranes to make contact and ultimately fuse.

4.5 Delivery of Transmembrane Proteins to the Sperm Surface via Membrane Fusion

We have previously provided evidence that in murine epididymis sperm are able to acquire PMCA4 during their maturation as they travel from the caput to the cauda and that epididymosomes can deliver it to caudal sperm *in vitro* (Patel et al., 2013). Similar findings were obtained for bovine sperm and epididymosomes (Schwarz et al., 2013) and OVS were also shown to deliver PMCA4 *in vitro* to murine sperm (Al-Dossary et al., 2013). Using 3D SR-SIM, I showed co-immunolocalization of PMCA4 and fluorescently-labeled OVS that were fused to the sperm surface, providing evidence that OVS deliver their cargo via fusion. Interestingly, I detected fusion and delivery of PMCA4 to be predominant on the midpiece, a location where it has not been reported in caudal sperm where it is found on the proximal principal piece in addition to being over the acrosome (Wennemuth et al., 2003; Okunade et al., 2004; Schuh et al., 2004; Aravindan et al., 2012). The plasma membrane over the proximal principal piece and the acrosome in murine sperm is known to be lipid rafts microdomains (Travis et al., 2001; Asano et al., 2009) which are locations where PMCA4 is found in somatic cells (Sepulveda et al., 2006) and where signal

transduction occurs (Sleight et al., 2005). It is likely that there is rearrangement of these domains to re-position PMCA4 in lipid rafts (Cross, 2004) in the midpiece.

In addition to PMCA4, I have observed that the αv subunit of $\alpha v\beta 3$ integrin can also be delivered to sperm, as merging of the fluorescent signals for OVS and the protein could be detected on sperm following co-incubation (**Fig. 18C**). Since $\alpha v\beta 3$ is an important sperm protein involved in sperm-egg fusion (Boissonnas et al., 2010) it seems clear that sperm-OVS fusion plays an important role in delivering transmembrane and other membrane-associated proteins to sperm during their final maturational period. Importantly, it should be noted that since PMCA4 is also delivered by epididymosomes (Patel et al., 2013; Schwarz et al., 2013) and by human prostasomes (unpublished observations from the DeLeon Lab), these EVs are likely to use the same fusogenic mechanism herein described.

4.6 The Functional Impact of Delivery Oviductosomal PMCA4 *in Vitro* to *Pmca4* null Sperm

Ca^{2+} -ATPase has been shown to play a crucial role in regulating sperm motility (Breitbart et al., 1985; Kanwar et al., 1993). Moreover, deletion of the gene encoding the major Ca^{2+} -ATPase efflux pump, PMCA4, in murine sperm (Wennemuth et al., 2003) leads to infertility due to loss of both progressive and hyperactivated motility (Okunade et al., 2004; Schuh et al., 2004). Hyperactivated motility is achieved by an increase in sperm $[\text{Ca}^{2+}]_i$ concentration (Ho et al., 2002; Ho and Suarez, 2003; Suarez and Ho, 2003). Lethal $[\text{Ca}^{2+}]_i$ levels were diminished when

bovine sperm were exposed to the apical plasma membrane of oviductal epithelial cells (Boilard et al., 2002). The authors concluded that anchored proteomic factors on the oviductal epithelial cells are responsible for maintaining sperm motility and viability (Boilard et al., 2002). The present study now allows us to identify PMCA4 as a potential major proteomic factor involved in diminishing toxic Ca^{2+} levels in bovine sperm co-incubated with oviductal epithelial cells. Thus I have evaluated the impact of: a) PMCA4 transfer from OVS to sperm *in vivo* and b) delivery of PMCA4 *in vitro* to *Pmca4* null sperm by assessing Ca^{2+} -ATPase activity, Ca^{2+} handling, and motility following PMCA4 delivery via OVS.

Although *Pmca4* null females are not sterile their level of fertility (their litter sizes), compared to WT, has never been investigated. Unsurprisingly, *Pmca4* null females are fully fertile and litter sizes are indistinguishable from WT and heterozygous females (**Fig. 22**). Interestingly, I found that PMCA1 expression is increased in *Pmca4* null oviduct, which likely explains the fertility of *Pmca4* null females observed. Overexpression of PMCA1 appears to compensate for the loss of PMCA4.

In this vein, sperm function was studied *in vitro* in capacitated sperm in the presence and absence of oviductosomal PMCA4. Recently, Schwarz and others provided evidence of improvement of Ca^{2+} -ATPase activity after the delivery of PMCA4 via epididymosomes to bovine caput sperm (Schwarz et al., 2013). However, they did not detect any increase in Ca^{2+} -ATPase activity in bovine caudal sperm after *in vitro* fusion with epididymosomes. Therefore, it would be important to demonstrate

the functionality of the impact of delivery of PMCA4 via OVS to caudal sperm. Interestingly, I found that mouse caudal sperm have a 3-fold increase in PMCA4 protein after *in vitro* fusion with OVS. Thus, I investigated the Ca^{2+} -ATPase activity after *in vitro* fusion with OVS. Indeed, I found a significant ($P = 0.01$ and $P = 0.003$) increased in Ca^{2+} -ATPase activity in WT and *Pmca4* KO caudal sperm, respectively, after *in vitro* fusion with OVS. Interestingly, the levels of Ca^{2+} -ATPase activity in *Pmca4* KO OVS and sperm were similar to those in WT and this is likely due to the expression of elevated levels of PMCA1, since mitochondrial Ca^{2+} -ATPases were blocked with oligomycin in the assays. Perhaps a modulation of Ca^{2+} -ATPase activity assay by adding calmodulin activator to the assay reaction, would stimulate the PMCA4 activity and distinguish between *Pmca4* KO and WT sperm.

In support of the finding of Ca^{2+} -ATPase activity in OVS, I was able to detect a significant ($P = 0.015$) decrease in $[\text{Ca}^{2+}]_i$ in *Pmca4* null sperm after co-incubation with OVS (**Fig. 25**). Moreover, in *Pmca4* null sperm intracellular Ca^{2+} levels were returned to normal, similar to those of WT sperm. Interestingly, I observed significant improvement in motility in *Pmca4* null sperm after co-incubation with OVS. These lines of evidence further support my hypothesis that oviductal PMCA4 that is transferred to sperm via OVS has a functional impact. It should be noted that during the Ca^{2+} loading assay OVS attached or unattached to sperm displayed the Ca^{2+} indicator fluorescence, revealing the presence of Ca^{2+} in these organelles (data not shown). This observation is parallel to that reported for prostasomes, which are

enriched with calcium and other divalent cations (Sullivan and Saez, 2013). It has been proposed that calcium carried by prostasomes could modulate sperm flagellar motility (Fabiani et al., 1995) or stimulate prostaomal ATPase activity (Ronquist et al., 1978). It is not unreasonable to propose that OVS may be performing dual roles in providing Ca^{2+} to modulate flagellar activity as well as the efflux pump to maintain homeostasis following the activity.

Taken together, my study has identified and characterized, for the first time the secretion of exosomes/microvesicles in the oviduct and named them "oviductosomes, OVS". OVS carry a key element of the Ca^{2+} handling toolkit, PMCA4 which is elevated during estrus and is one of the components that are responsible for sperm viability and their final maturation in the female tract, capacitation.

4.7 Conclusions

In light of this study, the following conclusions can be made:

1. For the first time the expression and secretion of PMCA4a in the female reproductive tissues and luminal fluids during estrus was identified.
2. The secretion occurs via EVs called oviductosomes (OVS), which were identified for the first time, from which PMCA4a, and likely 4b, can be acquired by sperm.
3. I have exploited the power of 3D SR-SIM and high magnification TEM to show that OVS fuse with the sperm membrane in delivering their cargo, with exosomes appearing to be more efficient than microvesicles in fusing.
4. I discovered that exosomes/microvesicles, OVS, do not carry/deliver the identical protein cargo and that they carry Ca^{2+} as do prostasomes.
5. The evidence indicates that OVS have both CD9 and integrin, both of which are present on sperm, and the latter is involved in their ability to fuse and deliver their cargo.
6. I localized PMCA4 for the first time on the posterior head, the neck, and on the IAM via nanoscopy, and have shown the physiological relevance of these localizations.
7. There is functional activity of PMCA4 in OVS and Ca^{2+} -ATPase activity is significantly increased in sperm after PMCA delivery via OVS, resulting in diminished $[\text{Ca}^{2+}]_i$.
8. There is an increase in the progressive motility of *Pmca4* null sperm after PMCA4 delivery via OVS.
9. These findings are important for the clinical application in IVF where the success rate is only 32%; this rate might be increased with modifications of current protocols to include the presence of PMCA4 and other fertility-modulating proteins to be discovered, via artificial vesicles.

4.8 Future Studies

1. Western blot used to determine if PMCA1 is differentially expressed in OVS from WT and *Pmca4* KO females.
2. Co-localization assay and 3D SR-SIM analysis to determine if PMCA1 is co-localize with FM4-64FX pre-labeled OVS and deliver to sperm membrane.
3. Uptake study to determine if OVS transfer PMCA1 to the sperm surface.
4. Modulation of Ca^{2+} -ATPase activity assay by adding calmodulin activator or PMCA inhibitors such as La^{3+} and caloxins to the assay reaction, will demonstrate increased PMCA function in between WT, compared to *Pmca4* KO sperm.

REFERENCES

- Adeoya-Osiguwa, S. A. and Fraser, L. R.** (1996). Evidence for Ca²⁺-dependent ATPase activity, stimulated by decapacitation factor and calmodulin, in mouse sperm. *Mol Reprod Dev* **44**, 111-120.
- Aitken, R. J.** (1995). Free radicals, lipid peroxidation and sperm function. *Reprod Fertil Dev* **7**, 659-668.
- Al-Dossary, A. A., Strehler, E. E. and Martin-DeLeon, P. A.** (2013). Expression and secretion of plasma membrane Ca²⁺-ATPase 4a (PMCA4a) during murine estrus: association with oviductal exosomes and uptake in sperm. *PloS one* **8**, e80181.
- Albers, R. W.** (1967). Biochemical aspects of active transport. *Annu Rev Biochem* **36**, 727-756.
- Andrews, J. C., Nolan, J. P., Hammerstedt, R. H. and Bavister, B. D.** (1994). Role of zinc during hamster sperm capacitation. *Biol Reprod* **51**, 1238-1247.
- Aravindan, R. G., Fomin, V. P., Naik, U. P., Modelski, M. J., Naik, M. U., Galileo, D. S., Duncan, R. L. and Martin-DeLeon, P. A.** (2012). CASK interacts with PMCA4b and JAM-A on the mouse sperm flagellum to regulate Ca²⁺ homeostasis and motility. *J Cell Physiol* **227**, 3138-3150.
- Armant, D. R. and Ellis, M. A.** (1995). Improved accuracy of sperm motility assessment using a modified Micro-Cell sperm counting chamber. *Fertil Steril* **63**, 1128-1130.
- Asano, A., Selvaraj, V., Buttke, D. E., Nelson, J. L., Green, K. M., Evans, J. E. and Travis, A. J.** (2009). Biochemical characterization of membrane fractions in murine sperm: identification of three distinct sub-types of membrane rafts. *J Cell Physiol* **218**, 537-548.

- Belan, P. V., Gerasimenko, O. V., Tepikin, A. V. and Petersen, O. H.** (1996). Localization of Ca²⁺ extrusion sites in pancreatic acinar cells. *J Biol Chem* **271**, 7615-7619.
- Boilard, M., Bailey, J., Collin, S., Dufour, M. and Sirard, M. A.** (2002). Effect of bovine oviduct epithelial cell apical plasma membranes on sperm function assessed by a novel flow cytometric approach. *Biol Reprod* **67**, 1125-1132.
- Boissonnas, C. C., Montjean, D., Lesaffre, C., Auer, J., Vaiman, D., Wolf, J. P. and Ziyat, A.** (2010). Role of sperm alphavbeta3 integrin in mouse fertilization. *Dev Dyn* **239**, 773-783.
- Brandenburger, T., Strehler, E. E., Filoteo, A. G., Caride, A. J., Aumuller, G., Post, H., Schwarz, A. and Wilhelm, B.** (2011). Switch of PMCA4 splice variants in bovine epididymis results in altered isoform expression during functional sperm maturation. *J Biol Chem* **286**, 7938-7946.
- Breitbart, H., Rubinstein, S. and Nass-Arden, L.** (1985). The role of calcium and Ca²⁺-ATPase in maintaining motility in ram spermatozoa. *J Biol Chem* **260**, 11548-11553.
- Bronson, R. A. and Fusi, F. M.** (1996). Integrins and human reproduction. *Mol Hum Reprod* **2**, 153-168.
- Caballero, J., Frenette, G. and Sullivan, R.** (2010). Post testicular sperm maturational changes in the bull: important role of the epididymosomes and prostasomes. *Vet Med Int* **2011**, 757194.
- Caballero, J. N., Frenette, G., Belleanne, C. and Sullivan, R.** (2013). CD9-positive microvesicles mediate the transfer of molecules to Bovine Spermatozoa during epididymal maturation. *PLoS one* **8**, e65364.
- Caride, A. J., Filoteo, A. G., Penniston, J. T. and Strehler, E. E.** (2007). The plasma membrane Ca²⁺ pump isoform 4a differs from isoform 4b in the mechanism of calmodulin binding and activation kinetics: implications for Ca²⁺ signaling. *J Biol Chem* **282**, 25640-25648.
- Chen, H., Griffiths, G., Galileo, D. S. and Martin-DeLeon, P. A.** (2006). Epididymal SPAM1 is a marker for sperm maturation in the mouse. *Biol Reprod* **74**, 923-930.
- Chernomordik, L. V. and Kozlov, M. M.** (2003). Protein-lipid interplay in fusion and fission of biological membranes. *Annu Rev Biochem* **72**, 175-207.

- Christen, R., Schackmann, R. W. and Shapiro, B. M.** (1983). Metabolism of sea urchin sperm. Interrelationships between intracellular pH, ATPase activity, and mitochondrial respiration. *J Biol Chem* **258**, 5392-5399.
- Cooper, T. G.** (1995). Role of the epididymis in mediating changes in the male gamete during maturation. *Adv Exp Med Biol* **377**, 87-101.
- Cooper, T. G.** (1998). Interactions between epididymal secretions and spermatozoa. *Reprod Fertil Suppl* **53**, 119-136.
- Costello, S., Michelangeli, F., Nash, K., Lefievre, L., Morris, J., Machado-Oliveira, G., Barratt, C., Kirkman-Brown, J. and Publicover, S.** (2009). Ca²⁺-stores in sperm: their identities and functions. *Reproduction* **138**, 425-437.
- Coy, P., Garcia-Vazquez, F. A., Visconti, P. E. and Aviles, M.** (2012). Roles of the oviduct in mammalian fertilization. *Reproduction* **144**, 649-660.
- Cross, N. L.** (2004). Reorganization of lipid rafts during capacitation of human sperm. *Biol Reprod* **71**, 1367-1373.
- Danen, E. H., Ten Berge, P. J., Van Muijen, G. N., Van 't Hof-Grootenboer, A. E., Brocker, E. B. and Ruiten, D. J.** (1994). Emergence of alpha 5 beta 1 fibronectin- and alpha v beta 3 vitronectin-receptor expression in melanocytic tumour progression. *Histopathology* **24**, 249-256.
- de Lamirande, E., Leclerc, P. and Gagnon, C.** (1997). Capacitation as a regulatory event that primes spermatozoa for the acrosome reaction and fertilization. *Mol Hum Reprod* **3**, 175-194.
- Deng, X., Czymmek, K. and Martin-DeLeon, P. A.** (1999). Biochemical maturation of Spam1 (PH-20) during epididymal transit of mouse sperm involves modifications of N-linked oligosaccharides. *Mol Reprod Dev* **52**, 196-206.
- Di Leva, F., Domi, T., Fedrizzi, L., Lim, D. and Carafoli, E.** (2008). The plasma membrane Ca²⁺ ATPase of animal cells: structure, function and regulation. *Arch Biochem Biophys* **476**, 65-74.
- Driscoll, M. D., Sathya, G., Muyan, M., Klinge, C. M., Hilf, R. and Bambara, R. A.** (1998). Sequence requirements for estrogen receptor binding to estrogen response elements. *J Biol Chem* **273**, 29321-29330.
- Escrevente, C., Keller, S., Altevogt, P. and Costa, J.** (2011). Interaction and uptake of exosomes by ovarian cancer cells. *BMC cancer* **11**, 108.

- Fabiani, R., Johansson, L., Lundkvist, O. and Ronquist, G.** (1995). Prolongation and improvement of prostasome promotive effect on sperm forward motility. *Eur J Obstet Gynecol Reprod Biol* **58**, 191-198.
- Filoteo, A. G., Elwess, N. L., Enyedi, A., Caride, A., Aung, H. H. and Penniston, J. T.** (1997). Plasma membrane Ca²⁺ pump in rat brain. Patterns of alternative splices seen by isoform-specific antibodies. *J Biol Chem* **272**, 23741-23747.
- Frenette, G. and Sullivan, R.** (2001). Prostasome-like particles are involved in the transfer of P25b from the bovine epididymal fluid to the sperm surface. *Mol Reprod Dev* **59**, 115-121.
- Fusi, F. M. and Bronson, R. A.** (1992). Sperm surface fibronectin. Expression following capacitation. *J Androl* **13**, 28-35.
- Fusi, F. M., Lorenzetti, I., Vignali, M. and Bronson, R. A.** (1992). Sperm surface proteins after capacitation. Expression of vitronectin on the spermatozoan head and laminin on the sperm tail. *J Androl* **13**, 488-497.
- Fusi, F. M., Tamburini, C., Mangili, F., Montesano, M., Ferrari, A. and Bronson, R. A.** (1996). The expression of alpha v, alpha 5, beta 1, and beta 3 integrin chains on ejaculated human spermatozoa varies with their functional state. *Mol Hum Reprod* **2**, 169-175.
- Gadella, B. M. and Luna, C.** (2014). Cell biology and functional dynamics of the mammalian sperm surface. *Theriogenology* **81**, 74-84.
- Geho, D. H., Smith, W. I., Jr., Liotta, L. A. and Roberts, D. D.** (2003). Fibronectin-based masking molecule blocks platelet adhesion. *Bioconjug Chem* **14**, 703-706.
- Giroux-Widemann, V., Jouannet, P., Pignot-Paintrand, I. and Feneux, D.** (1991). Effects of pH on the reactivation of human spermatozoa demembrated with Triton X-100. *Mol Reprod Dev* **29**, 157-162.
- Goldman, J. M., Murr, A. S. and Cooper, R. L.** (2007). The rodent estrous cycle: characterization of vaginal cytology and its utility in toxicological studies. *Birth Defects Res B Dev Reprod Toxicol* **80**, 84-97.
- Griffiths, G. S., Galileo, D. S., Reese, K. and Martin-DeLeon, P. A.** (2008a). Investigating the role of murine epididymosomes and uterosomes in GPI-linked protein transfer to sperm using SPAM1 as a model. *Mol Reprod Dev* **75**, 1627-1636.

- Griffiths, G. S., Miller, K. A., Galileo, D. S. and Martin-DeLeon, P. A.** (2008b). Murine SPAM1 is secreted by the estrous uterus and oviduct in a form that can bind to sperm during capacitation: acquisition enhances hyaluronic acid-binding ability and cumulus dispersal efficiency. *Reproduction* **135**, 293-301.
- Griffiths, G. S., Galileo, D. S., Aravindan, R. G. and Martin-DeLeon, P. A.** (2009). Clusterin facilitates exchange of glycosyl phosphatidylinositol-linked SPAM1 between reproductive luminal fluids and mouse and human sperm membranes. *Biol Reprod* **81**, 562-570.
- Hellstrom, W. J., Bell, M., Wang, R. and Sikka, S. C.** (1994). Effect of sodium nitroprusside on sperm motility, viability, and lipid peroxidation. *Fertil Steril* **61**, 1117-1122.
- Hermo, L. and Jacks, D.** (2002). Nature's ingenuity: bypassing the classical secretory route via apocrine secretion. *Mol Reprod Dev* **63**, 394-410.
- Herrick, S. B., Schweissinger, D. L., Kim, S. W., Bayan, K. R., Mann, S. and Cardullo, R. A.** (2005). The acrosomal vesicle of mouse sperm is a calcium store. *J Cell Physiol* **202**, 663-671.
- Hess, R. A. and de Franca, L. R.** (2008). Spermatogenesis and cycle of the seminiferous epithelium. *Adv Exp Med Biol* **535**:1-15.
- Hirst, R. A., Harrison, C., Hirota, K. and Lambert, D. G.** (1999). Measurement of [Ca²⁺] in whole cell suspensions Using Fura-2. *Methods Mol Biol* **114**:31-39.
- Ho, H. C. and Suarez, S. S.** (2003). Characterization of the intracellular calcium store at the base of the sperm flagellum that regulates hyperactivated motility. *Biol Reprod* **68**, 1590-1596.
- Ho, H. C., Granish, K. A. and Suarez, S. S.** (2002). Hyperactivated motility of bull sperm is triggered at the axoneme by Ca²⁺ and not cAMP. *Dev Biol* **250**, 208-217.
- Holton, M. L., Wang, W., Emerson, M., Neyses, L. and Armesilla, A. L.** (2010). Plasma membrane calcium ATPase proteins as novel regulators of signal transduction pathways. *World J Biol Chem* **1**, 201-208.
- Ito, C., Yamatoya, K., Yoshida, K., Maekawa, M., Miyado, K. and Toshimori, K.** (2010). Tetraspanin family protein CD9 in the mouse sperm: unique localization, appearance, behavior and fate during fertilization. *Cell Tissue Res* **340**, 583-594.

- Jones, R.** (1989). Membrane remodelling during sperm maturation in the epididymis. *Oxf Rev Reprod Biol* **11**, 285-337.
- Jones, R.** (1998). Plasma membrane structure and remodelling during sperm maturation in the epididymis. *J Reprod Fertil Suppl* **53**, 73-84.
- Kanwar, U., Anand, R. J. and Sanyal, S. N.** (1993). The effect of nifedipine, a calcium channel blocker, on human spermatozoal functions. *Contraception* **48**, 453-470.
- Kirchhoff, C. and Hale, G.** (1996). Cell-to-cell transfer of glycosylphosphatidylinositol-anchored membrane proteins during sperm maturation. *Mol Hum Reprod* **2**, 177-184.
- Kirchhoff, C., Pera, I., Derr, P., Yeung, C. H. and Cooper, T.** (1997). The molecular biology of the sperm surface. Post-testicular membrane remodelling. *Adv Exp Med Biol* **424**, 221-232.
- Kosk-Kosicka, D.** (1999). Measurement of Ca²⁺-ATPase activity (in PMCA and SERCA1). *Methods Mol Biol* **114**, 343-354.
- Kozlov, M. M., Leikin, S. L., Chernomordik, L. V., Markin, V. S. and Chizmadzhev, Y. A.** (1989). Stalk mechanism of vesicle fusion. Intermixing of aqueous contents. *Eu Biophys J* **17**, 121-129.
- Lakkaraju, A. and Rodriguez-Boulan, E.** (2008). Itinerant exosomes: emerging roles in cell and tissue polarity. *Trends Cell Biol* **18**, 199-209.
- Lee, M. G., Xu, X., Zeng, W., Diaz, J., Kuo, T. H., Wuytack, F., Racymaekers, L. and Muallem, S.** (1997). Polarized expression of Ca²⁺ pumps in pancreatic and salivary gland cells. Role in initiation and propagation of [Ca²⁺]_i waves. *J Biol Chem* **272**, 15771-15776.
- Leikin, S. L., Kozlov, M. M., Chernomordik, L. V., Markin, V. S. and Chizmadzhev, Y. A.** (1987). Membrane fusion: overcoming of the hydration barrier and local restructuring. *J Theor Biol* **129**, 411-425.
- Masyuk, A. I., Huang, B. Q., Ward, C. J., Gradilone, S. A., Banales, J. M., Masyuk, T. V., Radtke, B., Splinter, P. L. and LaRusso, N. F.** (2010). Biliary exosomes influence cholangiocyte regulatory mechanisms and proliferation through interaction with primary cilia. *Am J Physiol Gastrointest Liver Physiol* **299**, G990-999.

- Modelski, M. J., Menlah, G., Wang, Y., Dash, S., Wu, K., Galileo, D. S. and Martin-DeLeon, P. A.** (2014). Hyaluronidase 2: A Novel Germ Cell Hyaluronidase with Epididymal Expression and Functional Roles in Mammalian Sperm. *Biol Reprod*.
- O'Toole, C. M., Arnoult, C., Darszon, A., Steinhardt, R. A. and Florman, H. M.** (2000). Ca²⁺ entry through store-operated channels in mouse sperm is initiated by egg ZP3 and drives the acrosome reaction. *Mol Biol Cell* **11**, 1571-1584.
- Okunade, G. W., Miller, M. L., Pyne, G. J., Sutliff, R. L., O'Connor, K. T., Neumann, J. C., Andringa, A., Miller, D. A., Prasad, V., Doetschman, T. et al.** (2004). Targeted ablation of plasma membrane Ca²⁺-ATPase (PMCA) 1 and 4 indicates a major housekeeping function for PMCA1 and a critical role in hyperactivated sperm motility and male fertility for PMCA4. *J Biol Chem* **279**, 33742-33750.
- Patel, R., Al-Dossary, A. A., Stabley, D. L., Barone, C., Galileo, D. S., Strehler, E. E. and Martin-DeLeon, P. A.** (2013). Plasma Membrane Ca²⁺-ATPase 4 in Murine Epididymis: Secretion of Splice Variants in the Luminal Fluid and a Role in Sperm Maturation. *Biol Reprod* **89**, 6.
- Peddibhotla, S. S., Brinkmann, B. F., Kummer, D., Tuncay, H., Nakayama, M., Adams, R. H., Gerke, V. and Ebnet, K.** (2013). Tetraspanin CD9 links junctional adhesion molecule-A to alphavbeta3 integrin to mediate basic fibroblast growth factor-specific angiogenic signaling. *Mol Biol Cell* **24**, 933-944.
- Pedersen, P. L. and Carafoli, E.** (1987). Ion motive ATPases. I. Ubiquity, properties, and significance to cell function. *Trends Biochem Sci* **12**, 146-150.
- Pencer, J., Jackson, A., Kucerka, N., Nieh, M. P. and Katsaras, J.** (2008). The influence of curvature on membrane domains. *Eur Biophys J* **37**, 665-671.
- Pisitkun, T., Shen, R. F. and Knepper, M. A.** (2004). Identification and proteomic profiling of exosomes in human urine. *Proc Natl Acad Sci U S A* **101**, 13368-13373.
- Poburko, D., Santo-Domingo, J. and Demaurex, N.** (2011). Dynamic regulation of the mitochondrial proton gradient during cytosolic calcium elevations. *J Biol Chem* **286**, 11672-11684.

- Post, H., Wiche, R., Sen, P. C., Hoffbauer, G., Albrecht, M., Seitz, J., Aumuller, G. and Wilhelm, B.** (2002). Identification of a plasma membrane Ca²⁺-ATPase in epithelial cells and aposomes of the rat coagulating gland. *Prostate* **52**, 159-166.
- Post, R. L., Kume, S., Tobin, T., Orcutt, B. and Sen, A. K.** (1969). Flexibility of an active center in sodium-plus-potassium adenosine triphosphatase. *J Gen Physiol* **54**, 306-326.
- Qi, H., Moran, M. M., Navarro, B., Chong, J. A., Krapivinsky, G., Krapivinsky, L., Kirichok, Y., Ramsey, I. S., Quill, T. A. and Clapham, D. E.** (2007). All four CatSper ion channel proteins are required for male fertility and sperm cell hyperactivated motility. *Proc Natl Acad Sci U S A* **104**, 1219-1223.
- Raimondo, F., Morosi, L., Chinello, C., Magni, F. and Pitto, M.** (2011). Advances in membranous vesicle and exosome proteomics improving biological understanding and biomarker discovery. *Proteomics* **11**, 709-720.
- Reese, K. L., Aravindan, R. G., Griffiths, G. S., Shao, M., Wang, Y., Galileo, D. S., Atmuri, V., Triggs-Raine, B. L. and Martin-DeLeon, P. A.** (2010). Acidic hyaluronidase activity is present in mouse sperm and is reduced in the absence of SPAM1: evidence for a role for hyaluronidase 3 in mouse and human sperm. *Mol Reprod Devel* **77**, 759-772.
- Reid, A. T., Redgrove, K., Aitken, R. J. and Nixon, B.** (2011). Cellular mechanisms regulating sperm-zona pellucida interaction. *Asian J Androl* **13**, 88-96.
- Reinhardt, T. A., Filoteo, A. G., Penniston, J. T. and Horst, R. L.** (2000). Ca²⁺-ATPase protein expression in mammary tissue. *Cell Physiol* **279**, C1595-1602.
- Ritchie, A. J., Crawford, D. M., Ferguson, D. J., Burthem, J. and Roberts, D. J.** (2013). Normal prion protein is expressed on exosomes isolated from human plasma. *Br J Haematol* **163**, 678-680.
- Roca, J., Martinez, S., Vazquez, J. M., Lucas, X., Parrilla, I. and Martinez, E. A.** (2000). Viability and fertility of rabbit spermatozoa diluted in Tris-buffer extenders and stored at 15 degrees C. *Anim Reprod Sci* **64**, 103-112.
- Rodriguez-Martinez, H.** (2007). Role of the oviduct in sperm capacitation. *Theriogenology* **68 Suppl 1**, S138-146.
- Ronquist, G., Brody, I., Gottfries, A. and Stegmayr, B.** (1978). An Mg²⁺ and Ca²⁺-stimulated adenosine triphosphatase in human prostatic fluid--part II. *Andrologia* **10**, 427-433.

- Saez, F., Frenette, G. and Sullivan, R.** (2003). Epididymosomes and prostasomes: their roles in posttesticular maturation of the sperm cells. *J Androl* **24**, 149-154.
- Schorey, J. S. and Bhatnagar, S.** (2008). Exosome function: from tumor immunology to pathogen biology. *Traffic* **9**, 871-881.
- Schuh, K., Uldrijan, S., Telkamp, M., Rothlein, N. and Neyses, L.** (2001). The plasmamembrane calmodulin-dependent calcium pump: a major regulator of nitric oxide synthase I. *J Cell Biol* **155**, 201-205.
- Schuh, K., Cartwright, E. J., Jankevics, E., Bundschu, K., Liebermann, J., Williams, J. C., Armesilla, A. L., Emerson, M., Oceandy, D., Knobeloch, K. P. et al.** (2004). Plasma membrane Ca²⁺ ATPase 4 is required for sperm motility and male fertility. *J Biol Chem* **279**, 28220-28226.
- Schwarz, A., Wennemuth, G., Post, H., Brandenburger, T., Aumuller, G. and Wilhelm, B.** (2013). Vesicular transfer of membrane components to bovine epididymal spermatozoa. *Cell Tissue Res* **353**, 549-561.
- Seftor, R. E., Seftor, E. A., Gehlsen, K. R., Stetler-Stevenson, W. G., Brown, P. D., Ruoslahti, E. and Hendrix, M. J.** (1992). Role of the alpha v beta 3 integrin in human melanoma cell invasion. *Proc Natl Acad Sci U S A* **89**, 1557-1561.
- Sepulveda, M. R., Berrocal-Carrillo, M., Gasset, M. and Mata, A. M.** (2006). The plasma membrane Ca²⁺-ATPase isoform 4 is localized in lipid rafts of cerebellum synaptic plasma membranes. *J Biol Chem* **281**, 447-453.
- Shao, M., Ghosh, A., Cooke, V. G., Naik, U. P. and Martin-DeLeon, P. A.** (2008). JAM-A is present in mammalian spermatozoa where it is essential for normal motility. *Dev Biol* **313**, 246-255.
- Sikdar, R., Ganguly, U., Pal, P., Mazumder, B. and Sen, P. C.** (1991). Biochemical characterization of a calcium ion stimulated-ATPase from goat spermatozoa. *Mol Cell Biochem* **103**, 121-130.
- Simons, M. and Raposo, G.** (2009). Exosomes--vesicular carriers for intercellular communication. *Curr Opin Cell Biol* **21**, 575-581.
- Simpson, R. J., Jensen, S. S. and Lim, J. W.** (2008). Proteomic profiling of exosomes: current perspectives. *Proteomics* **8**, 4083-4099.

- Sleight, S. B., Miranda, P. V., Plaskett, N. W., Maier, B., Lysiak, J., Scrable, H., Herr, J. C. and Visconti, P. E.** (2005). Isolation and proteomic analysis of mouse sperm detergent-resistant membrane fractions: evidence for dissociation of lipid rafts during capacitation. *Biol Reprod* **73**, 721-729.
- Strehler, E. E.** (2013). Plasma membrane calcium ATPases as novel candidates for therapeutic agent development. *J Pharm Pharm Sci* **16**, 190-206.
- Strehler, E. E. and Zacharias, D. A.** (2001). Role of alternative splicing in generating isoform diversity among plasma membrane calcium pumps. *Physiol Rev* **81**, 21-50.
- Strehler, E. E., Filoteo, A. G., Penniston, J. T. and Caride, A. J.** (2007). Plasma-membrane Ca(2+) pumps: structural diversity as the basis for functional versatility. *Biochem Soc Trans* **35**, 919-922.
- Suarez, S. S. and Ho, H. C.** (2003). Hyperactivation of mammalian sperm. *Cell Mol Biol* **49**, 351-356.
- Suarez, S. S. and Pacey, A. A.** (2006). Sperm transport in the female reproductive tract. *Hum Reprod Update* **12**, 23-37.
- Sullivan, R. and Saez, F.** (2013). Epididymosomes, prostasomes, and liposomes: their roles in mammalian male reproductive physiology. *Reproduction* **146**, R21-35.
- Tan, S. S., Yin, Y., Lee, T., Lai, R. C., Yeo, R. W., Zhang, B., Choo, A. and Lim, S. K.** (2013). Therapeutic MSC exosomes are derived from lipid raft microdomains in the plasma membrane. *J Extracell Vesicles* **2**.
- Thery, C., Zitvogel, L. and Amigorena, S.** (2002). Exosomes: composition, biogenesis and function. *Nature reviews. Immunology* **2**, 569-579.
- Thery, C., Ostrowski, M. and Segura, E.** (2009). Membrane vesicles as conveyors of immune responses. *Nature reviews. Immunology* **9**, 581-593.
- Thys, M., Nauwynck, H., Vandaele, L., Bijttebier, J., Maes, D., Favoreel, H. and Van Soom, A.** (2012). Vitronectin and Its Receptor (Integrin $\alpha\beta 3$) During Bovine Fertilization In Vitro, p 503-522. In Perez-Marin CC (ed), A Bird's-Eye View of Veterinary Medicine, ISBN: 978-953-51-0031-7, InTech, Croatia, Europe. DOI: 10.5772/37408.

- Travis, A. J., Merdiushev, T., Vargas, L. A., Jones, B. H., Purdon, M. A., Nipper, R. W., Galatioto, J., Moss, S. B., Hunnicutt, G. R. and Kopf, G. S.** (2001). Expression and localization of caveolin-1, and the presence of membrane rafts, in mouse and Guinea pig spermatozoa. *Dev Biol* **240**, 599-610.
- Turturici, G., Tinnirello, R., Sconzo, G. and Geraci, F.** (2014). Extracellular membrane vesicles as a mechanism of cell-to-cell communication: advantages and disadvantages. *American journal of physiology. Cell Physiol* **306**, C621-633.
- Weinberg, J. B., Doty, E., Bonaventura, J. and Haney, A. F.** (1995). Nitric oxide inhibition of human sperm motility. *Fertil Steril* **64**, 408-413.
- Wennemuth, G., Babcock, D. F. and Hille, B.** (2003). Calcium clearance mechanisms of mouse sperm. *J Gen Physiol* **122**, 115-128.
- Wilhelm, B., Brandenburger, T., Post, H. and Aumuller, G.** (2008). Expression and localization of PMCA4 in rat testis and epididymis. *Histochem Cell Biol* **129**, 331-343.
- Yamashita, T., Kamada, H., Kanasaki, S., Maeda, Y., Nagano, K., Abe, Y., Inoue, M., Yoshioka, Y., Tsutsumi, Y., Katayama, S. et al.** (2013). Epidermal growth factor receptor localized to exosome membranes as a possible biomarker for lung cancer diagnosis. *Pharmazie* **68**, 969-973.
- Yeung, C. H., and Cooper, T.G.** (2002). Acquisition and development of sperm motility upon maturation in the epididymis, p 417–434. *In* Robaire B, Hinton BT, (ed), *The Epididymis: From Molecules to Clinical Practice*, Kluwer Academic/Plenum Publishers, New York, NY.
- Yoon, Y. J., Kim, O. Y. and Gho, Y. S.** (2014). Extracellular vesicles as emerging intercellular comunicasomes. *BMB reports*.
- Zalata, A. A., Christophe, A. B., Depuydt, C. E., Schoonjans, F. and Comhaire, F. H.** (1998). The fatty acid composition of phospholipids of spermatozoa from infertile patients. *Mol Hum Reprod* **4**, 111-118.
- Zhang, H. and Martin-DeLeon, P. A.** (2003). Mouse Spam1 (PH-20) is a multifunctional protein: evidence for its expression in the female reproductive tract. *Biol Reprod* **69**, 446-454.
- Zhou, Q., Li, M., Wang, X., Li, Q., Wang, T., Zhu, Q., Zhou, X., Wang, X., Gao, X. and Li, X.** (2012). Immune-related microRNAs are abundant in breast milk exosomes. *Int J Biol Sci* **8**, 118-123.

MANUSCRIPTS

1. *Patel, R., ***Al-Dossary, A. A.**, Stabley, D. L., Barone, C., Galileo, D. S., Strehler, E. E. and Martin-DeLeon, P. A. (2013). Plasma membrane Ca²⁺-ATPase 4 in murine epididymis: secretion of splice variants in the luminal fluid and a role in sperm maturation. *Biol Reprod* **89**, 6.***Co-first author**
2. **Al-Dossary, A. A.**, Strehler, E. E. and Martin-DeLeon, P. A. (2013). Expression and secretion of plasma membrane Ca²⁺-ATPase 4a (PMCA4a) during murine estrus: association with oviductal exosomes and uptake in sperm. *PLoS one* **8**, e80181.
3. **Al-Dossary, A. A.**, Caplan, J. L. and Martin-DeLeon, P. A. (2014). Oviductosomes-sperm membrane interaction in cargo delivery: Detection of fusion and underlying molecular players using 3D super-resolution structured illumination microscopy (SR-SIM). *Mol Cellular Biol, In Review*
4. **Al-Dossary, A. A.**, and Martin-DeLeon, P. A. (2014). JAM-A-CASK complex interacts with CD9 tetraspanin and $\alpha\beta3$ integrin to mediate Ca²⁺ signaling in Capacitation and the Acrosome reaction in Murine Sperm *Mol Cellular Biol, In preparation*
5. **Al-Dossary, A.A.**, Hurd, L.M., Dutt, R., and Martin-DeLeon, P.A. (2014). PMCA carried in Oviductosomal cargo delivered to sperm is functional and contributes to proper Ca²⁺ handling which significantly impacts sperm phenotype. *In preparation*
6. **Al-Dossary, A. A.**, Accerbi, M., Green, P.J. and Martin-DeLeon, P. A. (2014). The microRNA Population in Oviductosomes collected during Pro/estrus and Met/Diestrus. *In preparation*

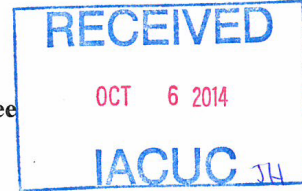
GLOSSARY OF ABBREVIATIONS

- AIJ: Ampullary Isthmus Junction
- ANOVA: Analysis of Variance
- AR: Acrosome Reaction
- CatSper: Cation Channels of Sperm
- CAP: Capacitation
- ELF: Epididymal Luminal Fluid
- EVs: Extracellular Vesicles
- FN: Fibronectin
- HTF: Human Tubal Fluid
- IAM: Inner Acrosomal Membrane
- LF: Luminal Fluid
- MVBs: Multivesicular Bodies
- NO: Nitric Oxide
- NOSs: Nitric Oxide Synthases
- $O_2^{\cdot-}$: Superoxide
- OLF: Oviductal Luminal Fluid
- $ONOO^-$: Peroxynitrite
- OVS: Oviductosomes
- PMCA: Plasma Membrane Calcium ATPase

- PUFA: Polyunsaturated Fatty Acids
- RGD: Arg-Gly-Asp
- SEM: Standard Error of the Mean
- SR-SIM: Super-Resolution Structured Illumination Microscopy
- SPAM1: Sperm Adhesion Molecule 1
- TEM: Transmission Electron Microscope
- ULF: Uterine Luminal Fluid
- VLF: Vaginal Luminal Fluid
- VN: Vitronectin

**INSTITUTIONAL ANIMAL CARE AND USE COMMITTEE (IACUC)
APPROVAL**

University of Delaware
Institutional Animal Care and Use Committee
Annual Review



Title of Protocol: Mechanism of Sperm motility defects seen in <i>Jam-A /Pmca4</i> null mice	
AUP Number: 1181-2015-1	← (4 digits only)
Principal Investigator: Patricia A. DeLeon	
Common Name: Mouse	
Genus Species: <i>Mus Musculus</i>	
Pain Category: (please mark one)	
USDA PAIN CATEGORY: (Note change of categories from previous form)	
Category	Description
<input type="checkbox"/> B	Breeding or holding where NO research is conducted
<input checked="" type="checkbox"/> C	Procedure involving momentary or no pain or distress
<input type="checkbox"/> D	Procedure where pain or distress is alleviated by appropriate means (analgesics, tranquilizers, euthanasia etc.)
<input type="checkbox"/> E	Procedure where pain or distress cannot be alleviated, as this would adversely affect the procedures, results or interpretation

Official Use Only
IACUC Approval Signature: 
Date of Approval: 12/1/2014

Principal Investigator Assurance

1. I agree to abide by all applicable federal, state, and local laws and regulations, and UD policies and procedures.
2. I understand that deviations from an approved protocol or violations of applicable policies, guidelines, or laws could result in immediate suspension of the protocol and may be reportable to the Office of Laboratory Animal Welfare (OLAW).
3. I understand that the Attending Veterinarian or his/her designee must be consulted in the planning of any research or procedural changes that may cause more than momentary or slight pain or distress to the animals.
4. I declare that all experiments involving live animals will be performed under my supervision or that of another qualified scientist listed on this AUP. All listed personnel will be trained and certified in the proper humane methods of animal care and use prior to conducting experimentation.
5. I understand that emergency veterinary care will be administered to animals showing evidence of discomfort, ailment, or illness.
6. I declare that the information provided in this application is accurate to the best of my knowledge. If this project is funded by an extramural source, I certify that this application accurately reflects all currently planned procedures involving animals described in the proposal to the funding agency.
7. I assure that any modifications to the protocol will be submitted to the UD-IACUC and I understand that they must be approved by the IACUC prior to initiation of such changes.
8. I understand that the approval of this project is for a maximum of one year from the date of UD-IACUC approval and that I must re-apply to continue the project beyond that period.
9. I understand that any unanticipated adverse events, morbidity, or mortality must be reported to the UD-IACUC immediately.
10. I assure that the experimental design has been developed with consideration of the three Rs: reduction, refinement, and replacement, to reduce animal pain and/or distress and the number of animals used in the laboratory.
11. I assure that the proposed research does not unnecessarily duplicate previous experiments. (<i>Teaching Protocols Exempt</i>)
12. I understand that by signing, I agree to these assurances.

<hr/> Signature of Principal Investigator
10-4-2014 <hr/> Date

SIGNATURE(S) OF ALL PERSONS LISTED ON THIS PROTOCOL

I certify that I have read this protocol, accept my responsibility and will perform only the procedures that have been approved by the IACUC.

Name	Signature
1. Amal Aldossary	<i>Amal Aldossary</i>
2. Kathie Wu	<i>Kathie Wu</i>
3. Lauren Coffua	<i>Lauren Coffua</i>
4. Rebecca Pollak	<i>Rebecca Pollak</i>
5. Pradeepthi Bathala	<i>Pradeepthi Bathala</i>
6. Patricia A. DeLeon	<i>Patricia A DeLeon</i>
7. Click here to enter text.	
8. Click here to enter text.	
9. Click here to enter text.	
10. Click here to enter text.	
11. Click here to enter text.	
12. Click here to enter text.	
13. Click here to enter text.	
14. Click here to enter text.	
15. Click here to enter text.	

IACUC approval of animal protocols must be renewed on an annual basis.

1. Previous Approval Date: 12/1/13

Is Funding Source the same as on original, approved AUP?

Yes No

If no, please state Funding Source and Award Number: [Click here to enter text.](#)

2. Record of Animal Use:

Common Name	Genus Species	Total Number Previously Approved	Number Used To Date
1. Mouse	<i>Mus Musculus</i>	1920	1043
2. Click here to enter text.	Click here to enter text.	Click here to enter text.	Click here to enter text.
3. Click here to enter text.	Click here to enter text.	Click here to enter text.	Click here to enter text.
4. Click here to enter text.	Click here to enter text.	Click here to enter text.	Click here to enter text.
5. Click here to enter text.	Click here to enter text.	Click here to enter text.	Click here to enter text.

3. Protocol Status: *(Please indicate by check mark the status of project.)*

Request for Protocol Continuance:

A. Active: Project ongoing

B. Currently inactive: Project was initiated but is presently inactive

C. Inactive: Project never initiated but anticipated starting date is:

[Click here to enter text.](#)

Request for Protocol Termination:

D. Inactive: Project never initiated

E. Completed: No further activities with animals will be done.

PLOS JOURNALS STATEMENT OF AUTHORS' RIGHTS

Open-Access License

No Permission Required

PLOS applies the [Creative Commons Attribution \(CC BY\) license](#) to all works we publish (read the [human-readable summary](#) or the [full license legal code](#)). Under the CC BY license, authors retain ownership of the copyright for their article, but authors allow anyone to download, reuse, reprint, modify, distribute, and/or copy articles in PLOS journal long as the original authors and source are cited. **No permission is required from the authors or the publishers**

In most cases, appropriate attribution can be provided by simply citing the original article (e.g., Kaltenbach LS et al. (2007) Huntingtin Interacting Proteins Are Genetic Modifiers of Neurodegeneration. *PLOS Genet* 3(5): e82. doi:10.1371/journal.pgen.0050082). If you plan to reuse is not part of a published article (e.g., a featured issue image), then please indicate the originator of the item and the journal in which the item appeared. For any reuse or redistribution of a work, you must also make clear the license under which the work was published.

This broad license was developed to facilitate open access to, and free use of, original works of all types. Applying it ensures your right to make your work freely and openly available. Learn more about [open access](#). For queries about